

EXCITON PHOTON AND PHONON INTERACTIONS IN SEMICONDUCTOR
QUANTUM DOTS

By

Kaijie Xu

A DISSERTATION

Submitted to
Michigan State University
in partial fulfillment of the requirements
for the degree of

DOCTOR OF PHILOSOPHY

Physics

2012

ABSTRACT

EXCITON PHOTON AND PHONON INTERACTIONS IN SEMICONDUCTOR QUANTUM DOTS

By

Kaijie Xu

Excitons, photons, and phonons are elementary excitations that have been widely investigated in semiconductor systems. This thesis focuses on the exciton energy transfer between quantum dots, which is a physical process that involves all these elementary excitations. Exciton energy transfer is a common process in many artificial systems such as solar cells, lasers, and quantum gates.

In order to study the exciton energy transfer, we develop a full quantum theory to describe the exciton-photon interaction and exciton-phonon interaction. We derive the exciton-photon interaction from the quantized field operator representing the electromagnetic field. In the derivation, the effect of a planar cavity, which modifies the photon density of states is considered. We also obtain the exciton-phonon interaction starting from the deformation potential. With both types of interaction given, we study the dynamics of the exciton transfer in a cavity by solving the Schrödinger equation for the coupled system of excitons, photons and phonons. Both elastic and inelastic exciton energy transfer are simulated. We find that the coupling to phonons enhances the exciton energy transfer when two dots are off-resonant. In addition to the theoretical and numerical study of the exciton energy transfer, two applications of the theory are discussed. As an application to quantum computing, phonon-assisted exciton energy transfer is proposed as the key ingredient in the implementation of a Quantum Zeno gate. In another application, we expand our approach to a multi-dot array, which can be applied to the design of novel light-harvesting devices.

ACKNOWLEDGMENTS

I would like to thank my advisor Professor Carlo Piermarocchi for his full support academically and personally in the past years. Also, I would like to express my gratitude to the members of my Guidance Committee: Professor Michael Moore, Professor Chih-Wei Lai, Professor Wayne Repko, Professor Gary Westfall and Professor S.D. Mahanti. Special thanks to Debbie Barratt for your patience and help.

TABLE OF CONTENTS

List of Tables	vi
List of Figures	vii
1 Introduction	1
2 Theoretical framework	7
2.1 Excitons in semiconductors	7
2.1.1 Wannier-Mott exciton theory	8
2.1.2 Excitons in quantum dots	11
2.2 Exciton energy transfer in photon-confined systems	17
2.2.1 Photon Hamiltonian in a microcavity	17
2.2.2 Exciton-photon interaction in a microcavity	20
2.2.3 Exciton-phonon interaction	23
3 Exciton dynamics in quantum dots	27
3.1 Exciton dynamics for a single dot in planar cavity	28
3.2 Two dots in a planar cavity	33
3.3 Super-radiance and Sub-radiance	37
3.4 Phonon-assisted energy transfer	39
3.5 Conclusion	45
4 Applications	47
4.1 Conditional phase gate using quantum dots	47
4.1.1 Brief introduction to quantum computing	47
4.1.2 Quantum gates	49
4.1.3 Quantum Zeno gate	52
4.1.4 Fidelity of the controlled phase gate by Quantum Zeno effect	54
4.1.5 Analytical estimation of the fidelity	59
4.1.6 Numerical calculation of the fidelity	61
4.2 Energy transfer in quantum dot arrays	63
4.2.1 Non-Markovian quantum process TCL method	64
4.2.2 Multi-dot array	72
5 Conclusion and outlook	81

A	Projection operator techniques	87
A.1	Projection operators	87
A.2	The Nakajima-Zwanzig equation	88
A.3	Time-convolutionless projection operator method	91
B	Perturbation theory check	97
B.1	Exciton energy transfer between two dots	99
B.2	Phonon assisted exciton energy transfer	102
B.3	Exciton-photon-phonon interaction	106
	Bibliography	112

LIST OF TABLES

3.1	Materials parameters used in the numerical simulations	28
4.1	Output coefficients	60

LIST OF FIGURES

1.1	Schematic view of the two dots in a planar cavity.	4
2.1	The conduction and valence band of the semiconductor with a direct bandgap E_g	8
2.2	Schematic view of spatial band structure of semiconductor heterostructure.	12
2.3	Three typical Quantum Dots	13
3.1	Real part of $F(\tau, \omega, \mathbf{R})$ in the case of quantum dots resonant (a and b) and off-resonant (c and d) with respect to the lowest cavity mode. Panels a and c : on-site memory effects (single dot case). Panels b and d : memory effects in the light propagation at finite distance.	31
3.2	Single dot dynamics with two different energy for the dot: (a) Quantum dot exciton energy resonant with the lowest cavity mode. (b) Quantum dot exciton energy far detuned at half the energy of the lowest cavity mode. The decay in both cases is the result of the coupling of the dot to the continuum of cavity modes.	32
3.3	Schematic view of the two dots in a planar cavity. L is the separation between the two planar mirrors in the cavity. We assume the dots to be disk-like. L_{dot} is the size of the dot in the growth direction (z), and β is the in-plane radius of the dot. R_{ab} is the separation between the two dots.	33
3.4	Photon dispersion relation in a planar cavity, the photon energy ($\hbar\omega$) is on the horizontal axis and the in-plane photon momentum \mathbf{k}_γ is on the vertical axis. Note that photon frequency has a minimum, which is determined by the photon wavevector quantization in the z direction. Arrows indicate the exciton energy of QD $_a$ (red) and QD $_b$ (green).	34
3.5	Exciton dynamics in two dots system. (a), (b) show the dynamics of the exciton population in QD $_a$ and QD $_b$. (c), (d) energy transfer time T_{tran} for different detuning Δ and inter-dot separation R_{ab} . Here ω_a and ω_b are the excitation energy for QD $_a$ and QD $_b$, respectively. $\omega_{\mathbf{k}\gamma=0}$ is the frequency of the lowest cavity mode.	36

3.6	Comparison between superradiance, subradiance and single dot spontaneous emission. For superradiance, the initial condition is $ \psi_i(t)\rangle = a, 0\rangle + b, 0\rangle$. For subradiance, the initial condition is $ \psi_i(t)\rangle = a, 0\rangle - b, 0\rangle$	39
3.7	Phonon assisted energy transfer. (a) no phonon included. (b) the phonon-assisted exciton energy transfer with phonon energy equals the detuning between the two dots (phonon-assisted resonance).	44
4.1	Schematic view of three dots based quantum zeno gate configuration	53
4.2	Scheme of the dynamics of the system under different initial states. The narrow blue (bold gray) arrow represents the electron (hole) spins. The energy levels for QD1 are the empty dot (lower) and the first exciton level (upper), while the energy levels in QD2 and QD3 are charged dot ground states (lower) and trion states (upper). Figures (a)-(d) correspond to the four possible initial states of the two qubits. (a)-(c) If the electron in QD2 or QD3 is spin down, the exciton in QD1 can decay into one of the neighboring dots, in which case the Quantum Zeno effect prevents the Rabi Oscillation in QD1. (d) If both decay channels are closed, QD1 will undergo a 2π -Rabi oscillation. The photon emission rate γ is too weak to induce a Quantum Zeno effect.	56
4.3	Dynamical evolution of several density matrix elements for the initial state $ \Psi_i^0\rangle$ during the gate operation via numerical simulation.	62

Chapter 1

Introduction

The physics of semiconductor nanostructures has been an active research field in condensed matter physics in recent decades. Semiconductor quantum dots, which are zero dimensional quantum heterostructures are among the most studied systems in this novel area [1, 2]. The properties of excitons, which are the elementary optical excitations of semiconductors, depend strongly on the dimensionality of the system. In quantum dots, excitons have discrete energy levels due to the confinement in all three spatial dimensions. This is a typical property of the electronic levels in atoms. Quantum dots with dimensions from a few nanometers to hundreds of nanometers are at least ten times larger than atoms. Hence, semiconductor quantum dots have properties that combine those of bulk semiconductors and atoms [3]. For this reason, the research of excitons in semiconductor quantum dots has become an exciting field in which concepts from both condensed matter physics and atomic physics can be applied.

Being the bound state of an electron and a hole, an exciton can transport energy without transporting net charges. Exciton energy transfer is a common process in materials science

and biology. This process is important in many artificial systems designed to harvest and generate light, for instance, in devices based on organic materials such as solar cells [4], light emitting diodes [5], and lasers [6]. Energy transfer may also be a key ingredient to the application of quantum dots system to quantum computing. [7].

Energy transfer is often classified in terms of short-range transfer (also called Förster transfer) and long-range (radiative) transfer. In the short-range transfer, the distance R between donor and acceptor is smaller compared to the wavelength of the transferred excitons. In this case, the transfer is dominated by the electrostatic dipole-dipole interaction, and the free-space transfer rate behaves as R^{-6} . In the long-range radiative case, the observed R^{-2} dependence of the transfer rate can be seen as the result of the emission and reabsorption of photons. Many theoretical and experimental investigations on exciton energy transfer in solids and liquids have been carried out in the past [8, 9, 10, 11, 12].

The object of this thesis is to study theoretically the exciton energy transfer between quantum dots, which has also been studied with different methods by other groups [13, 14, 15, 16, 17, 18, 19, 20, 21]. We develop a full quantum theory to explain this energy transfer process. We also incorporate two new aspects to this problem: quantum dots interacting with light in a photon confined system and the phonon effects on the light matter interaction.

The physics of exciton energy transfer in systems in which both photons and excitons are confined can be qualitatively different. A photon-confined system is a structure in which the electromagnetic modes are quantized in one or more directions and the photon density of states is modified with respect to the vacuum. For a planar microcavity, in which two planar mirrors quantize the photon wavevector in the direction perpendicular to the mirror planes, the in-plane photon wavevector is not confined. The idea of controlling the exciton

energy transfer by modifying the optical environment has been theoretically explored in the case of planar microcavity systems [22, 23, 24, 25].

In solid state materials such as semiconductor quantum dots, phonon effects can not be neglected. Phonon absorption and emission can modify the exciton dynamics [26, 27, 28] and affect the efficiency of the exciton energy transfer process. The effect of a phonon bath on the energy transfer in the general case has been the subject of many theoretical investigations [29, 30, 31]. Due to the large deformation potentials in semiconductors, the energy transfer in quantum dots systems can be strongly affected by phonons. Phonon effects in the emission linewidth of quantum dots have been recently investigated both experimentally and theoretically [32, 33]. Phonon effects help us to obtain a better understanding of exciton energy transfer in semiconductor quantum dots.

To be more specific, our goal for this thesis is to study the dynamics of both elastic and inelastic exciton energy transfer between quantum dots in a planar microcavity. We will develop a full theory of quantum dots in a microcavity interaction with photons and phonons [34]. We have applied our theory to quantum computing and light harvesting systems. This thesis is organized in the following way.

Chapter 2 starts with a review of the theoretical concepts of the physics covered in this thesis. We provide a quantum mechanical treatment of excitons in quantum dots. Furthermore, the photon Hamiltonian in the planar microcavity and the exciton-photon interaction Hamiltonian are derived. The exciton-photon interaction, which is usually treated semiclassically is derived in a full quantum picture. Moreover, we show how to recover the Förster coupling between the quantum dots from the Coulomb interaction [18, 19, 20, 21]. In our model, we start from the quantized EM field operator in the planar cavity [35, 22] to calculate

the coupling constant of the exciton-photon interaction. In our approach, the Coulomb interaction between electrons and holes is not included explicitly. As a result, the exciton-photon coupling constant is expressed as a function of experimentally measured physical parameters of the semiconductor quantum dots. In addition, to study the inelastic energy transfer, we provide a theoretical description of the exciton-phonon interaction originated from the deformation potential coupling between the excitons and longitudinal acoustic phonons [36]. The coupling constant for the exciton-phonon interaction is expressed as a function of the deformation potential of the semiconductor, which can be experimentally measured in bulk materials. The purpose of this chapter is to give the reader a theoretical view of all the terms of the full Hamiltonians treated in this thesis.

In Chapter 3, we explicitly consider the dynamics of the exciton transfer in a cavity by solving the Schrödinger equation for the coupled system of excitons, photons and phonons. We will focus on a system that contains one or two semiconductor quantum dots embedded in a planar microcavity. The schematic view of the system considered is shown in Fig.1.1.

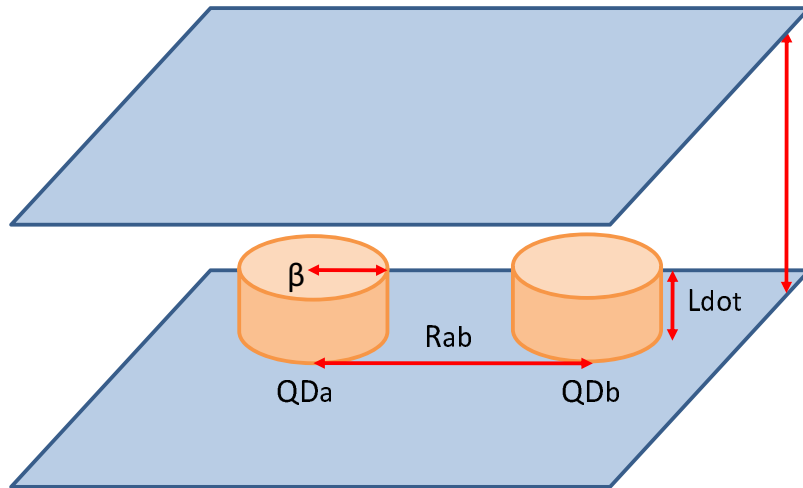


Figure 1.1: Schematic view of the two dots in a planar cavity.

Starting from the Hamiltonians given in Chapter 2, we derive the equation of motion from

the Schrödinger equation in the interaction picture. Equations of motion including the phonon degrees of freedom are also derived with the same method, using an effective exciton-photon-phonon interaction and truncating the phonon Hilbert space. With the equations of motion established, we simulate the dynamics with realistic parameters. The complete simulation of elastic energy transfer demonstrates a good agreement with the theoretical prediction. In the case of inelastic energy transfer, in which both photons and phonons participate in the exciton transfer process, the simulation shows the possibility to gain a relatively efficient exciton energy transfer between two detuned dots. In addition, the collective effect on the spontaneous emission in multiple quantum dots which is known as super-radiance, is also observed in our simulation. It serves as a proof of the validity and versatility of our model.

In Chapter 4, two potential applications of this developed model are discussed. As an application in quantum computation, phonon-assisted energy transfer has been proposed as a key mechanism for realizing quantum gates based on the Quantum Zeno effect [7]. This idea of applying Quantum Zeno effect to quantum computing is contributed by our colleagues Dr. Y.P. Huang and Prof. M. Moore [37]. We apply their idea from atomic physics to semiconductor physics. We explain the system configuration and the physical requirements for successful gate operation. In the end, the fidelity of the quantum gate is optimized for given physical characteristic parameters.

Another application relates to the exciton energy transfer in dot arrays which are considered in novel light harvesting device architecture. Exciton energy transfer is believed to be a major source of the transition of the energy in these processes. A prototype model which simplifies the multi dot system to a one dimensional dot array is proposed. In order to study the dynamics of the exciton in dot arrays, a theory with good scalability is required to effi-

ciently deal with the system with more than two dots. The time-convolutionless technique developed by Breuer and Petruccione in their book [38] is extended to solve the problem. In the book, this technique is used to explain the spontaneous emission in a single two level system. We first extend this method to a two dot system. Then it is straight forward to apply the same technique to deal with an N dot problem. As a result, the complexity of the problem goes quadratically with the number of dots. For a dot array, if only the nearest neighbors are considered, the complexity of the problem scales linearly with the number of dots.

The thesis ends with comments on the result of the dynamics simulation and the possible applications we proposed. Future directions of research that may use our exciton energy transfer model are presented and briefly discussed.

The results presented in this thesis have been published in

1. K. J. Xu, Y. P. Huang, M. G. Moore, and C. Piermarocchi. Two-qubit conditional phase gate in laser-excited semiconductor quantum dots using the quantum Zeno effect. *Phys. Rev. Lett.*, 103(3):037401, Jul 2009.
2. K. J. Xu and C. Piermarocchi. Dynamics of elastic and inelastic energy transfer between quantum dots in a microcavity. *Phys. Rev. B*, 84:115316, Sep 2011.

Chapter 2

Theoretical framework

2.1 Excitons in semiconductors

Optical properties of semiconductors are determined by interband transitions between valence and conduction bands. Excitons in a material are quasiparticles that can be considered as hydrogenic bound states of an excited electron in the conduction band and the remaining hole in the valence band. The electron and the hole interact through Coulomb interaction. Excitons may be classified into two different types, Frenkel excitons and Wannier-Mott excitons [39, 40]. This classification is determined by the properties of the material, in particular by the value of the dielectric constant and effective mass of electron and hole. Frenkel excitons are typically found in alkali halide crystals and in organic molecular crystals which have a small dielectric constant. In these materials, the Coulomb interaction between the electrons and the holes may be strong and the effective Bohr radius of Frenkel excitons tend to be small due to the strong binding. In inorganic semiconductor, the dielectric constant is generally large and excitons are typically of the Wannier-Mott type. Electric field screening,

due to the larger dielectric constant reduces the Coulomb interaction between the electrons and the holes, thus the Bohr radius of Wannier-Mott excitons is much larger compared to the one of Frenkel excitons. Typically, a Wannier-Mott exciton has a Bohr radius much larger than the interatomic spacing of the crystal. We will only study Wannier-Mott excitons in this thesis.

2.1.1 Wannier-Mott exciton theory

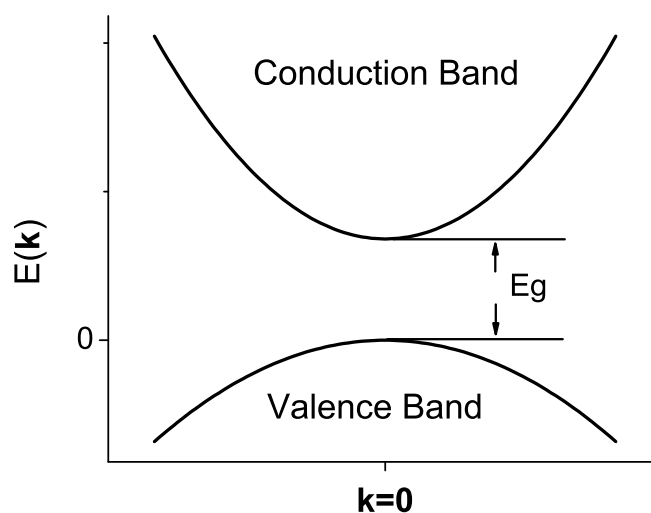


Figure 2.1: The conduction and valence band of the semiconductor with a direct bandgap E_g .

An intuitive explanation for the Wannier-Mott exciton concept can be given based on the scheme in Fig. 2.1. For simplicity, we assume a quadratic dispersion for valence and conduction band electrons, as well as a direct bandgap with energy E_g . Initially, the system is assumed to be in its ground state, which means that the valence band is filled, and all conduction band states are unoccupied. Optical transitions induced by photons may excite an electron in the valence band to an unoccupied state in the conduction band. With our assumption, and the zero energy point shown in Fig. 2.1, the single electron energies in

valence and conduction band are

$$E_v(\mathbf{k}) = \frac{\hbar^2 k^2}{2m_v^*}, \quad E_c(\mathbf{k}) = E_g + \frac{\hbar^2 k^2}{2m_c^*}. \quad (2.1)$$

Here m_v^* and m_c^* are the effective mass of the valence and conduction electrons, respectively. According to the definition of the effective mass $m^* = \hbar^2 \cdot \left[\frac{d^2 E}{dk^2} \right]^{-1}$, m_c^* is positive, meanwhile, m_v^* is negative. Before excitation, all the valence band states are completely filled, the removal of an electron from this band is accompanied by the creation of an excitation termed a hole. The hole can be treated as a particle with an effective mass $m_h^* = -m_v^*$, positive charge e and energy $E_h(\mathbf{k}) = \frac{\hbar^2 k^2}{2m_h^*}$. The absorption of a photon of energy $\hbar\omega$ in the semiconductor creates two excitations: one is the electron in the conduction band of wavevector \mathbf{k} and energy $E_c(\mathbf{k}) = E_g + \frac{\hbar^2 k^2}{2m_c^*}$ and the second one is the hole in the valence band of wavevector $-\mathbf{k}$ and energy $E_h(\mathbf{k}) = \frac{\hbar^2 k^2}{2m_h^*}$. According to conservation of energy, for this process, we have

$$\hbar\omega = E_g + \frac{\hbar^2 k^2}{2m_e^*} + \frac{\hbar^2 k^2}{2m_h^*}. \quad (2.2)$$

Here, m_c^* is replaced by m_e^* to indicate that it represents the effective mass of the electron in the conduction band.

Exciton is a quasi-particle representing the bound state of the electron and hole pair. The essential idea is that the electron and the hole are particles with opposite charges. Therefore there is a Coulomb attraction $-e^2/\epsilon r$ between them. Here, ϵ is the dielectric constant for the semiconductor, which effectively causes screening.

The state of the electron hole pair can be described by a two-particle Schrödinger equation

$$\left[-\frac{\hbar^2 \nabla_e^2}{2m_e^*} - \frac{\hbar^2 \nabla_h^2}{2m_h^*} - \frac{e^2}{\epsilon |\mathbf{r}_e - \mathbf{r}_h|} \right] \Phi(\mathbf{r}_e, \mathbf{r}_h) = E \Phi(\mathbf{r}_e, \mathbf{r}_h). \quad (2.3)$$

The problem of Eq.(2.3) can be transformed using relative $\mathbf{r} = \mathbf{r}_e - \mathbf{r}_h$ and center of mass coordinates \mathbf{R} to obtain the effective mass equation for excitons in real space representation

$$\left[-\frac{\hbar^2 \nabla_{\mathbf{R}}^2}{2M} - \frac{\hbar^2 \nabla_{\mathbf{r}}^2}{2\mu_x} - \frac{e^2}{\epsilon r} \right] \Phi(\mathbf{R}, \mathbf{r}) = E \Phi(\mathbf{R}, \mathbf{r}). \quad (2.4)$$

Here, $M = m_e^* + m_h^*$ is the total mass and $\mu_x = m_e^* m_h^* / (m_e^* + m_h^*)$ is the reduced mass of the electron-hole pair. The center of mass motion can be separated as

$$\Phi(\mathbf{R}, \mathbf{r}) = \Psi(\mathbf{R}) \psi(\mathbf{r}). \quad (2.5)$$

With this separation of variables we have two equations; one for the center of mass motion and one for the relative motion.

$$-\frac{\hbar^2 \nabla_{\mathbf{R}}^2}{2M} \Psi(\mathbf{R}) = E_{\mathbf{R}} \Psi(\mathbf{R}). \quad (2.6)$$

Obviously, the center of mass motion is a plane-wave, $\Psi(\mathbf{R}) \propto e^{i\mathbf{q}\mathbf{R}}$ with energy $E_{\mathbf{R}} = \frac{\hbar^2 q^2}{2M}$. The Coulomb interaction enters only in the equation for the electron-hole relative motion

$$\left[-\frac{\hbar^2 \nabla_{\mathbf{r}}^2}{2\mu_x} - \frac{e^2}{\epsilon r} \right] \psi(\mathbf{r}) = E_{\mathbf{r}} \psi(\mathbf{r}). \quad (2.7)$$

This equation has the same form of the Schrödinger equation for the hydrogen atom. Excitons are therefore quasiparticles in the solid which have the hydrogenic wavefunctions

of an excited electron in the conduction band and the hole in the valence band Eq.(2.7) is known as the Wannier equation.

We should mention that the effective mass equation in Eq.(2.7) can be derived from first principles, taking into account the full electron-electron interaction. By using a Green's function formalism, Eq.(2.4) can be obtained in the lowest order approximation to the effective electron-hole interaction [41]. From the well-known solution to the Hydrogen atom problem, we can find the energies of the exciton to be

$$E_n(\mathbf{q}) = E_g + \frac{\hbar^2 q^2}{2M} - \frac{\mu_x e^4}{2\epsilon^2 \hbar^2} \frac{1}{n^2}. \quad (2.8)$$

Note that exciton energies are found to be below the uncorrelated electron-hole energies. The missing energy defines the exciton binding energy. The index n here is the principal quantum number in the solution to the hydrogen atom problem. In the following discussion we will focus on the lowest internal state $\psi_n = \psi_{1s}$ only and thus drop the index n .

2.1.2 Excitons in quantum dots

Up to now, our review of excitons has only considered bulk materials. In the following, we will describe excitons in low dimensional quantum structures, which have distinct features. In order to confine excitons, it is required that both conduction electrons and holes are confined in the same region. Conventional confinement potentials such as electric or magnetic traps are not strong enough to confine the exciton. Since electrons and holes have opposite charge, an electron potential $V(\mathbf{r})$ acts on holes like a potential $-V(\mathbf{r})$. Semiconductor heterostructures confine excitons because they create a variation of the bandgap energy at the interface of different materials. With a proper choice of the configuration, electrons and holes

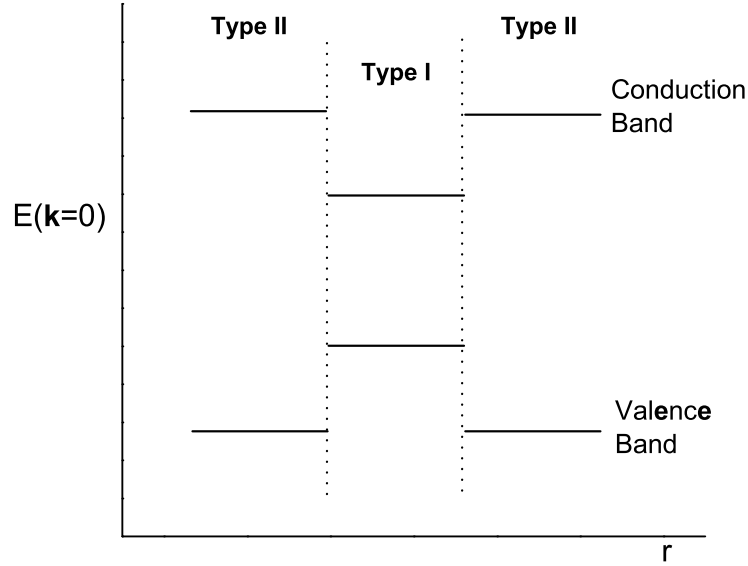


Figure 2.2: Schematic view of spatial band structure of semiconductor heterostructure.

can be confined in the same region as shown in Fig 2.2. Given the technological advances in crystal growth techniques, it is now possible to fabricate various types of semiconductor heterostructures with characteristic dimensions of the order of nanometers, which is comparable to the carrier's de Broglie wavelength in bulk material. In this regime, the electronic and optical properties of the exciton are altered due to confinement. For example, the excitation energy of the $1s$ exciton depends on the width and depth of the confinement. In contrast, for bulk material, the $1s$ exciton energy only depends on the bandgap energy. The excitation energy dependence on the confinement potential provides another parameter to control the optical properties of the excitons. Nanostructures such as quantum dots (QD) are typical systems where the potential of confined excitons can be engineered.

A semiconductor quantum dot is a simple nanostructure of typical size ranging from nanometers to a few microns. It normally contains hundreds or thousands of atoms and thus the Bloch functions do not deviate very much from the bulk case. However the envelope of

the electron and hole wavefunction is strongly modified due to the finite size of the structure. They are generally composed of atoms from groups II and VI elements (e.g. CdSe and CdTe) or groups III and V elements (e.g. InP, InAs and GaAs) of the periodic table. The reason 'quantum' prefixes the name is because the dots exhibit quantum confinement properties in all three dimensions. The only thing that behaves like this in nature is the atom, but a quantum dot is at least ten times bigger. As a result, quantum dots have properties that are between those of bulk semiconductors and those of atoms. There are different types of quantum dots such as nanocrystal quantum dots, self-assembled quantum dots and vertical quantum dots in a pillar heterostructure which are shown in Fig. 2.3.

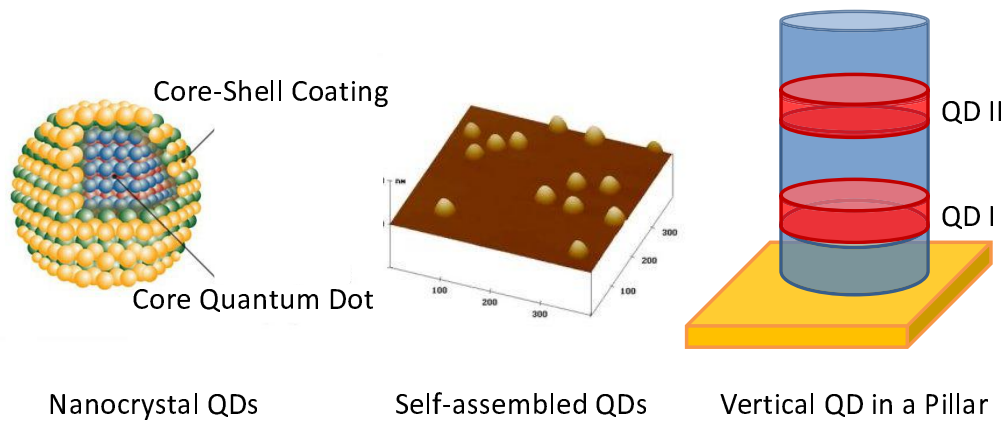


Figure 2.3: Three typical Quantum Dots

Nanocrystal quantum dots which consist of only a few hundred to a few hundred thousand atoms can be synthesized from precursor compounds dissolved in solutions, much like traditional chemical processes [42]. Interestingly, the emission wavelength (the emission color) of quantum dots depends on the dot size, and in the case of semiconductor nanocrystals, color can be controlled precisely through simple chemistry. This unique optical properties make nanocrystal quantum dots as a new type of color-selectable lasing medium. For example, CdSe nanocrystal quantum dots of different radii, under ultraviolet illumination, emit dif-

ferent colors because of the quantum size effect. A 2.4-nm-radius dot has an energy gap of about 2 eV and emits in the orange, whereas a dot of radius 0.9 nm has a gap of about 2.7 eV and emits a blue color.

Self-assembled quantum dots nucleate spontaneously under certain conditions during molecular beam epitaxy (MBE) and metalorganic vapor phase epitaxy (MOVPE), when a material is grown on a substrate to which it is not lattice matched. MBE grown quantum dots are mostly from III-V group materials, such as GaAs, InGaAs, InAs and InP, and occasionally from other groups, such as PbSe and CdSe. This fabrication method has potential for applications in quantum cryptography (i.e. single photon sources) and quantum computing. The main limitations of this method are the cost of fabrication and the lack of control over positioning and the size of individual dots.

For vertical quantum dots, current nanofabrication technology (lithography, etching) [3] allows us to precisely control the size and shape of the dots. Disk-like quantum dots which belong to the type of vertical pillar quantum dots have been shown to provide a two-dimensional analogy for real atoms, due to their strong confinement in the growth dimensions.

In this thesis, we mainly study disk-like quantum dots. The effective mass Hamiltonian in Eq.(2.4) for the electron hole system with confinement potentials reads as

$$\left[-\frac{\hbar^2 \nabla_{\mathbf{r}_e}^2}{2m_e^*} - \frac{\hbar^2 \nabla_{\mathbf{r}_h}^2}{2m_h^*} - \frac{e^2}{\epsilon |\mathbf{r}_e - \mathbf{r}_h|} + V_e(\mathbf{r}_e) + V_h(\mathbf{r}_h) \right] \Phi(\mathbf{r}_e, \mathbf{r}_h) = E\Phi(\mathbf{r}_e, \mathbf{r}_h), \quad (2.9)$$

where $V_e(\mathbf{r}_e)$ and $V_h(\mathbf{r}_h)$ are the effective confinement potential for electron and hole respectively [43].

For a disk-like quantum dot, we assume the z -direction confinement potentials to be strong enough to confine the exciton in the x - y plane. Therefore the Coulomb potential

can be simplified as an in-plane potential which only depends on the in-plane distance $\rho = \rho_e - \rho_m$. In the case of a very strong confinement in z -direction, the potentials can be separated into z and in-plane components as

$$V_e(\mathbf{r}_e) = V_e(\rho_e) + U_e(z_e), \quad V_h(\mathbf{r}_h) = V_h(\rho_h) + U_h(z_h). \quad (2.10)$$

This choice makes the Hamiltonian separable in z and ρ and the exciton wave function can be written as

$$\Phi(\mathbf{r}_e, \mathbf{r}_h) = \Psi(\rho_e, \rho_h) \psi_e(z_e) \psi_h(z_h), \quad (2.11)$$

with the notation $\mathbf{r}_{e/h} = (\rho_{e/h}, z_{e/h})$.

In case of a strong and narrow confinement in the z direction, it is plausible to assume a rectangular potential for both electron and hole [44]. So the functions ψ_e and ψ_h are just the eigenfunction for a particle in a one dimensional potential well. The remaining problem to solve is the in-plane Schrödinger equation

$$\left[-\frac{\hbar^2 \nabla_{\rho_e}^2}{2m_e^*} - \frac{\hbar^2 \nabla_{\rho_h}^2}{2m_h^*} - \frac{e^2}{\epsilon|\rho|} + V_e(\rho_e) + V_h(\rho_h) \right] \Psi(\rho_e, \rho_h) = E' \Psi(\rho_e, \rho_h). \quad (2.12)$$

$E' = E - E_{ze} - E_{zh}$ is the in plane energy. Here E_{ze} and E_{zh} are the eigenenergy for electron and hole in a one dimensional potential well. Similarly to the treatment in bulk, we introduce the center of mass and relative motion coordinates:

$$\rho = \rho_e - \rho_h, \quad \mathbf{R} = \frac{m_e^* \rho_e + m_h^* \rho_h}{M}, \quad M = m_e^* + m_h^*. \quad (2.13)$$

We may expand the potential in powers of ρ as

$$V_e(\rho_e) = V_e(\mathbf{R} + \frac{m_h^*}{M}\rho) = V_e(\mathbf{R}) + \nabla V_e(\mathbf{R})\frac{m_h^*}{M}\rho + O(\rho^2), \quad (2.14)$$

$$V_h(\rho_h) = V_h(\mathbf{R} - \frac{m_e^*}{M}\rho) = V_h(\mathbf{R}) - \nabla V_h(\mathbf{R})\frac{m_e^*}{M}\rho + O(\rho^2). \quad (2.15)$$

Since the exciton Bohr radius is much smaller than the in plane confinement radius, we only keep the zeroth order of the expansion

$$V_e(\rho_e) \approx V_e(\mathbf{R}), \quad V_h(\rho_h) \approx V_h(\mathbf{R}). \quad (2.16)$$

With this approximation, the in plane Hamiltonian can be separates in the relative and center of mass motion and we separate the in-plane wavefunction as

$$\Psi(\rho_e, \rho_h) = \chi(\mathbf{R})\Psi(\rho). \quad (2.17)$$

The solution to $\Psi(\rho)$ is the two dimensional hydrogen-like problem

$$\left(-\frac{\hbar^2}{2\mu}\nabla_\rho^2 - \frac{e^2}{\epsilon|\rho|} \right) \Psi(\rho) = E_\rho\Psi(\rho), \quad (2.18)$$

and $\chi(\mathbf{R})$ is the solution of the equation

$$\left(-\frac{\hbar^2}{2M}\nabla_{\mathbf{R}}^2 + V_e(\mathbf{R}) + V_h(\mathbf{R}) \right) \chi(\mathbf{R}) = E_{\mathbf{R}}\chi(\mathbf{R}). \quad (2.19)$$

The eigenenergies of a confined 2D exciton state are

$$E = E_g + E_{ze} + E_{zh} + E_\rho + E_{\mathbf{R}}. \quad (2.20)$$

This treatment is very similar to the exciton in bulk matter. Instead of getting a 3D hydrogen-like problem for the relative motion, we obtain a 2D hydrogen-like problem, since we only have strong confinement in the z -direction. The modification to the exciton energy due to the confinement comes from two parts. First is the quantization energy E_{ze} and E_{zh} . Second is the difference between the hydrogenic eigenenergies for the 3D and 2D problems. We notice that the excitation energy of the confined exciton can be tuned by changing the quantization energy which is directly related to the dimension of the confinement.

2.2 Exciton energy transfer in photon-confined systems

2.2.1 Photon Hamiltonian in a microcavity

In this section, we are going to provide a quantum mechanical description of electromagnetic field inside a semiconductor microcavity. A microcavity is basically a nano or micro scale cavity to confine the electromagnetic field. The simplest semiconductor microcavity structure is the Fabry-Pérot resonator. The Fabry-Pérot resonator is a planar structure made of two parallel mirrors. The mirror can be of any kind, the mirrors are described by their reflection and transmission coefficients. Ideally, an electromagnetic field can only exist between the mirrors, only when the successive passes of the wave interfere constructively. This leads to the condition for the wave vector perpendicular to the mirror

k_z , which satisfies the equation

$$k_z L = n\pi, \quad (2.21)$$

where n is integer. Equivalently, for $\mathbf{k} = (\mathbf{k}_\gamma, k_z)$,

$$L\sqrt{\frac{\omega^2}{c^2}n_r^2 - \mathbf{k}_\gamma^2} = n\pi, \quad (2.22)$$

here \mathbf{k}_γ is the component of photon wavevector parallel to the mirrors, L is the cavity spacing and n_r is the material index of refraction. In a planar microcavity, the electromagnetic field is quantized in the direction of the confinement, denoted as z -direction. The energy dispersion relation of the cavity mode photon is very different from the free photon. The energy for a free photon reads as $E = \hbar c|\mathbf{k}|$ which, in principle, can range from 0 to ∞ . In contrast, the energy for a cavity photon is $E = \hbar c\sqrt{\mathbf{k}_\gamma^2 + k_z^2} \geq \hbar c\pi/L$ according to Eq.(2.21). In other words, there exists a forbidden band for the photon in cavity. With this, we may study the excitonic energy of the quantum dots embedded in the cavity under two different conditions: resonant or off-resonant to the cavity photon mode. As pointed out by Purcell [45], the relaxation time of the excitation depends on the resonance condition. This means the dynamics of the exciton in the quantum dot can be affected by the configuration of the microcavity.

G. Barton showed how to derive the electromagnetic vector potential $\mathbf{A}(\mathbf{r})$ between the conducting plates in his 1970 paper [35]. We can apply his result to the planar microcavity, since we assume that the microcavity is ideal, which has a similar function to confine the electromagnetic field as the conducting plates. Due to the symmetry of the microcavity, it is convenient to define the photon polarization according to the cavity E-modes ($E_z = 0$)

and M-modes ($B_z = 0$). The field operators for the E and M modes can be written as

$$\begin{aligned}\mathbf{A}_{\mathbf{k}E}(\mathbf{r}) &= \sqrt{\frac{\hbar}{\epsilon_0 n_r^2 \omega_{\mathbf{k}} V}} \cos(k_z z) \hat{k}_\gamma \times \hat{z} e^{i\mathbf{k}_\gamma \mathbf{r}_\parallel} a_{\mathbf{k}E} + h.c. , \\ \mathbf{A}_{\mathbf{k}M}(\mathbf{r}) &= \sqrt{\frac{\hbar}{\epsilon_0 n_r^2 \omega_{\mathbf{k}} V}} \left(-\frac{k_\gamma}{k} \sin(k_z z) \hat{z} \right. \\ &\quad \left. - i \frac{k_z}{k} \cos(k_z z) \hat{k}_\gamma \right) \times \hat{z} e^{i\mathbf{k}_\gamma \mathbf{r}_\parallel} a_{\mathbf{k}M} + h.c. ,\end{aligned}\tag{2.23}$$

where $a_{\mathbf{k}E}$ and $a_{\mathbf{k}M}$ are annihilation operators for photons in the E and M modes. The notation for the in-plane and perpendicular components of vectors with respect to the cavity plane is defined by the relations $\mathbf{k} = (\mathbf{k}_\gamma, k_z)$ and $\mathbf{r} = (\mathbf{r}_\parallel, z)$. V is an arbitrary quantization volume, and n_r is the material index of refraction. In principle we have to consider all the possible photon wavevector \mathbf{k} . However, k_z is quantized in the cavity and we focus here on quantum dots with exciton energy near the lowest cavity branch corresponding to $k_z = \frac{\pi}{L}$. Therefore, we neglect off-resonant branches with higher values of k_z and we will label the cavity modes in the lowest branch using only the in-plane component \mathbf{k}_γ .

Operators $a_{\mathbf{k}E}$ and $a_{\mathbf{k}M}$ are normalized, so that the photon Hamiltonian can be written as

$$\mathcal{H}_{em} = \sum_{k_z} \sum_{\mathbf{k}_\gamma, \nu} \hbar \omega_{\mathbf{k}} a_{\mathbf{k}\nu}^\dagger a_{\mathbf{k}\nu}.\tag{2.24}$$

Since we will study the case that the exciton energy is lower or matches the first cavity mode ($k_z = \pi/L$), we can neglect the rest of the higher energy modes. Therefore the Hamiltonian simplifies to

$$\mathcal{H}_{em} = \sum_{\mathbf{k}_\gamma, \nu} \hbar \omega_{\mathbf{k}} a_{\mathbf{k}\nu}^\dagger a_{\mathbf{k}\nu},\tag{2.25}$$

with $\mathbf{k} = (\mathbf{k}_\gamma, \pi/L)$ and $\nu = E, M$.

2.2.2 Exciton-photon interaction in a microcavity

In this section, we derive the interaction between the exciton in the QD and the cavity photon in the microcavity.

First we describe the coupling of the exciton in the quantum dot with the radiation field. The exciton-photon interaction is expressed in terms of the electron-photon Hamiltonian in first quantization as

$$\mathcal{H} = \sum_i \frac{1}{2m_0} (\mathbf{p}_i - e\mathbf{A}(\mathbf{r}_i))^2, \quad (2.26)$$

where $\mathbf{A}(\mathbf{r}_i)$ is the electromagnetic vector potential and e and m_0 are the electron charge and mass. Moreover, \mathbf{r}_i and \mathbf{p}_i are the position and momentum of the i th electron. In the Coulomb gauge, by expanding the square in the above equation, we obtain

$$\mathcal{H} = \sum_i \frac{\mathbf{p}_i^2}{2m_0} - \frac{e}{m_0} \mathbf{A}(\mathbf{r}_i) \mathbf{p}_i + \frac{e^2}{2m_0} \mathbf{A}^2(\mathbf{r}_i). \quad (2.27)$$

The first term represents the exciton Hamiltonian \mathcal{H}_0 , the interaction Hamiltonian can be recognized as

$$\mathcal{H}_I = \sum_i -\frac{e}{m_0} \mathbf{A}(\mathbf{r}_i) \mathbf{p}_i + \frac{e^2}{2m_0} \mathbf{A}^2(\mathbf{r}_i). \quad (2.28)$$

For low-intensity radiation the term quadratic in $\mathbf{A}(\mathbf{r}_i)$ becomes negligible [46], and we are left with

$$\mathcal{H}_I = \sum_i -\frac{e}{m_0} \mathbf{A}(\mathbf{r}_i) \mathbf{p}_i. \quad (2.29)$$

With $\mathbf{A}(\mathbf{r})$ given in Eq.(2.23), we can derive, the coupling of one quantum dot located at position \mathbf{R} with the radiation field. After a lengthy calculation which has been done in [47], the Hamiltonian for a single quantum dot in the cavity can be written as $\mathcal{H} = \mathcal{H}_0 + \mathcal{H}_I$,

where

$$\begin{aligned}\mathcal{H}_0 &= \sum_{\mathbf{k}\gamma\lambda} \hbar\omega_{\mathbf{k}\gamma} a_{\mathbf{k}\gamma\lambda}^\dagger a_{\mathbf{k}\gamma\lambda} + \hbar\omega c^\dagger c \quad \text{and} \\ \mathcal{H}_I &= \sum_{\mathbf{k}\gamma\lambda} \hbar \left[g_{\mathbf{k}\gamma\lambda}^*(\mathbf{R}) c^\dagger a_{\mathbf{k}\gamma\lambda} + g_{\mathbf{k}\gamma\lambda}(\mathbf{R}) a_{\mathbf{k}\gamma\lambda}^\dagger c \right].\end{aligned}\tag{2.30}$$

The photon energy is given by $\hbar\omega_{\mathbf{k}\gamma} = \frac{\hbar c}{nr} \sqrt{\mathbf{k}_\gamma^2 + \frac{\pi^2}{L^2}}$. The exciton-photon coupling constants are given by $g_{\mathbf{k}\gamma\lambda}(\mathbf{R})$ where λ is the photon polarization, which can be E or M . The operator c^\dagger (c) denotes creation (annihilation) of one exciton with energy $\hbar\omega$ in the quantum dot. For a cavity mode \mathbf{k}_γ , the exciton-photon coupling constants can be expressed as

$$g_{\mathbf{k}\gamma E}(\mathbf{R}) = ie\omega\Phi_{1s}(0)\frac{1}{\hbar}C_{\mathbf{k}\gamma}\chi(\mathbf{k}_\gamma)I(\pi/L)u_{cv}\tag{2.31}$$

for the E mode. The interband dipolar coupling is indicated by u_{cv} . The coupling constants for the M modes are obtained if we make comparison between field operator $\mathbf{A}_{\mathbf{k}E}(\mathbf{r})$ and $\mathbf{A}_{\mathbf{k}M}(\mathbf{r})$ in Eq.(2.23)

$$g_{\mathbf{k}\gamma M}(\mathbf{R}) = -i\frac{\pi}{Lk}g_{\mathbf{k}\gamma E}(\mathbf{R}).\tag{2.32}$$

The coefficient $\Phi_{1s}(0) = \sqrt{\frac{2}{\pi a_B^2}}$ is the ground state wavefunction of the two dimensional hydrogen-like problem taken at zero electron-hole distance, with a_B being the exciton Bohr radius. Note that we are considering here quantum dots with size comparable to the exciton Bohr radius. For smaller dots, this electron-hole overlap coefficient appearing in the matrix element can be larger. The other quantities appearing in the coupling constants are defined

as

$$C_{\mathbf{k}\gamma} = \sqrt{\frac{\hbar}{\epsilon_0 n_r^2 \omega_{\mathbf{k}\gamma} V}} \quad (2.33)$$

$$I(\pi/L) = \int dz \phi_e(z) \phi_h(z) \cos(\pi z/L) \quad (2.34)$$

$$\chi(\mathbf{k}\gamma) = e^{-i\mathbf{k}\gamma \mathbf{R}} \sqrt{2\pi\beta} e^{-\frac{1}{4}\mathbf{k}\gamma^2 \beta^2}, \quad (2.35)$$

where $\phi_e(z)$ and $\phi_h(z)$ are the z component of electron and hole wave functions in the dot, and β is the in plane size of the dot. To simplify, we express $g_{\mathbf{k}\gamma E}(\mathbf{R})$ as

$$g_{\mathbf{k}\gamma E}(\mathbf{R}) = i e^{-i\mathbf{k}\gamma \mathbf{R}} g_{\mathbf{k}\gamma E}. \quad (2.36)$$

Explicitly,

$$g_{\mathbf{k}\gamma E} = \frac{e}{\hbar} \omega \sqrt{\frac{\hbar}{\epsilon_0 n_r^2 \omega_{\mathbf{k}\gamma} V}} \sqrt{2\pi\beta} e^{-\frac{1}{4}\mathbf{k}\gamma^2 \beta^2} \Phi_{1s}(0) I\left(\frac{\pi}{L}\right) u_{cv}. \quad (2.37)$$

Here, $g_{\mathbf{k}\gamma E}$ is a real number, which depends on $\mathbf{k}\gamma$ as $g_{\mathbf{k}\gamma E} = \frac{1}{\sqrt{\omega_{\mathbf{k}\gamma}}} e^{-\frac{1}{4}\mathbf{k}\gamma^2 \beta^2} g_E$. In the same way we have for the M modes

$$g_{\mathbf{k}\gamma M}(\mathbf{R}) = e^{-i\mathbf{k}\gamma \mathbf{R}} g_{\mathbf{k}\gamma M}, \quad (2.38)$$

where $g_{\mathbf{k}\gamma M} = \frac{1}{\sqrt{\omega_{\mathbf{k}\gamma}}} \frac{\pi}{Lk} e^{-\frac{1}{4}\mathbf{k}\gamma^2 \beta^2} g_M$.

2.2.3 Exciton-phonon interaction

In this section we extend our approach to take phonon effects into consideration. A phonon is a quasi-particle that represents the collective vibrational motion of the atoms or molecules in condensed matter. It is a quantum mechanical description of a special type vibrational motion, in which a lattice uniformly oscillates at the same frequency. In classical mechanics these are known as normal modes. The normal modes are important because any arbitrary lattice vibration can be considered as a superposition of these elementary vibrations. While normal modes are wave-like phenomena in classical mechanics, they have particle-like properties in the wave-particle duality of quantum mechanics. Phonons play a major role in many of the physical properties of bulk materials. As mentioned in the previous section, quantum dots contain thousands of atoms whose collective motion may cause dissipative effects and these effects can not be neglected in physical processes. Just like its classical analogy, there are two different types of phonon, longitudinal and transversal phonon which can be classified by the relation between its wavevector and vibration direction. For a transversal phonon, the vibration is perpendicular to its wavevector. For longitudinal phonon, its vibration and wavevector are parallel. Phonon can be also classified as acoustic phonon and optical phonon by their different vibration modes. Optical phonon represents the vibration mode which has strong relative motion between the atoms. Acoustic phonon has much lower energy due to its lack of relative motion. In addition, the dispersion relation of acoustic phonon and optical phonon are totally different [48].

In this thesis, we do not consider the phonon as a thermal bath at finite temperature, instead, we study the case at zero temperature. The zero temperature model can provide insight on the role that phonon plays in the exciton energy transfer process. Moreover,

since we consider quantum dots detuned with respect to each other only by a few meV, we will restrict the discussion to acoustic phonons. We neglect the coupling between different exciton levels through phonons. This approximation is known as the independent boson model [49, 50]. The total Hamiltonian for the coupled exciton-phonon system is written as

$$\mathcal{H}_0 = \sum_{\mathbf{q}} \hbar\omega_{\mathbf{q}} b_{\mathbf{q}}^{\dagger} b_{\mathbf{q}} + c^{\dagger} c [\hbar\omega + \sum_{\mathbf{q}} M_{\mathbf{q}} (b_{\mathbf{q}}^{\dagger} + b_{-\mathbf{q}})]$$

where $b_{\mathbf{q}}^{\dagger}$ ($b_{\mathbf{q}}$) are the creation (annihilation) operator of the phonon (with wave vector \mathbf{q} and energy $\hbar\omega_{\mathbf{q}}$). The last term indicates the exciton-phonon interaction, which is determined by the coupling matrix element $M_{\mathbf{q}}$.

As shown by Takagahara [51, 36], the most effective interaction between excitons and acoustic phonons originates from the deformation potential coupling to the longitudinal acoustic phonon modes. The interaction with transverse acoustic phonon modes and piezoelectric coupling is therefore neglected here. The acoustic phonon energy is taken to be $\omega_{\mathbf{q}} = c_p |\mathbf{q}|$. With these assumptions, $M_{\mathbf{q}}$ describing the exciton-phonon interaction via the deformation potential coupling is given by [52]

$$M_{\mathbf{q}} = \sqrt{\frac{\hbar|\mathbf{q}|}{2\rho c_p V}} (D_e \langle X | e^{i\mathbf{q}\mathbf{r}} e | X \rangle - D_h \langle X | e^{i\mathbf{q}\mathbf{r}} h | X \rangle)$$

where D_e and D_h are the deformation potential constants for electrons and holes. ρ is the mass density, c_p is the speed of the sound in the material, and V is the quantization volume. $|X\rangle$ is the exciton wave function. For simplicity, we assume that the exciton wave function is described by a product of electron and hole wave functions. In our disk-like dot, the electron and hole wave function is a product of Gaussian functions characterized by the

confinement in the xy plane and in the z direction. As shown in Fig. 3.3, the confinement length parameters in the xy plane and in z direction are β and L_{dot} , respectively. Since we have two dots in our system, the position of the dot introduces a phase factor to the coupling $M_{\mathbf{q}}(\mathbf{R}_j) = e^{-i\mathbf{q}\mathbf{R}_j} M_{\mathbf{q}}$ [53]. The final expression of the exciton-phonon coupling is given by

$$M_{\mathbf{q}}(\mathbf{R}_j) = \sqrt{\frac{\hbar|\mathbf{q}|}{2\rho c_p V}} e^{-i\mathbf{q}\mathbf{R}_j} (D_e - D_h) e^{-(q_x^2 + q_y^2)\beta^2/4 - q_z^2 L_{dot}^2/4}.$$

We add the new phonon-related terms into the Hamiltonian which becomes

$$\begin{aligned} \mathcal{H} &= \mathcal{H}_0 + \mathcal{H}_I \\ \mathcal{H}_0 &= \sum_{\mathbf{k}\gamma\lambda} \hbar\omega_{\mathbf{k}\gamma} a_{\mathbf{k}\gamma\lambda}^\dagger a_{\mathbf{k}\gamma\lambda} + \sum_{\mathbf{q}} \hbar\omega_{\mathbf{q}} b_{\mathbf{q}}^\dagger b_{\mathbf{q}} \\ &+ \sum_j c_j^\dagger c_j [\hbar\omega_j + \sum_{\mathbf{q}} M_{\mathbf{q}}(\mathbf{R}_j) (b_{\mathbf{q}}^\dagger + b_{-\mathbf{q}})] \\ \mathcal{H}_I &= \sum_{j\mathbf{k}\gamma\lambda} \hbar \left[g_{\mathbf{k}\gamma\lambda}^*(\mathbf{R}_j) c_j^\dagger a_{\mathbf{k}\gamma\lambda} + g_{\mathbf{k}\gamma\lambda}(\mathbf{R}_j) a_{\mathbf{k}\gamma\lambda}^\dagger c_j \right]. \end{aligned} \quad (2.39)$$

Note that we have $M_{\mathbf{q}}^*(\mathbf{R}_j) = M_{-\mathbf{q}}(\mathbf{R}_j)$. It was shown by Mahan [49] that \mathcal{H}_0 can be diagonalized by a canonical transformation $\bar{A} = e^s A e^{-s}$, where $s = \sum_j c_j^\dagger c_j \sum_{\mathbf{q}} \frac{M_{\mathbf{q}}(\mathbf{R}_j)}{\omega_{\mathbf{q}}} (b_{\mathbf{q}}^\dagger - b_{-\mathbf{q}})$, which transforms the full Hamiltonian into

$$\begin{aligned}
\mathcal{H}_0 &= \sum_{\mathbf{k}\gamma\lambda} \hbar\omega_{\mathbf{k}\gamma} a_{\mathbf{k}\gamma\lambda}^\dagger a_{\mathbf{k}\gamma\lambda} + \sum_{\mathbf{q}} \hbar\omega_{\mathbf{q}} b_{\mathbf{q}}^\dagger b_{\mathbf{q}} \\
&\quad + \sum_j c_j^\dagger c_j (\hbar\omega_j - \sum_{\mathbf{q}} \frac{M_{\mathbf{q}}^2}{\omega_{\mathbf{q}}}) \\
\mathcal{H}_I &= \sum_{j\mathbf{k}\gamma\lambda} \hbar g_{\mathbf{k}\gamma\lambda}^*(\mathbf{R}_j) c_j^\dagger X_j^\dagger a_{\mathbf{k}\gamma\lambda} \\
&\quad + \hbar g_{\mathbf{k}\gamma\lambda}(\mathbf{R}_j) a_{\mathbf{k}\gamma\lambda}^\dagger c_j X_j,
\end{aligned} \tag{2.40}$$

where $X_j = \exp[-\sum_{\mathbf{q}} \frac{M_{\mathbf{q}}(\mathbf{R}_j)}{\omega_{\mathbf{q}}} (b_{\mathbf{q}}^\dagger - b_{-\mathbf{q}})]$.

Chapter 3

Exciton dynamics in quantum dots

In the previous chapter, we have developed a theoretical description of exciton-photon interaction in a planar microcavity and exciton-phonon interaction. In this chapter, we study the dynamics of the exciton energy transfer between two quantum dots in three different cases: (i) a single dot coupled only to cavity modes, (ii) two dots coupled to cavity modes, and (iii) two dots coupled to cavity modes and to acoustic phonons. In the latter case, we focus on the process of phonon-assisted inelastic exciton energy transfer between the quantum dots. We take into account phonon effects by introducing a light-matter Hamiltonian with three operators describing the exciton-photon-phonon coupling in a non-perturbative way with a truncation of phonon number in the Hilbert space. Using this non-perturbative approach, we simulate the exciton dynamics with realistic parameters in the zero temperature limit. From the dynamics, we extract the dependence of the characteristic energy transfer rate as a function of the interdot separation. This theoretical approach can be used to optimize exciton energy transfer by designing structures with engineered photon and phonon density of states.

3.1 Exciton dynamics for a single dot in planar cavity

We use the Hamiltonian derived in Chapter 2 to study the system dynamics with numerical simulations. In the numerical calculations, we have taken parameters from AlGaAs/GaAs systems [54, 55, 47, 56, 57]. (See Tab. 3.1 for the parameters) to estimate the coupling constant according to Eq.(2.37).

Table 3.1: Materials parameters used in the numerical simulations

L (nm)	100	a_B (nm)	10
β (nm)	10	u_{cv}^2 (nm ²)	0.0228
ω (meV)	1680	n_r	3.5

Before dealing with the exciton energy transfer between two dots, we study the dynamics of an exciton in a single dot (dot a) confined in a planar cavity. We introduce the interaction picture with respect to \mathcal{H}_0 defined in Eq.(2.30) and we transform the light-matter Hamiltonian as

$$\begin{aligned}
 \tilde{\mathcal{H}}_I &= e^{i\mathcal{H}_0 t/\hbar} \mathcal{H}_I e^{-i\mathcal{H}_0 t/\hbar} \\
 &= \sum_{\mathbf{k}\gamma\lambda} \hbar [g_{\mathbf{k}\gamma\lambda}^*(\mathbf{R}) c^\dagger a_{\mathbf{k}\gamma\lambda} e^{i(\omega - \omega_{\mathbf{k}\gamma})t} \\
 &\quad + g_{\mathbf{k}\gamma\lambda}(\mathbf{R}) a_{\mathbf{k}\gamma\lambda}^\dagger c e^{-i(\omega - \omega_{\mathbf{k}\gamma})t}].
 \end{aligned} \tag{3.1}$$

Then, we write the wave function for the system of a single exciton coupled to photon modes in the cavity as

$$|\psi(t)\rangle = C_a(t) |a, 0, 0\rangle + \sum_{\mathbf{k}\gamma\lambda} C_{\mathbf{k}\gamma\lambda}(t) |0, (\mathbf{k}\gamma\lambda), 0\rangle, \tag{3.2}$$

where $|a, 0, 0\rangle$ indicates a state in which the exciton is in the quantum dot and there is no photon in the cavity, while $|0, (\mathbf{k}_\gamma \lambda), 0\rangle$ indicates a cavity photon with wavevector \mathbf{k}_γ and polarization λ and no exciton. The last quantum number in the kets refers to the phonon number, which will be discussed later and is set to zero for the moment. Note that we are considering the case here in which we start with a quantum dot excited with a single exciton. We therefore have the total number of exciton/photon excitations in the system fixed to one. We don't need to deal with biexciton since we only have single excitation. From the equation of motion

$$|\psi(t)\rangle = \frac{-i}{\hbar} \tilde{\mathcal{H}}_I(t) |\psi(t)\rangle, \quad (3.3)$$

we derive equations for the coefficients $C_a(t)$ and $C_{\mathbf{k}_\gamma \lambda}$ defined in Eq.(3.2).

$$\begin{aligned} \dot{C}_a(t) &= -i \sum_{\mathbf{k}_\gamma \lambda} g_{\mathbf{k}_\gamma \lambda}^*(\mathbf{R}) C_{\mathbf{k}_\gamma \lambda}(t) e^{i(\omega - \omega_{\mathbf{k}_\gamma})t} \\ \dot{C}_{\mathbf{k}_\gamma \lambda}(t) &= -i g_{\mathbf{k}_\gamma \lambda}(\mathbf{R}) C_a(t) e^{-i(\omega - \omega_{\mathbf{k}_\gamma})t}. \end{aligned} \quad (3.4)$$

By inserting the equation for $\dot{C}_{\mathbf{k}_\gamma \lambda}(t)$ into the time derivative of the equation for $\dot{C}_a(t)$, explicitly the equation for $\ddot{C}_a(t)$. The dependence on the photon degrees of freedom can be eliminated by defining the function

$$\begin{aligned} F(\tau, \omega, \mathbf{R}) &= \sum_{\mathbf{k}_\gamma \lambda} g_{\mathbf{k}_\gamma \lambda}^2 e^{i\mathbf{k}_\gamma \mathbf{R}} e^{i(\omega - \omega_{\mathbf{k}_\gamma})\tau} \\ &= F_E(\tau, \omega, \mathbf{R}) + F_M(\tau, \omega, \mathbf{R}). \end{aligned} \quad (3.5)$$

Note that in the case of a single dot we can set $\mathbf{R} = 0$, while the function for $\mathbf{R} \neq 0$ describes memory effects due to photon propagation and is important in the case of the energy transfer

between two dots. For the E mode we have

$$F_E(\tau, \omega, \mathbf{R}) = \sum_{\mathbf{k}_\gamma} \frac{\alpha}{V \omega_{\mathbf{k}_\gamma}} e^{i\mathbf{k}_\gamma \mathbf{R}} e^{-\frac{1}{2} \mathbf{k}_\gamma^2 \beta^2} e^{i(\omega - \omega_{\mathbf{k}_\gamma})\tau}, \quad (3.6)$$

where $\alpha = \frac{e^2}{\hbar^2} \omega^2 \frac{\hbar}{\epsilon_0 n_r^2} 2\pi \beta^2 \Phi_{1s}^2(0) I^2(\frac{\pi}{L}) u_{cv}^2$ which is a constant independent of \mathbf{k}_γ . We can replace the summation over \mathbf{k}_γ by an integral

$$F_E(\tau, \omega, \mathbf{R}) = \frac{A\alpha}{4\pi^2 V} \int_0^\infty d^2 \mathbf{k}_\gamma \frac{1}{\omega_{\mathbf{k}_\gamma}} e^{i\mathbf{k}_\gamma \mathbf{R}} e^{-\frac{1}{2} \mathbf{k}_\gamma^2 \beta^2} e^{i(\omega - \omega_{\mathbf{k}_\gamma})\tau}.$$

After replacing $\mathbf{k}_\gamma \mathbf{R} = k_\gamma R \cos \theta$, and changing variable according to $d\omega_{k_\gamma} = \frac{dk_\gamma \cdot k_\gamma c}{\sqrt{(\frac{\pi}{L})^2 + k_\gamma^2}}$, we obtain

$$F_E(\tau, \omega, \mathbf{R}) = \frac{\alpha}{2\pi c^2 L} e^{\frac{\beta^2 \pi^2}{2L^2}} e^{i\omega\tau} \times \int_{c\frac{\pi}{L}}^\infty d\omega_{k_\gamma} e^{-i\omega_{k_\gamma} \tau} e^{-\frac{\beta^2}{2c^2} \omega_{k_\gamma}^2} J_0 \left(R \sqrt{\frac{\omega_{k_\gamma}^2}{c^2} - \frac{\pi^2}{L^2}} \right). \quad (3.7)$$

In the same way, keeping in mind that $g_{\mathbf{k}_\gamma M}(\mathbf{R}) = -i \frac{ck_z}{\omega_{\mathbf{k}_\gamma}} g_{\mathbf{k}_\gamma E}(\mathbf{R})$, we find

$$F_M(\tau, \omega, \mathbf{R}) = \frac{\alpha}{2\pi c^2 L} e^{\frac{\beta^2 \pi^2}{2L^2}} e^{i\omega\tau} \times \int_{c\frac{\pi}{L}}^\infty d\omega_{k_\gamma} \frac{c^2 \frac{\pi^2}{L^2}}{\omega_{k_\gamma}^2} e^{-i\omega_{k_\gamma} \tau} e^{-\frac{\beta^2}{2c^2} \omega_{k_\gamma}^2} J_0 \left(R \sqrt{\frac{\omega_{k_\gamma}^2}{c^2} - \frac{\pi^2}{L^2}} \right). \quad (3.8)$$

Using the function $F(\tau, \omega, \mathbf{R})$, the equation of motion leads to an integro-differential equa-

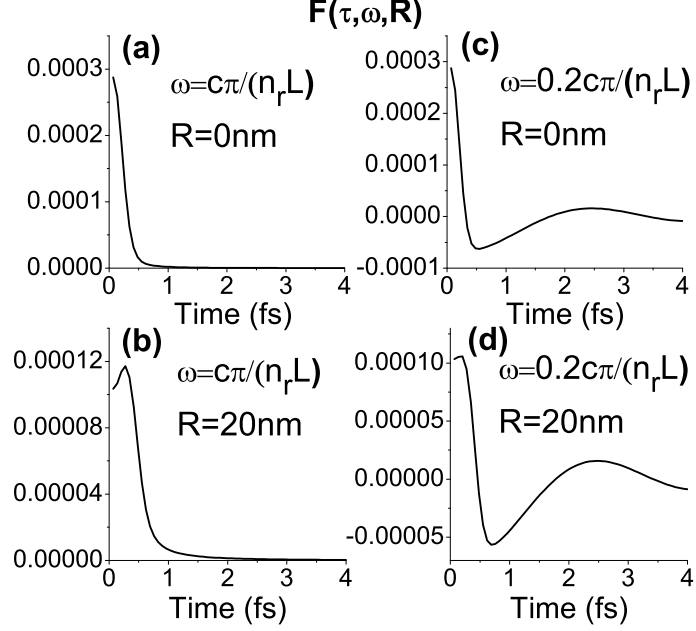


Figure 3.1: Real part of $F(\tau, \omega, \mathbf{R})$ in the case of quantum dots resonant (*a* and *b*) and off-resonant (*c* and *d*) with respect to the lowest cavity mode. Panels *a* and *c*: on-site memory effects (single dot case). Panels *b* and *d*: memory effects in the light propagation at finite distance.

tion for the amplitude $C_a(t)$

$$\dot{C}_a(t) = - \int_0^t dt' F(t-t', \omega, 0) C_a(t'). \quad (3.9)$$

This function $F(\tau, \omega, \mathbf{R})$ includes non-Markovian effects in the light-matter interaction process. The real part of this function is shown in Fig.3.1(a) for $\mathbf{R}=0$. The system only has a short memory effects of about 0.5 fs. In Fig.3.1(b) we plot the function with $\mathbf{R}=20$ nm. In this case, the function is peaked at about 0.25 fs, corresponding to the time needed by the light to travel 20 nm. In Fig.3.1(c) and (d) the exciton energy $\hbar\omega$ in the quantum dots is below the lowest branch of the cavity, $F(\tau, \omega, \mathbf{R})$ shows an oscillation around the zero point, and the system has longer memory effects in this case.

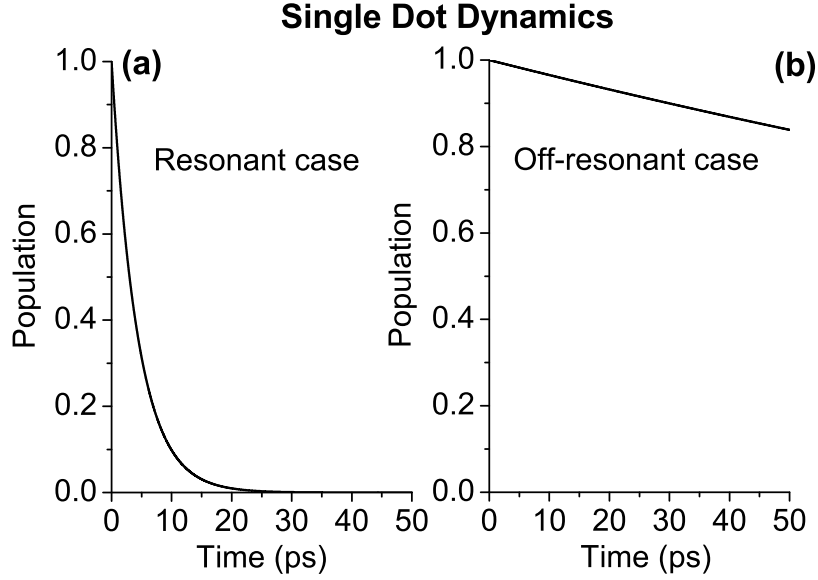


Figure 3.2: Single dot dynamics with two different energy for the dot: (a) Quantum dot exciton energy resonant with the lowest cavity mode. (b) Quantum dot exciton energy far detuned at half the energy of the lowest cavity mode. The decay in both cases is the result of the coupling of the dot to the continuum of cavity modes.

In principle, to calculate $\dot{C}_a(t)$ we need to integrate from 0 to t . However due to the very short memory effects in $F(t - t', \omega, 0)$ the integral converges quickly after a few time steps in t' . We have integrated numerically this integro-differential equation in two different cases. In Fig.3.2(a), the exciton energy of the quantum dot is resonant with the lowest cavity mode, while in Fig.3.2(b), the exciton energy in the quantum dot is far detuned with respect to the lowest cavity mode. Note that in our approach we do not add a phenomenological decay parameter. The decay observed in Fig.3.2 is the result of the coupling of the discrete quantum dot level with the continuum of modes of the cavity. Note also that the decay time in (b) is much longer than in (a), in agreement with the Purcell effect [45, 58, 59].

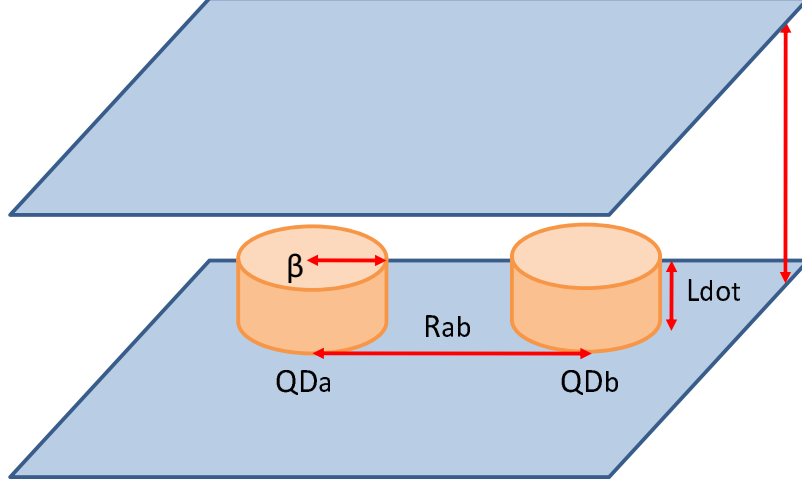


Figure 3.3: Schematic view of the two dots in a planar cavity. L is the separation between the two planar mirrors in the cavity. We assume the dots to be disk-like. L_{dot} is the size of the dot in the growth direction (z), and β is the in-plane radius of the dot. R_{ab} is the separation between the two dots.

3.2 Two dots in a planar cavity

In this section, we extend the approach to the case of two quantum dots in the planar cavity, and focus on the dynamics of the exciton energy transfer. The total Hamiltonian reads

$$\begin{aligned}
\mathcal{H} &= \mathcal{H}_0 + \mathcal{H}_I \\
\mathcal{H}_0 &= \sum_{\mathbf{k}\gamma\lambda} \hbar\omega_{\mathbf{k}\gamma} a_{\mathbf{k}\gamma\lambda}^\dagger a_{\mathbf{k}\gamma\lambda} + \sum_j \hbar\omega_j c_j^\dagger c_j \\
\mathcal{H}_I &= \sum_j \sum_{\mathbf{k}\gamma\lambda} \hbar \left[g_{\mathbf{k}\gamma\lambda}^*(\mathbf{R}_j) c_j^\dagger a_{\mathbf{k}\gamma\lambda} + g_{\mathbf{k}\gamma\lambda}(\mathbf{R}_j) a_{\mathbf{k}\gamma\lambda}^\dagger c_j \right],
\end{aligned} \tag{3.10}$$

where we have added a new index j to denote the quantum dot a or b . In principle, the coupling constant $g_{\mathbf{k}\gamma\lambda}(\mathbf{R}_j)$ are different for different dots due to the dependence on the dot size, energy, and oscillator strength. However, we assume that the two dots are nearly identical and we neglect these corrections. As in the previous section, we use the interaction

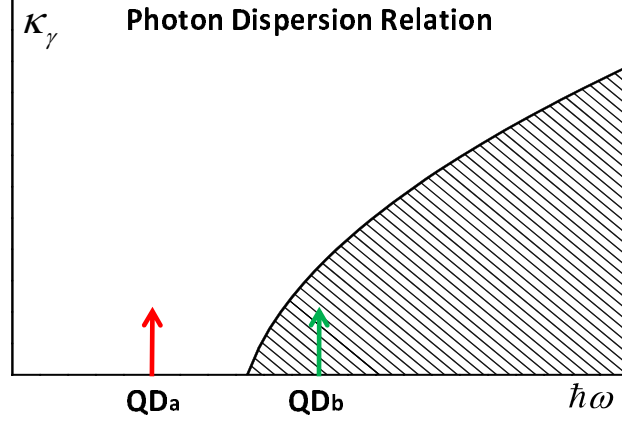


Figure 3.4: Photon dispersion relation in a planar cavity, the photon energy ($\hbar\omega$) is on the horizontal axis and the in-plane photon momentum \mathbf{k}_γ is on the vertical axis. Note that photon frequency has a minimum, which is determined by the photon wavevector quantization in the z direction. Arrows indicate the exciton energy of QD_a (red) and QD_b (green).

representation and we choose our wave function as

$$\begin{aligned}
|\psi(t)\rangle &= C_a(t) |a, 0, 0\rangle + C_b(t) |b, 0, 0\rangle \\
&+ \sum_{\mathbf{k}_\gamma \lambda} C_{\mathbf{k}_\gamma \lambda}(t) |0, (\mathbf{k}_\gamma \lambda), 0\rangle .
\end{aligned} \tag{3.11}$$

In this case we obtain two coupled integro-differential equations for the coefficient $C_a(t)$ and $C_b(t)$

$$\begin{aligned}
\dot{C}_a(t) &= - \int_0^t dt' F(t-t', \omega_a, 0) C_a(t') \\
&\quad - \int_0^t dt' F(t-t', \omega_b, \mathbf{R}_{ab}) C_b(t') e^{i(\omega_a - \omega_b)t} \\
\dot{C}_b(t) &= - \int_0^t dt' F(t-t', \omega_a, -\mathbf{R}_{ab}) C_a(t') e^{i(\omega_b - \omega_a)t} \\
&\quad - \int_0^t dt' F(t-t', \omega_b, 0) C_b(t') ,
\end{aligned} \tag{3.12}$$

$$\tag{3.13}$$

Without additional degrees of freedom, such as phonons, the exciton energy transfer

between QD_a and QD_b only occurs when the two dots are resonant, and we restrict our discussion to such case in this section. However, we can have a qualitatively different dynamics depending on the overlap of the energy of the two quantum dots at resonance and the cavity photon density of states. The detuning Δ discussed in this section is a dimensionless quantity which indicates the energy difference between the exciton energy and the energy of the lowest cavity photon mode. The system dynamics is shown in Fig.3.5. From Fig.3.5 (a) and (b), we can see that the exciton energy transfer is more effective when Δ is larger. This can be interpreted in the following way: when the energy of the two dots overlap significantly with the cavity density of states, the exciton population is more likely to leak to the continuum of cavity modes, leading to strong decay effects. When the two dots have a large Δ , the exciton population transfer between the two dots occurs through a slow adiabatic process. Fig.3.5 (c) shows the relation between transfer time, which is the time taken by the exciton population in QD_b to reach its first maximum, and the detuning Δ . The detuning is expressed in units of the lowest cavity mode $\omega_{\mathbf{k}\gamma=0}$, which is explicitly $c\pi/(n_r L)$. In this simulation the distance between the dots is fixed to 20 nm. Fig.3.5 (d), shows the R dependence of the transfer time. In this simulation we set $\omega_a = \omega_b = \omega_{\mathbf{k}\gamma=0}$. The transfer time is proportional to R , which means that the transfer rate Γ is proportional to R^{-1} , and the interdot coupling proportional to $1/\sqrt{R}$. As mentioned in the introduction, the R dependence on Γ for energy transfer in the free space is either R^{-6} for Föster transfer or R^{-2} for radiative transfer. The R^{-1} dependence is the effect of the two dimensional character of the density of the states. As pointed out in Ref. [14], in a 2D cavity the exciton energy transfer can be seen as an ultra-long range effect when compared to the exciton energy transfer in free space in similar conditions.

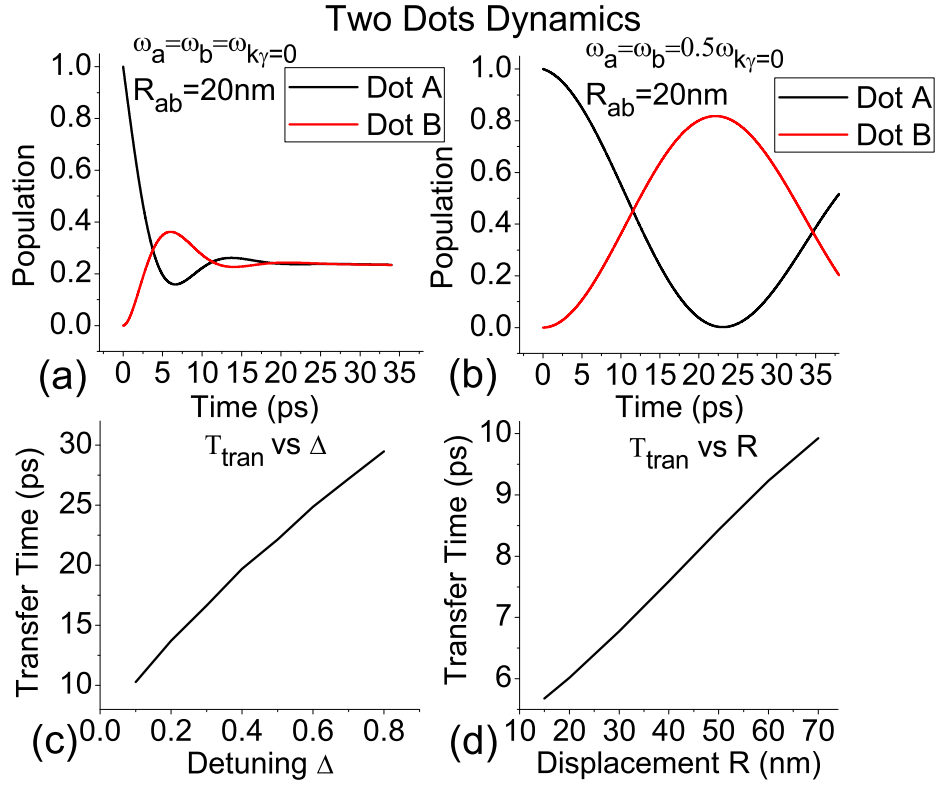


Figure 3.5: Exciton dynamics in two dots system. (a), (b) show the dynamics of the exciton population in QD_a and QD_b . (c), (d) energy transfer time T_{tran} for different detuning Δ and inter-dot separation R_{ab} . Here ω_a and ω_b are the excitation energy for QD_a and QD_b , respectively. $\omega_{\mathbf{k}\gamma=0}$ is the frequency of the lowest cavity mode.

3.3 Super-radiance and Sub-radiance

In the discussion of spontaneous emission so far, only one dot was considered. For multiple dots system, it is plausible to assume that different dots become coupled virtually by their interaction with the radiation field. Under these circumstances, the excitations in quantum dots behave in a collective, rather than an independent fashion, with the result that the spontaneous emission from N excited quantum dots is proportional to N^2 rather than N [60]. This effect is named super-radiance. As shown by Weissbluth [61], the spontaneous emission rate in atoms depends on the initial state of atoms. In this section, we will show how this comes for the double dot system. As discussed in the previous section, the Hamiltonian for our two dot system is given in Eq.(3.10). Without losing generality, we may simplify the Hamiltonian assuming the the two quantum dots have the same exciton energy ω_0 and the quantum dots interact with a single mode ω_0 of radiation field:

$$\begin{aligned}
 \mathcal{H} &= \mathcal{H}_0 + \mathcal{H}_I \\
 \mathcal{H}_0 &= \hbar\omega a^\dagger a + \sum_j \hbar\omega_0 c_j^\dagger c_j \\
 \mathcal{H}_I &= \sum_j \hbar|g| \left(c_j^\dagger a + a^\dagger c_j \right).
 \end{aligned} \tag{3.14}$$

Since the above Hamiltonian conserves the total number of excitation, if we choose single excitation as the initial condition, the wavefunction of the system can be written as $|\psi(t)\rangle = C_a(t) |a, 0\rangle + C_b(t) |b, 0\rangle + C_{\mathbf{k}}(t) |0, 1\rangle$. The computation of nonvanishing matrix elements of \mathcal{H}_I is straightforward,

$$\langle a, 0 | \mathcal{H}_I | 0, 1 \rangle = \langle 0, 1 | \mathcal{H}_I | a, 0 \rangle = \langle b, 0 | \mathcal{H}_I | 0, 1 \rangle = \langle 0, 1 | \mathcal{H}_I | b, 0 \rangle = \hbar |g|. \quad (3.15)$$

Now consider two initial states,

$$\begin{aligned} |\psi_1\rangle &= \frac{1}{\sqrt{2}} (|a, 0\rangle - |b, 0\rangle), \\ |\psi_2\rangle &= \frac{1}{\sqrt{2}} (|a, 0\rangle + |b, 0\rangle). \end{aligned} \quad (3.16)$$

With the results from Eq.(3.15), we simply get,

$$\begin{aligned} \langle 0, 1 | \mathcal{H}_I | \psi_1 \rangle &= 0, \\ \langle 0, 1 | \mathcal{H}_I | \psi_2 \rangle &= \sqrt{2} \hbar |g|. \end{aligned} \quad (3.17)$$

From perturbation theory, the spontaneous emission rate is proportional to $|\langle \psi_f | \mathcal{H}_I | \psi_i \rangle|^2$. For the initial state $|\psi_1\rangle$, the matrix element of \mathcal{H}_I for the transition $|\psi_1\rangle \rightarrow |0, 1\rangle$ is zero. This is known as subradiance. In Contrast, for initial state $|\psi_2\rangle$, the matrix element of \mathcal{H}_I for the transition $|\psi_2\rangle \rightarrow |0, 1\rangle$ is $\sqrt{2} \hbar |g|$. So the spontaneous emission rate is proportional to $2 \hbar |g|^2$ which is twice as for the single dot case. This phenomenon is called superradiance.

Up to this point, we studied a simple model which shows the basic properties of superradiance and subradiance. With the numerical approach developed in the previous section, we are able to simulate the collective behavior of the excitonic dynamics in two quantum dots with the interacting Hamiltonian given in Eq.(3.10) without simplification.

In Fig. 3.6, all three simulations are done with the same time scale and exciton energy below the lowest cavity mode which is referred to as the off-resonant regime. The difference of

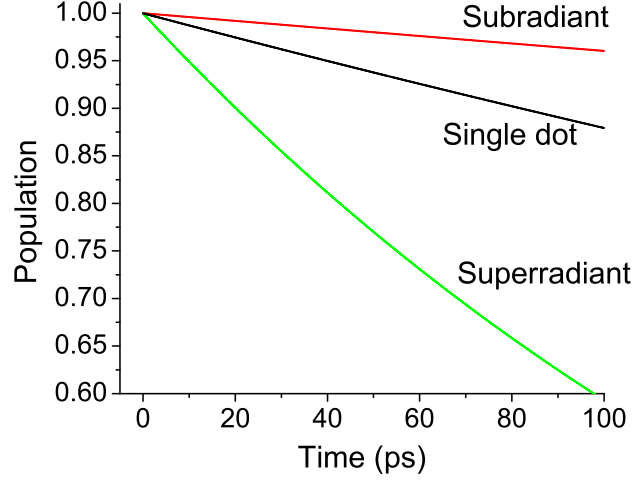


Figure 3.6: Comparison between superradiance, subradiance and single dot spontaneous emission. For superradiance, the initial condition is $|\psi_i(t)\rangle = |a, 0\rangle + |b, 0\rangle$. For subradiance, the initial condition is $|\psi_i(t)\rangle = |a, 0\rangle - |b, 0\rangle$.

the initial conditions between superradiance and subradiance are the relative phase between the exciton in the quantum dots. As shown in the figure, for superradiance, the excitons in the double quantum dots system have a much shorter life time. For subradiance, these two excitons are nearly frozen in the quantum dots without recombination. It is interesting that due to the interaction between the two dots, the spontaneous emission is drastically affected by the relative phase between the two excitons. This is an example that shows how important the relative phase is in a quantum system. Moreover, this study of super-radiance shows the robustness of our full quantum mechanical model.

3.4 Phonon-assisted energy transfer

In this section, we simulate the system dynamics when exciton-phonon interaction is included in the Hamiltonian. As shown in Chapter 2, the full Hamiltonian reads,

$$\begin{aligned}
\mathcal{H}_0 &= \sum_{\mathbf{k}\gamma\lambda} \hbar\omega_{\mathbf{k}\gamma} a_{\mathbf{k}\gamma\lambda}^\dagger a_{\mathbf{k}\gamma\lambda} + \sum_{\mathbf{q}} \hbar\omega_{\mathbf{q}} b_{\mathbf{q}}^\dagger b_{\mathbf{q}} \\
&\quad + \sum_j c_j^\dagger c_j (\hbar\omega_j - \sum_{\mathbf{q}} \frac{M_{\mathbf{q}}^2}{\omega_{\mathbf{q}}}) \\
\mathcal{H}_I &= \sum_{j\mathbf{k}\gamma\lambda} \hbar g_{\mathbf{k}\gamma\lambda}^*(\mathbf{R}_j) c_j^\dagger X_j^\dagger a_{\mathbf{k}\gamma\lambda} \\
&\quad + \hbar g_{\mathbf{k}\gamma\lambda}(\mathbf{R}_j) a_{\mathbf{k}\gamma\lambda}^\dagger c_j X_j,
\end{aligned} \tag{3.18}$$

where $X_j = \exp[-\sum_{\mathbf{q}} \frac{M_{\mathbf{q}}(\mathbf{R}_j)}{\omega_{\mathbf{q}}} (b_{\mathbf{q}}^\dagger - b_{-\mathbf{q}})]$.

In a similar way to what have been done in the previous sections, we choose our wave function as

$$\begin{aligned}
|\psi(t)\rangle &= C_a(t) |a, 0, 0\rangle + \sum_{\mathbf{q}} C_{a,\mathbf{q}}(t) |a, 0, \mathbf{q}\rangle \\
&\quad + C_b(t) |b, 0, 0\rangle + \sum_{\mathbf{q}} C_{b,\mathbf{q}}(t) |b, 0, \mathbf{q}\rangle \\
&\quad + \sum_{\mathbf{k}\gamma\lambda} C_{\mathbf{k}\gamma\lambda}(t) |0, (\mathbf{k}\gamma\lambda), 0\rangle \\
&\quad + \sum_{\mathbf{k}\gamma\lambda\mathbf{q}} C_{\mathbf{k}\gamma\lambda\mathbf{q}}(t) |0, (\mathbf{k}\gamma\lambda), \mathbf{q}\rangle .
\end{aligned} \tag{3.19}$$

As discussed above, the last quantum number in the kets refers the phonon degrees of freedom. This choice of wavefunction truncates the Hilbert space to one phonon at most.

To calculate the matrix element of the Hamiltonian (\mathcal{H}_I) in our truncated Hilbert space, we

first rewrite the operator X_j as

$$\begin{aligned} X_j &= e^{-\sum_{\mathbf{q}} \frac{M_{\mathbf{q}}(\mathbf{R}_j)}{\omega_{\mathbf{q}}} (b_{\mathbf{q}}^\dagger - b_{-\mathbf{q}})} \\ &= e^{-\sum_{\mathbf{q}} \frac{M_{\mathbf{q}}(\mathbf{R}_j)}{\omega_{\mathbf{q}}} b_{\mathbf{q}}^\dagger} e^{\sum_{\mathbf{q}} \frac{M_{-\mathbf{q}}(\mathbf{R}_j)}{\omega_{\mathbf{q}}} b_{\mathbf{q}}} e^{-1/2 \sum_{\mathbf{q}} \frac{M_{\mathbf{q}}^2}{\omega_{\mathbf{q}}^2}}. \end{aligned}$$

X_j is an operator that contains phonon operators only. In the discussion of X_j , we neglect exciton and phonon degrees of freedom. $|0\rangle$ and $|\mathbf{q}\rangle$ are operators in the phonon space. The nonzero matrix elements of the operator X_j can be expressed as

$$\begin{aligned} \langle 0|X_j|0\rangle &= e^{-1/2 \sum_{\mathbf{q}} \frac{M_{\mathbf{q}}^2}{\omega_{\mathbf{q}}^2}} \langle 0|0\rangle \\ \langle \mathbf{q}|X_j|\mathbf{q}\rangle &= e^{-1/2 \sum_{\mathbf{q}} \frac{M_{\mathbf{q}}^2}{\omega_{\mathbf{q}}^2}} \langle \mathbf{q}|(1 - \frac{M_{\mathbf{q}}^2}{\omega_{\mathbf{q}}^2} b_{\mathbf{q}}^\dagger b_{\mathbf{q}})|\mathbf{q}\rangle \\ \langle 0|X_j|\mathbf{q}\rangle &= e^{-1/2 \sum_{\mathbf{q}} \frac{M_{\mathbf{q}}^2}{\omega_{\mathbf{q}}^2}} \langle 0|\frac{M_{-\mathbf{q}}(\mathbf{R}_j)}{\omega_{\mathbf{q}}} b_{\mathbf{q}}|\mathbf{q}\rangle \\ \langle \mathbf{q}|X_j|0\rangle &= e^{-1/2 \sum_{\mathbf{q}} \frac{M_{\mathbf{q}}^2}{\omega_{\mathbf{q}}^2}} \langle \mathbf{q}|-\frac{M_{\mathbf{q}}(\mathbf{R}_j)}{\omega_{\mathbf{q}}} b_{\mathbf{q}}^\dagger|0\rangle. \end{aligned}$$

Therefore, our truncation of the Hilbert space is equivalent to expand X_j to the second order

in the $\frac{M_{\mathbf{q}}}{\omega_{\mathbf{q}}}$ dimensionless coupling as $X_j = e^{-1/2 \sum_{\mathbf{q}} \frac{M_{\mathbf{q}}^2}{\omega_{\mathbf{q}}^2}} [1 + \sum_{\mathbf{q}} -\frac{M_{\mathbf{q}}(\mathbf{R}_j)}{\omega_{\mathbf{q}}} (b_{\mathbf{q}}^\dagger - b_{-\mathbf{q}}) - \frac{M_{\mathbf{q}}^2}{\omega_{\mathbf{q}}^2} b_{\mathbf{q}}^\dagger b_{\mathbf{q}}]$. Keeping in mind the ansatz for the wavefunction, the interaction hamiltonian

can then be written as

$$\begin{aligned}\mathcal{H}_I &= \sum_{j\mathbf{k}\gamma\lambda} \hbar g'_{\mathbf{k}\gamma\lambda}{}^*(\mathbf{R}_j) c_j^\dagger a_{\mathbf{k}\gamma\lambda} \left[1 - \sum_{\mathbf{q}} \frac{M_{\mathbf{q}}^2}{\omega_{\mathbf{q}}^2} b_{\mathbf{q}}^\dagger b_{\mathbf{q}} \right] + h.c. \\ &+ \sum_{j\mathbf{k}\gamma\lambda\mathbf{q}} \hbar g'_{\mathbf{k}\gamma\lambda}{}^*(\mathbf{R}_j) c_j^\dagger a_{\mathbf{k}\gamma\lambda} \frac{M_{\mathbf{q}}(\mathbf{R}_j)}{\omega_{\mathbf{q}}} (b_{\mathbf{q}}^\dagger - b_{-\mathbf{q}}) + h.c. ,\end{aligned}$$

where $g'_{\mathbf{k}\gamma\lambda}(\mathbf{R}_j)$ is defined as $e^{-1/2 \sum_{\mathbf{q}} \frac{M_{\mathbf{q}}^2}{\omega_{\mathbf{q}}^2}} g_{\mathbf{k}\gamma\lambda}(\mathbf{R}_j)$. The first term in \mathcal{H}_I describes a renormalization of the exciton-photon interaction due to the presence of phonons. The factor $\left[1 - \sum_{\mathbf{q}} \frac{M_{\mathbf{q}}^2}{\omega_{\mathbf{q}}^2} b_{\mathbf{q}}^\dagger b_{\mathbf{q}} \right]$ can be seen as a saturation coefficient that depends on the phonon number. The second term in \mathcal{H}_I derives from the first order expansion of X , which gives an effective exciton-photon-phonon coupling term involving three operators. Keeping in mind that $M_{\mathbf{q}}(\mathbf{R}_j) = e^{-i\mathbf{q}\mathbf{R}_j} M_{\mathbf{q}}$, the effective coupling constant for this interaction can be simplified as $g'_{\mathbf{k}\gamma\lambda}{}^*(\mathbf{R}_j) G_{\mathbf{q}} e^{-i\mathbf{q}\mathbf{R}_j}$. Using $\frac{M_{\mathbf{q}}}{\omega_{\mathbf{q}}} = G_{\mathbf{q}}$ we rewrite the interaction Hamiltonian as

$$\begin{aligned}\mathcal{H}_I &= \sum_{j\mathbf{k}\gamma\lambda} \hbar g'_{\mathbf{k}\gamma\lambda}{}^*(\mathbf{R}_j) c_j^\dagger a_{\mathbf{k}\gamma\lambda} \left[1 - \sum_{\mathbf{q}} G_{\mathbf{q}}^2 b_{\mathbf{q}}^\dagger b_{\mathbf{q}} \right] + h.c. \\ &+ \sum_{j,\mathbf{k}\gamma\lambda\mathbf{q}} \hbar g'_{\mathbf{k}\gamma\lambda}{}^*(\mathbf{R}_j) c_j^\dagger a_{\mathbf{k}\gamma\lambda} G_{\mathbf{q}}(\mathbf{R}_j) (b_{\mathbf{q}}^\dagger - b_{-\mathbf{q}}) + h.c. .\end{aligned}$$

As in the previous sections, we use the interaction picture and we define new kernel functions that depend also on the phonon momentum

$$F(\tau, \omega, \mathbf{R}, \mathbf{q}) = \sum_{\mathbf{k}\gamma\lambda} g'_{\mathbf{k}\gamma\lambda} e^{i\mathbf{k}\gamma\mathbf{R}} e^{i(\omega - \sum_{\mathbf{q}} \frac{M_{\mathbf{q}}^2}{\hbar\omega_{\mathbf{q}}} - \omega_{\mathbf{k}\gamma} + c_p q)\tau} .$$

Using these new functions we can write the integro-differential equations for the coefficients of the wavefunction in the ansatz of Eq.(3.19), and we obtain for $C_a(t)$

$$\begin{aligned}
\dot{C}_a(t) = & - \int_0^t dt' F(t-t', \omega'_a, 0, 0) C_a(t') - \int_0^t dt' F(t-t', \omega'_b, \mathbf{R}_{ab}, 0) C_b(t') e^{i(\omega_a - \omega_b)t} \\
& - \sum_{\mathbf{q}} G_{\mathbf{q}} \int_0^t dt' F(t-t', \omega'_a, 0, \mathbf{q}) C_{a,\mathbf{q}}(t') e^{i\mathbf{q}\mathbf{R}_a} e^{-ic_p q t} \\
& - \sum_{\mathbf{q}} G_{\mathbf{q}} \int_0^t dt' F(t-t', \omega'_b, \mathbf{R}_{ab}, \mathbf{q}) C_{b,\mathbf{q}}(t') e^{i(\omega_a - \omega_b)t} e^{i\mathbf{q}\mathbf{R}_b} e^{-ic_p q t} \\
& + \sum_{\mathbf{q}} G_{\mathbf{q}} \int_0^t dt' F(t-t', \omega'_a, 0, 0) (1 - G_{\mathbf{q}}^2) C_{a,\mathbf{q}}(t') e^{i\mathbf{q}\mathbf{R}_a} e^{-ic_p q t} \quad (3.20) \\
& + \sum_{\mathbf{q}} G_{\mathbf{q}} \int_0^t dt' F(t-t', \omega'_b, \mathbf{R}_{ab}, 0) (1 - G_{\mathbf{q}}^2) C_{b,\mathbf{q}}(t') e^{i(\omega_a - \omega_b)t} e^{i\mathbf{q}\mathbf{R}_a} e^{-ic_p q t} \\
& - \sum_{\mathbf{q}} G_{\mathbf{q}}^2 \int_0^t dt' F(t-t', \omega'_a, 0, -\mathbf{q}) C_a(t') \\
& - \sum_{\mathbf{q}} G_{\mathbf{q}}^2 \int_0^t dt' F(t-t', \omega'_b, \mathbf{R}_{ab}, -\mathbf{q}) C_b(t') e^{i(\omega_a - \omega_b)t} e^{i\mathbf{q}\mathbf{R}_{ab}} .
\end{aligned}$$

The equations for $\dot{C}_b(t)$, $\dot{C}_{a,\mathbf{q}}$ and $\dot{C}_{b,\mathbf{q}}$ are derived in a similar way and are not shown here. Moreover, the dynamics of the energy transfer can be well understood by looking at the time evolution of $\dot{C}_a(t)$ only.

In Eq.(3.20), We have the sum over all possible values of \mathbf{q} . We replace the sum $\sum_{\mathbf{q}}$ by the integral $\frac{V}{(2\pi)^3} \int q^2 dq \sin\theta d\theta d\phi$, where we integrate over q . Here V is the quantization volume. As shown in Ref. [52], the coupling G_q of acoustic phonons and a quantum dot excitons has a peak value at a specific value of q_{\max} that depends on the quantum dot size. For $q \neq q_{\max}$ the matrix element decreases drastically due to a mismatch between the phonon wavelength and the quantum dot size. We find that for a given size of the

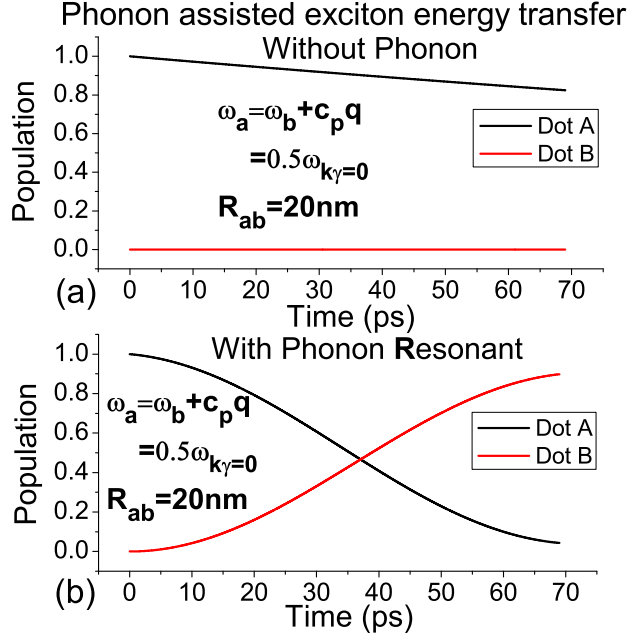


Figure 3.7: Phonon assisted energy transfer. (a) no phonon included. (b) the phonon-assisted exciton energy transfer with phonon energy equals the detuning between the two dots (phonon-assisted resonance).

two quantum dots in the cavity, the phonon assisted energy transfer process is efficient only when the energy of the phonon at q_{\max} matches the difference in energy of the two excitons. Since the G_q is peaked at q_{\max} we approximate the integral $\int q^2 dq \sin \theta d\theta d\phi G_q$ by $q_{\max}^2 \delta q G_{q_{\max}}$ with the θ and ϕ dependence integrated exactly. δq here is an effective width in q space dependent on the quantum dot size. With this approximation, we can replace the summation over all possible phonon modes by a single mode phonon q_{\max} with the coupling constant $\tilde{G}_{q_{\max}}$.

With all the realistic parameters for GaAs quantum dots, $\hbar c_p q_{\max}$ is around 0.5 meV, and the dimensionless interaction $\tilde{G}_{q_{\max}}$ is around 0.1. The parameter values used in this estimation are $D_e = -4.8$ eV, $D_h = -14.6$ eV, $\rho = 5350$ kg/m³, and $c_p = 5150$ m/s. [30, 51] With these assumptions and the estimation of $G_{q_{\max}}$, we run simulations in

which the exciton is initially in the dot a with an energy higher than the exciton in the dot b . In this case, $\omega_a > \omega_b$, a phonon is emitted in the final state to take away the extra energy. As shown in Fig.3.7(a), when the phonon coupling is switched off, the exciton in the first quantum dot decays spontaneously like in the case of a single dot in the cavity, and the second quantum dot remains unexcited. This result indicates that the QD $_a$ cannot transfer the exciton to QD $_b$ in this off-resonant configuration. Fig.3.7 (b), shows that the energy transfer between QD $_a$ and QD $_b$ can occur when we turn the phonon coupling on. However, the phonon-assisted exciton energy transfer only occurs when the phonon energy matches the detuning between the two dots, leading to a phonon assisted resonant energy transfer. We should note that the phonon-assisted transfer rate is much slower, because the equivalent phonon-exciton-photon coupling is weaker than the exciton-photon coupling.

3.5 Conclusion

In this chapter, we have studied the dynamics of the exciton energy transfer process between two quantum dots in a planar cavity. We have used the coupling constant for the exciton-photon interaction calculated in Chapter 2 using quantized field operators for E and M cavity modes. In our numerical simulation, we have described the spontaneous exciton recombination as a result of the coupling of the discrete exciton modes with the continuum of modes of the planar cavity, without including a phenomenological damping term in the equations. We have solved the equations of motion and we have simulated the dynamics of the exciton energy transfer process. In the simulation, we have found that the exciton energy transfer only occurs when the two dots have the same exciton energy, which corresponds to the resonant condition or the elastic transfer. Due to the confinement, the photon density

of state is changed and there is a minimum allowed value for the photon energy. We found that if the exciton energy is lower than the lowest cavity mode energy, the spontaneous decay of the exciton is highly suppressed. We have also found that the inter-dot separation dependence of the effective transfer rate is R^{-1} in the planar cavity, compared with the energy transfer rate in the free space which is either R^{-6} for Förster transfer or R^{-2} for radiative transfer. This difference originates from the different photon density of states. We have also taken phonons into consideration to describe the inelastic energy transfer. We have considered the exciton-phonon interaction originating from the deformation potential coupling between the exciton and the longitudinal acoustic phonon. Using the independent boson model discussed in Chapter 2, we have derived an effective exciton-photon-phonon interaction. The phonon can bring in or take away the extra energy to compensate the energy detuning between the two dots, and can lead to a phonon-assisted energy transfer process between the two dots in the presence of detuning.

Chapter 4

Applications

4.1 Conditional phase gate using quantum dots

In this chapter we will discuss two applications of systems containing quantum dots coupled to the electromagnetic field. The first application is related to quantum computing, which is briefly introduced in this chapter. We propose a system containing three semiconductor quantum dots to realize a two qubit quantum phase gate by applying the Quantum Zeno effect. This idea originates from the intriguing work by Dr. Y.P. Huang and Prof. M. Moore [37]. The second application concerns the theoretical description of energy transfer in a chain of quantum dots, which can be used in light-harvesting systems.

4.1.1 Brief introduction to quantum computing

Quantum computation is the study of operations on information that can be accomplished using quantum mechanical phenomena, such as superposition and entanglement. Quantum computation combines fundamental ideas from quantum mechanics and computer science.

The main difference between a classical computer and a quantum computer is the definition of a bit. A classical bit only contains two possible values, 0 and 1. A quantum bit, or a “qubit”, it could be in any superposition of state $|0\rangle$ and state $|1\rangle$. The possibility of having qubits in superposition states leads to quantum parallelism, which is a fundamental feature of quantum algorithms. In 1994, Peter Shor demonstrated that the problem of finding the prime factors of an integer could be solved more efficiently on a quantum computer than on a classical computer. In 1995, Lov Grover showed that another important problem, the problem of searching through some unstructured search space could also be sped up on a quantum computer. Shor and Grover’s results indicate that quantum computers are more powerful than classical computer for certain problem. However, the ability to control single quantum systems is essential if we want to make quantum computing feasible in real life. Since the 1970s, many techniques for controlling single quantum systems have been developed. For example, atom traps [62] were developed for trapping a single atom and isolating it from the rest of the world. Excitons have been confined in the self-assembled quantum dots and their dynamics have been controlled by laser pulses [63]. In 1998, Daniel Loss and David DiVincenzo [64] proposed a new implementation of a universal set of gates for quantum computing using the spins of the electrons in coupled quantum dots as qubits. In this thesis, we also use electron spins in quantum dots as qubits, but we focus on a quantum control that use lasers. We will show in this chapter a new scheme for the implementation of a quantum gate in a double-dot system.

4.1.2 Quantum gates

Classical computer circuits consist of wires and logic gates. The wires are used to transport information around the circuit, while the logic gates perform manipulations of the information. For example, a classical NOT gate converts 0 to 1 and 1 to 0, i.e. the value of the bit is flipped. Similarly, a quantum NOT gate takes the state $|0\rangle$ to the state $|1\rangle$ and vice versa, and is a quantum analogue to the classical NOT gate. The quantum NOT gate can be defined more generally as the quantum transformation that takes the state $\alpha|0\rangle + \beta|1\rangle$ to the state $\beta|0\rangle + \alpha|1\rangle$. There is a convenient way to represent the quantum NOT gate. We can define a matrix X to represent the quantum NOT gate as follows

$$X = \begin{pmatrix} 0 & 1 \\ 1 & 0 \end{pmatrix}, \quad (4.1)$$

while the quantum state $\alpha|0\rangle + \beta|1\rangle$ can be written in a vector form as

$$\begin{pmatrix} \alpha \\ \beta \end{pmatrix}, \quad (4.2)$$

then the corresponding output for the quantum NOT gate is

$$X \begin{pmatrix} \alpha \\ \beta \end{pmatrix} = \begin{pmatrix} \beta \\ \alpha \end{pmatrix}. \quad (4.3)$$

According to the normalization condition required for a quantum state, the constraint for the matrix U describing the single qubit gate is unitarity, that is $U^\dagger U = I$. There are many

non-trivial single qubit gates, one important gate is called the Hadamard gate,

$$H = \frac{1}{\sqrt{2}} \begin{pmatrix} 1 & 1 \\ 1 & -1 \end{pmatrix}. \quad (4.4)$$

The Hadamard gate is one of the most useful quantum gates which is often used to create a two-qubit entanglement by combining it with a two qubit controlled-NOT gate as explained below.

In order to do computation, a multi-qubit logic gate is required. One commonly used multi-qubit quantum logic gate is the controlled-NOT or CNOT gate. It has two input qubits, the first qubit is the control qubit and the second bit is the target qubit. If the control qubit is set to 0, then the target qubit is left untouched. If the control qubit is set to 1, then a quantum NOT is applied to the target qubit. The CNOT gate can be expressed in matrix form as

$$C^{NOT} = \begin{pmatrix} 1 & 0 & 0 & 0 \\ 0 & 1 & 0 & 0 \\ 0 & 0 & 0 & 1 \\ 0 & 0 & 1 & 0 \end{pmatrix}, |00\rangle = \begin{pmatrix} 1 \\ 0 \\ 0 \\ 0 \end{pmatrix}, |01\rangle = \begin{pmatrix} 0 \\ 1 \\ 0 \\ 0 \end{pmatrix}, |10\rangle = \begin{pmatrix} 0 \\ 0 \\ 1 \\ 0 \end{pmatrix}, |11\rangle = \begin{pmatrix} 0 \\ 0 \\ 0 \\ 1 \end{pmatrix}. \quad (4.5)$$

An important theoretical result in classical computation is that any function on bits can be computed from the composition of NAND gates alone, which is known as a universal gate. In analogy to this, in quantum computing, it is proved that any multiple qubit logic gate may be composed from CNOT gate and single qubit gates. This is a remarkable universality result. Since arbitrary single qubit operator can be realized by different methods, the most

challenging problem is to design a CNOT gate, or alternatively, a two-qubit gate which is equivalent to a CNOT gate.

Another interesting quantum gate is the controlled-Z gate(also called as controlled phase gate). As a special property of quantum mechanics which is not shown in classical computer, the relative phase between two qubits could be functional to perform a logic gate. The controlled Z gate could be shown in matrix form as

$$C_{ij}^Z = \begin{pmatrix} 1 & 0 & 0 & 0 \\ 0 & 1 & 0 & 0 \\ 0 & 0 & 1 & 0 \\ 0 & 0 & 0 & -1 \end{pmatrix}, \quad (4.6)$$

here i denotes the control qubit and j denotes the target qubit. Only when both qubits are in state $|11\rangle$, a π phase ($e^{i\pi} = -1$) would be added after this gate. With a CNOT gate

$$C_{ij}^{NOT} = \begin{pmatrix} 1 & 0 & 0 & 0 \\ 0 & 1 & 0 & 0 \\ 0 & 0 & 0 & 1 \\ 0 & 0 & 1 & 0 \end{pmatrix}, \quad (4.7)$$

and Hadamard gate on the target qubit j

$$H_j = \frac{1}{\sqrt{2}} \begin{pmatrix} 1 & 1 & 0 & 0 \\ 1 & -1 & 0 & 0 \\ 0 & 0 & 1 & 1 \\ 0 & 0 & 1 & -1 \end{pmatrix}. \quad (4.8)$$

It is easily shown, $C_{ij}^Z = H_j C_{ij}^{NOT} H_j$. First of all, this is an example of the universality of the controlled-NOT gate. Secondly, we could equivalently get $C_{ij}^{NOT} = H_j C_{ij}^Z H_j$ since $H_j^2 = 1$. This means that the controlled Z gate can be also considered as an universal two qubit gate which could be converted in the CNOT gate with only help of single qubit Hadamard gate.

4.1.3 Quantum Zeno gate

The Quantum Zeno effect [65, 66, 67, 68] occurs when a rapid sequence of measurements is performed on a slowly evolving quantum system, with the result that the system is *frozen* in its initial state. To explain this effect, suppose we have a system in the initial state I, which is the eigenstate of the measurement operator. The system can decay into state II with a certain probability p under free time evolution. If measurements are made periodically, with some finite interval between each one, at each measurement, the wave function collapses to an eigenstate of the measurement operator, for instance, the initial state I or the state II. For a rapid sequence of measurements, in which the time interval between the measurements are much shorter compared to the system evolution time, the probability for the system initially in I collapsing into state II goes to zero.

An analogous effect to the Quantum Zeno effect occurs when a system is strongly coupled to a reservoir, as the transfer of information from the system into the reservoir can be seen as a continuous measurement. If coupling to the reservoir can be made contingent on the joint quantum state of two qubits, the Quantum Zeno effect can be used in conjunction with control pulses to efficiently drive the qubits into an entangled state. This general approach has been discussed within the framework of interaction free measurements [69,

70, 37], decoherence free subspaces [71, 72]. Proposed physical implementations vary from purely photonic systems [73, 74, 75], to atom-cavity systems [76, 37], and superconducting qubits [77], yet without reported experimental realization.

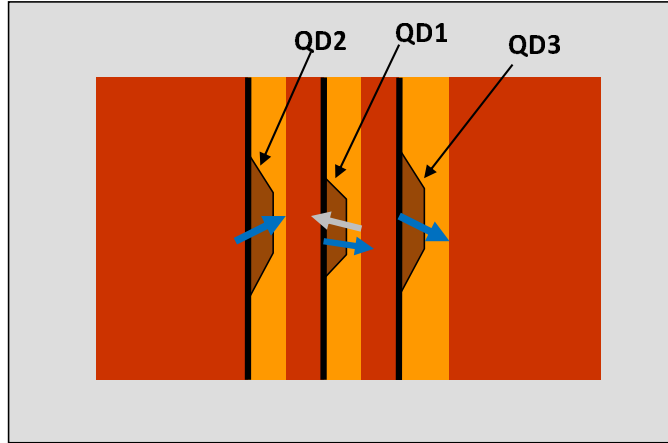


Figure 4.1: Schematic view of three dots based quantum zeno gate configuration

Following a generalized Quantum Zeno effect phase-gate recently proposed in [37], we have devised a two-qubit conditional phase gate using electron spins in semiconductor quantum dots. This system has the advantage over atomic systems that decoherence rates are of the order of picoseconds, which, in Zeno-based schemes, leads to significant improvements in gate time and/or fidelity.

We consider a system composed of three quantum dots (QDs), two of which are singly charged with electrons (see Fig.4.1). The spins of these two electrons are then the logical qubits on which the phase-gate acts. A laser field is then applied, tuned to the exciton resonance of the uncharged dot. The energy levels and laser polarization are chosen so that the electron generated in the neutral dot will be spin up. If formed, the exciton can relax to the neighboring dots by a spin-conserving dissipative phonon-assisted process [30]. The emission of a phonon and relocation of the exciton would clearly indicate that at least one

qubit spin did not match the electron spin of the exciton. Thus the possibility of phonon emission is equivalent to a strong continuous partial measurement [29, 37] of the collective spin state of the two qubits.

Despite the widely-held belief that decoherence must always be minimized in quantum information processing, it has been known for some time [76] that decoherence can in principle be harnessed to generate high-fidelity entanglement by use of the Quantum Zeno effect. In our scheme, the Quantum Zeno effect occurs when the strong dissipation rate of the exciton state suppresses the laser induced Rabi oscillations in the neutral dot, effectively freezing it in its ground state. As the dissipation mechanism is subject to Pauli blocking, the spin-qubits in the charged dots can thus be seen as *quantum switches* that control the Quantum Zeno effect. After a single Rabi cycle, a two level system will return to its original state times a π phase shift. In our system, only the up-up spin-qubit state undergoes Rabi oscillation, and acquires the -1 factor, thus realizing a conditional phase gate.

4.1.4 Fidelity of the controlled phase gate by Quantum Zeno effect

In order to predict the fidelity of the gate, we will use parameters appropriate for vertically grown (In,As)Ga/GaAs self-assembled quantum dots. Structures with vertically coupled neutral and charged quantum dots have been recently demonstrated [78]. The central neutral dot will be QD1, and the two lateral charged dots will be referred to as QD2 and QD3. Absorption of a photon creates an exciton state in QD1, and trion states in QD2 and QD3. We assume that the ground trion energies in the two lateral dots are similar, and are lower than the ground exciton energy in the central dot, so that phonon-mediated exciton relaxation is energetically allowed. In the absence of the Quantum Zeno effect, the driving laser

will induce Rabi oscillations between the zero- and one-exciton states of QD1. Assuming that the driving laser field is σ_- polarized, the standard selection rules lead to the creation of an exciton with electron spin up($+\frac{1}{2}$) and a heavy hole spin down($-\frac{3}{2}$) in QD1. Due to the difference between the exciton and trion energy, QD2 and QD3 are far-detuned and thus not driven by the laser. The exciton and trion linewidths in InAs/GaAs quantum dots are of the order of one μeV [59]. Moreover, in our scheme we will use weak lasers so that both the Rabi energy and the linewidths are much smaller than the typical separation between the levels.

There are several exciton decay mechanisms that can spoil the Rabi oscillations. Many such processes depend on the intensity of the laser and have been experimentally characterized [79, 80]. In the weak excitation limit, phonon-mediated processes are dominant. The role of the phonon is to carry away excess energy. For concreteness, we will assume that the phonon-assisted excitation transfer [30] is the dominant dissipation channel from QD1 to QD2 or QD3 since phonon-assisted relaxation of a *single* carrier between two dots via tunneling is exponentially suppressed for QD separations of several nm. Nonetheless, the scheme for the gate and our analytical results, can be easily adapted to the case in which quantum dots are close and the phonon emission involves only the electron. In this short-range case the energy levels of the central and lateral dots have to be engineered so that hole transfer is forbidden. For a weak resonant 2π laser pulse with Rabi energy $\Omega \ll \Gamma$, where Γ is the phonon emission rate, then the three spin states (up-down, down-up and down-down) trigger the Quantum Zeno effect and freeze the system. A schematic view of the different possible Quantum Zeno effect scenarios for different initial states is shown in Fig.4.2.

The quantum state of the system can be expressed in the triple-particle basis $|\lambda\sigma\sigma'\rangle =$

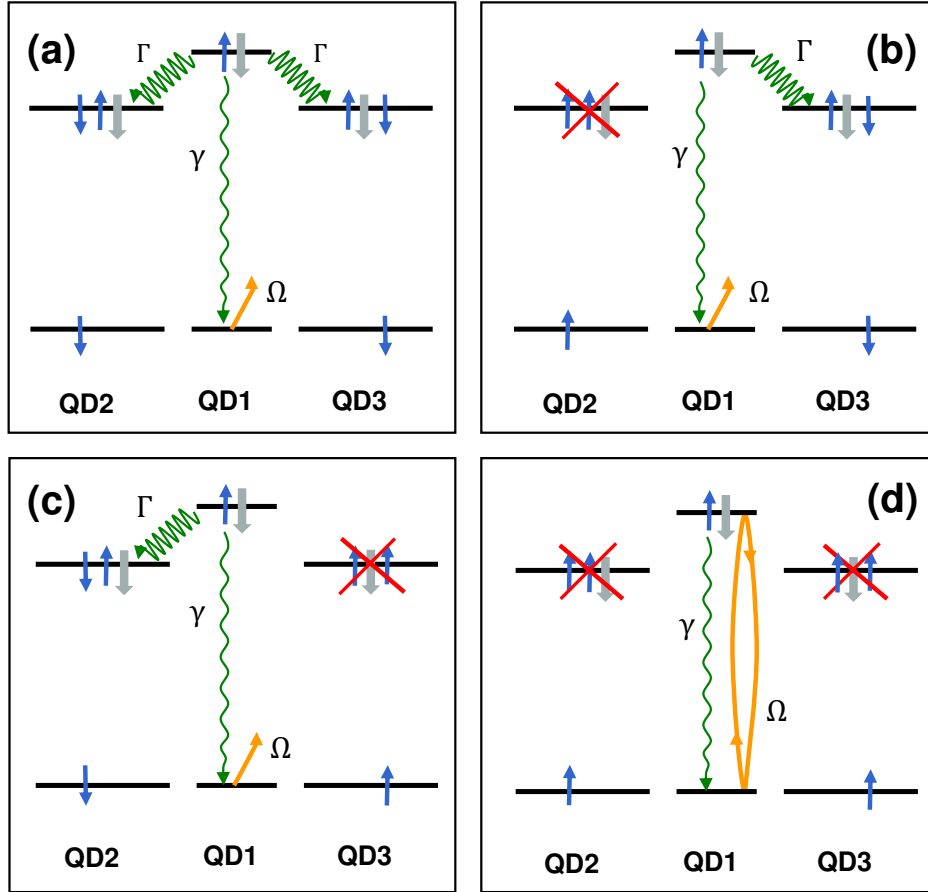


Figure 4.2: Scheme of the dynamics of the system under different initial states. The narrow blue (bold gray) arrow represents the electron (hole) spins. The energy levels for QD1 are the empty dot (lower) and the first exciton level (upper), while the energy levels in QD2 and QD3 are charged dot ground states (lower) and trion states (upper). Figures (a)-(d) correspond to the four possible initial states of the two qubits. (a)-(c) If the electron in QD2 or QD3 is spin down, the exciton in QD1 can decay into one of the neighboring dots, in which case the Quantum Zeno effect prevents the Rabi Oscillation in QD1. (d) If both decay channels are closed, QD1 will undergo a 2π -Rabi oscillation. The photon emission rate γ is too weak to induce a Quantum Zeno effect.

$|\lambda\rangle_a \otimes |\sigma\sigma'\rangle_{23}$. Here, $|\lambda\rangle_a$ ($\lambda = 0, 1, 2, 3$) represents the state of the ancillary electron-hole pair created in QD1, where $\lambda = 0$ is the vacuum state with no exciton, while $\lambda = 1, 2, 3$ indicates the exciton residing in QD1, QD2, or QD3, respectively. $|\sigma\sigma'\rangle_{23}$ represents the combined state of the two logical qubits, with $\sigma, \sigma' \in \{\uparrow, \downarrow\}$ indicating the spin (up or down) states of the electrons in QD2 and QD3, respectively. The states $|2\uparrow\sigma'\rangle$ and $|3\sigma\uparrow\rangle$ are forbidden by the Pauli exclusion principle, and therefore excluded from our model.

Our goal is to realize a two-qubit phase gate for the electron spins in QD2 and QD3, with the electron-hole pair acting only as an ancillary system. Ideally, such a gate transforms an initial logical state $|\Psi_i\rangle_{23}$ of QD2 and QD3 to the final state $\hat{U}_\pi|\Psi_i\rangle_{23}$, with the π -phase gate operator defined via $\hat{U}_\pi|\sigma\sigma'\rangle_{23} = (1 - 2\delta_{\sigma,\uparrow}\delta_{\sigma',\uparrow})|\sigma\sigma'\rangle_{23}$. The ancillary system, initially prepared in $|0\rangle_a$ state, becomes entangled with the logical qubits during the 2π pulse, becoming once again disentangled by the end of the pulse. Due to errors, the ancillary qubit might still be entangled with the logical qubits after the gate operation, so that the final density matrix representing QD2 and QD3 should be obtained by tracing over λ .

The system's Hamiltonian is given by

$$H = \epsilon_2 c_2^\dagger c_2 + \epsilon_3 c_3^\dagger c_3 + \frac{\Omega}{2}(c_1 + c_1^\dagger) \quad (4.9)$$

Here, the c_i^\dagger (c_i) is the exciton creation (annihilation) operator, with $i = 1, 2, 3$ labeling the three quantum dots. Ω is the Rabi strength of the driving laser. In contrast to the state-selectivity of the phonon-mediated relaxation process, the decay of the exciton in QD1 via spontaneous photon emission is independent of QD2 and QD3 states, and will only cause the exciton to relax back to the initial $|0\rangle_a$ state. This is the primary source of error in the gate operation, and is mitigated by choosing $\Omega \gg \gamma$, where γ is the exciton spontaneous

photon-emission rate.

To model the system's dynamics, we employ Linblad formalism [81] to arrive at the master equation

$$i\frac{\partial\rho}{\partial t} = -[\rho, H] + i\mathcal{L}[\rho], \quad (4.10)$$

where ρ is the density operator for the system. The superoperator \mathcal{L} is given by

$$\mathcal{L}[\rho] = \frac{1}{2} \sum_{i=1}^3 \left[L_i \rho L_i^\dagger - L_i^\dagger L_i \rho + H.c. \right], \quad (4.11)$$

where $L_1 = \sqrt{\gamma}c_1$ describes spontaneous photon decay in QD1, and $L_2 = \sqrt{\Gamma_2}c_2^\dagger c_1$, $L_3 = \sqrt{\Gamma_3}c_3^\dagger c_1$ describes phonon-assisted dissipation from QD1 to QD2 and QD3. Since the phonon-decay channels are independent, having a symmetric or asymmetric exciton decay rate will not significantly affect gate performance as long as $\Gamma_2, \Gamma_3 \gg \Omega$. Thus, we choose $\Gamma_2 = \Gamma_3 = \Gamma$ for convenience. We note that other channels could as well be characterized by generalizing the Γ -terms to include any spin-selective relaxation channels, while γ -terms to include spin-independent ones.

During the gate operation, the system is initially in the state $\rho_i = |\Psi_i\rangle\langle\Psi_i| \otimes |0\rangle_a\langle 0|_a$, and then evolves under equation (4.10) for a duration of $t = 2\pi/\Omega$, resulting in a final density ρ_f . The fidelity is defined as

$$\mathcal{F} = \text{tr}\{\rho_f \hat{U}_\pi |\Psi_i\rangle\langle\Psi_i|_{23} \hat{U}_\pi^\dagger \otimes \hat{P}_1\}, \quad (4.12)$$

where $\hat{P}_1 = |0\rangle_a\langle 0|_a + |1\rangle_a\langle 1|_a$. This gives the probability that two logical qubits are in the proper phase-gate output state with the electron-hole pair remaining in QD1. This later condition is required because relaxation of the exciton to either QD2 or QD3 results in a

doubly-charged dot and collapse of the two-qubit entangled state.

4.1.5 Analytical estimation of the fidelity

Before presenting numerical results, we first seek approximate analytical solutions to the dissipative dynamics of equation (4.10). Defining density matrices $\rho_{mn} = \langle m|_{23} \hat{P}_1 \rho \hat{P}_1 |n\rangle_{23}$, with $m, n \in \{\uparrow\uparrow, \uparrow\downarrow, \downarrow\uparrow, \downarrow\downarrow\}$, the master equation (4.10) can be divided into a set of uncoupled equations, leading to

$$\begin{aligned} \frac{\partial \rho_{mn}}{\partial t} &= i[\rho_{mn}, H_0] + \frac{\gamma}{2} \left(c_1 \rho_{mn} c_1^\dagger - c_1^\dagger c_1 \rho_{mn} + H.c. \right) \\ &\quad - \alpha_m \Gamma c_1^\dagger c_1 \rho_{mn} - \alpha_n \Gamma \rho_{mn} c_1^\dagger c_1, \end{aligned} \quad (4.13)$$

where α_m is a logical-qubit dependent parameter, defined as $\alpha_m = 0, \frac{1}{2}, \frac{1}{2}, 1$, for $m = \uparrow\uparrow, \uparrow\downarrow, \downarrow\uparrow, \downarrow\downarrow$, respectively.

Successful operation requires $\Gamma \gg \Omega$ to impose the Quantum Zeno effect, while $\gamma \ll \Omega$ is required to suppress spontaneous photon-emission, the primary failure mechanism. Hence, the operational range of the present Zeno phase gate is $\gamma \ll \Omega \ll \Gamma$. This separation of time-scales enables us to solve Eq.(4.13) perturbatively. With the definition $\rho_{mn}^{\lambda\lambda'} = \langle \lambda m | \rho | \lambda' n \rangle$, the matrix elements of the final density are given to second order in $\frac{\gamma}{\Omega}$ and $\frac{\Omega}{\Gamma}$ by $\rho_{mn}^{\lambda\lambda'} = \mu_{mn}^{\lambda\lambda'} \langle m | \Psi_i \rangle \langle \Psi_i | n \rangle$. The output coefficients $\mu_{mn}^{\lambda\lambda'}$ are given by Table 1, with $f(x) = 1 - \frac{\pi}{2}x + \frac{3\pi^2}{50}x^2$, $g(x) = \frac{\pi}{100}x + \frac{3\pi^2}{500}x^2$. Note that the population and coherence dynamics in the subspace $\lambda = 2, 3$ are completely decoupled from the $\lambda = 0, 1$ subspace. In fact, we only need equations for the diagonal matrix elements with respect to the $\lambda = 0, 1$ subspace, as only they contribute to the fidelity (4.12). We see from Table 1 that to leading order, the gate output coefficients are consistent with only the state $|\uparrow\uparrow\rangle_{23}$ having acquired

a π -phase shift, as desired for the π -phase gate.

Table 4.1: Output coefficients

m	n	μ_{mn}^{00}	μ_{mn}^{11}
$\uparrow\uparrow$	$\uparrow\uparrow$	$(1 + \frac{3\pi}{4} \frac{\gamma}{\Omega})^{-1}$	$1 - (1 + \frac{3\pi}{4} \frac{\gamma}{\Omega})^{-1}$
$\uparrow\uparrow$	$\neq\uparrow\uparrow$	$-f(\frac{\Omega}{\alpha_n \Gamma}) \exp(-\frac{\pi}{2} \frac{\gamma}{\Omega})$	$g(\frac{\Omega}{\alpha_n \Gamma}) \left(\frac{\gamma}{\Omega} + \pi \frac{\gamma^2}{\Omega^2} \right)$
$\neq\uparrow\uparrow$	$\uparrow\uparrow$	$-f(\frac{\Omega}{\alpha_m \Gamma}) \exp(-\frac{\pi}{2} \frac{\gamma}{\Omega})$	$g(\frac{\Omega}{\alpha_m \Gamma}) \left(\frac{\gamma}{\Omega} + \pi \frac{\gamma^2}{\Omega^2} \right)$
$\neq\uparrow\uparrow$	$\neq\uparrow\uparrow$	$\exp(-\frac{\pi}{2} \frac{\alpha_m + \alpha_n}{\alpha_m \alpha_n} \frac{\Omega}{\Gamma})$	0

The fidelity defined in Eq.(4.12) is now explicitly given by $\mathcal{F} = \sum_{mn} (-1)^{\delta_{m,\uparrow\uparrow} + \delta_{n,\uparrow\uparrow}} (\mu_{mn}^{00} + \mu_{mn}^{11}) |\langle n | \Psi_i \rangle|^2 |\langle m | \Psi_i \rangle|^2$, which depends on γ, Ω, Γ , as well as on the initial logical state $|\Psi_i\rangle$.

In practice, while Γ and γ are known parameters for a given QD system, $|\Psi_i\rangle$ is in general arbitrary, making it impossible to simultaneously optimize Ω for all input states. For a given Ω , however, there is a lower bound $\mathcal{F}_{LB}(\Omega) = \text{Min}\{\mathcal{F}(\Omega), |\Psi_i\rangle \in \mathcal{H}\}$, where \mathcal{H} is the full two-qubit Hilbert space. Maximizing the lower bound then gives $\mathcal{F}_{\text{opt}} = \text{Max}\{\mathcal{F}_{LB}(\Omega), \forall \Omega\}$, for $\Omega_{\text{opt}} = \sqrt{\gamma\Gamma/8}$ and

$$\mathcal{F}_{\text{opt}} \geq \mathcal{F}(\Omega_{\text{opt}}) = \exp\left[-\frac{10}{3} \sqrt{\frac{\gamma}{\Gamma}}\right], \quad (4.14)$$

so that the fidelity is improved only by increasing Γ/γ .

Considering recent theoretical calculations, the phonon-assisted transfer rate between two quantum dots can be as fast as several tens of picoseconds for favorable alignments [30]. The lifetime τ of the exciton in (In,As)Ga/GaAs QD is of the order of 1 ns [82], which only marginally meets our operational criteria. Nonetheless, τ can be significantly extended by

embedding the QD system into an optical cavity. In fact, $\tau \sim 10$ ns has been demonstrated in a recent experiment [59]. For accessible parameters of $\Gamma = 20$ ns⁻¹, $\gamma = 0.08$ ns⁻¹, we find $\Omega_{\text{opt}} = 0.45$ ns⁻¹ and $\mathcal{F}_{\text{opt}} = 0.810$. For these parameters, we have also calculated the mean fidelity averaged over all the initial states as defined in Refs. [83, 63], which gives $\mathcal{F}_{\text{avg}} = 0.850$. As we will describe, a much higher fidelity can be obtained probabilistically by measuring the final state of the ancillary system to *herald* successful gate operation.

4.1.6 Numerical calculation of the fidelity

To verify the analytical results, we now solve exactly the dissipative dynamics Eq.(4.9) via numerical simulations. For comparison, we choose $\Gamma = 20$ ns⁻¹, $\gamma = 0.08$ ns⁻¹, $\Omega = 0.45$ ns⁻¹ and initial state $|\Psi_i^0\rangle = \frac{1}{2}(|\uparrow\uparrow\rangle + |\uparrow\downarrow\rangle + |\downarrow\uparrow\rangle + |\downarrow\downarrow\rangle)$. The dynamics of matrix elements $\rho_{\uparrow\uparrow,\uparrow\uparrow}^{00}$, $\rho_{\uparrow\downarrow,\uparrow\uparrow}^{00}$ and $\rho_{\downarrow\uparrow,\downarrow\uparrow}^{00}$, $\rho_{\downarrow\downarrow,\downarrow\downarrow}^{00}$ are shown in Fig.4.3. From the figure we can see that both $\rho_{\uparrow\uparrow,\uparrow\uparrow}^{00}$ and $\rho_{\uparrow\downarrow,\uparrow\uparrow}^{00}$ undergo damped oscillation, due to $\gamma \ll \Omega$. At the end of the 2π -pulse, we find $\rho_{\uparrow\uparrow,\uparrow\uparrow}^{00} = 0.180$, and $\rho_{\uparrow\downarrow,\uparrow\uparrow}^{00} = -0.176$, compared with 0.176 and -0.175 respectively from the analytical results. The off-diagonal matrix element $\rho_{\uparrow\downarrow,\uparrow\uparrow}^{00}$ gains a minus sign after the 2π -pulse, which is the key ingredient of our phase gate. In contrast, both $\rho_{\downarrow\uparrow,\downarrow\uparrow}^{00}$ and $\rho_{\downarrow\downarrow,\downarrow\downarrow}^{00}$ are shown to be frozen in its initial state, due to Quantum Zeno effect since $\Omega \ll \Gamma$. The final values of $\rho_{\downarrow\uparrow,\downarrow\uparrow}^{00}$ and $\rho_{\downarrow\downarrow,\downarrow\downarrow}^{00}$ are found to be 0.217 and 0.233, in agreement with the analytical results. The fidelity from the numerical simulation is with the initial state given above is 0.829, which is very close to the approximate analytical value of 0.831.

The gate fidelity can be further improved by measuring the final state of the ancillary electron-hole pair, which can ‘herald’ successful gate operation. If it is detected in $|2\rangle_a, |3\rangle_a$

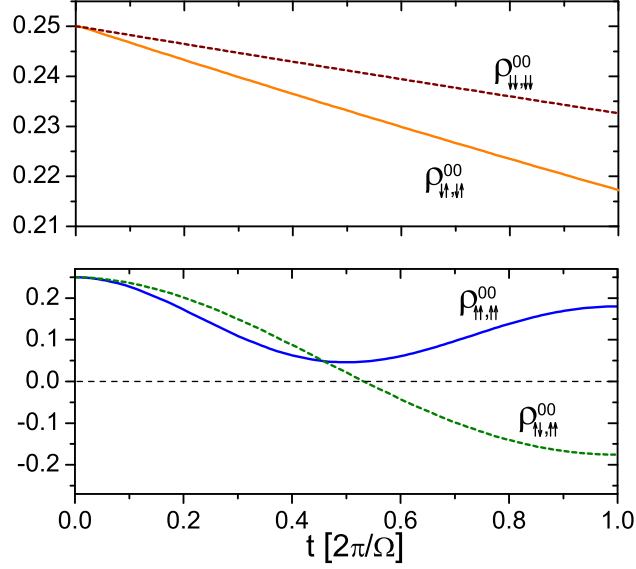


Figure 4.3: Dynamical evolution of several density matrix elements for the initial state $|\Psi_i^0\rangle$ during the gate operation via numerical simulation.

or $|1\rangle_a$ states, which correspond to a trion in QD2, QD3, or an exciton in QD1, failure is indicated. Only if the state $|0\rangle_a$ is obtained, is successful operation a possibility. In this case we obtain $\mathcal{F}_h = \mathcal{F}/(1 - P_f)$, where P_f is the failure probability. For the input state $|\Psi_i^0\rangle$, this heralded fidelity is $\mathcal{F}_h = 0.986$, a significant improvement from the unheralded value of 0.829. Similar improvements are found for other input states. The reason for the large improvement is that the dominant failure mechanism is photon emission via exciton decay in QD1. This is most likely to occur at the halfway point of gate operation, where the probability to have an exciton in QD1 reaches its maximum. This results in QD1 returning to $|0\rangle_a$ and begin a new Rabi cycle. In this scenario, only half of a Rabi cycle will have occurred, leaving QD1 in the exciton states. Thus gate failure will correlate highly with the ancillary system being found in state $|1\rangle_a$ at the end of gate operation.

In practice, the final state of the ancillary electron-hole pair might be measured by applying two driving lasers to the three quantum dots and detecting the resulting fluorescence

photons. One of the lasers is tuned to be resonant with the trion and charged biexciton transition in QD2 and QD3, yet far detuned from other transitions. Similarly, the other laser is resonant with the exciton and biexciton transition in QD1, and as well far detuned from other transitions. A trion in QD2 and QD3, or an exciton in QD1, will then lead to resonance fluorescence, indicating the failure of the gate operation. On the other hand, the absence of fluorescence photons heralds the electron-hole being in the $|0\rangle_a$ state. We note that in the non-fluorescence case, the logical qubits are preserved, since they are driven far from resonance.

The results of this work demonstrate the possibility of realizing a two-qubit controlled phase gate via the Quantum Zeno effect in (In,As)Ga/GaAs self-assembled quantum dots. Using realistic values for all parameters, the obtained fidelity is around 0.85. If the final state of the exciton can successfully be measured, the heralded fidelity can be as high as 0.99. The fidelity can be improved further only if the phonon-assisted exciton transfer rate can and/or the lifetime of the exciton in the ancillary dot is increased. In principle, there could be different ways to scale our system to multiple qubits. For example, consider a chain of coupled cavities with one dot in each cavity. The ancillary dots will be off resonant with their cavity modes, so to reduce the γ , and the charged dots can be tuned in resonance to their cavity mode so to enhance the energy transfer rate Γ .

4.2 Energy transfer in quantum dot arrays

In the previous section, we have investigated the possibility of a quantum phase gate based on a three dots nanostructure as an application of our simulation of exciton energy transfer. In addition, exciton energy transfer contributes to light harvesting processes in organic and

inorganic semiconductor-based solar cells [84, 85, 86]. In these systems, a two-dot model is no longer sufficient. A multi-dot model is required. In this section, we apply a new method to study the dynamics of the exciton energy transfer in a dot array.

4.2.1 Non-Markovian quantum process TCL method

As discussed in previous chapter, we can study the dynamics of dot systems by deriving the equation of motion starting from the system's Hamiltonian. It ends up with integro-differential equations Eq.(3.12, 3.13) involving a retarded time integration over the history of the system. This non-Markovian approach provides us with a more precise description of the system dynamics. However, integro-differential equations are harder to solve than partial differential equations. In order to simplify the integro-differential equation to a partial differential equation, we may use Markovian approximation to get rid of the integral part from history of the system. Alternatively, without losing the non-Markovian feature of the system dynamics, we may use a perturbative time-convolutionless (TCL) technique [87] based on well-developed projection operator techniques [88, 89].

The method we develop in this section is based on an extension to two dots of an exactly solvable model for a single dot two-level system with TCL projection operator techniques discussed in [38]. Our goal is to use this approach to solve the excitonic dynamics of a multi-dot array. We will first investigate the behavior of a two dot system. If we have two dots, QD1 and QD2 which have different excitation energy $\hbar\omega_1$ and $\hbar\omega_2$, the system is described by the Hamiltonian,

$$\begin{aligned}
\mathcal{H} &= \mathcal{H}_0 + \mathcal{H}_I \\
\mathcal{H}_0 &= \sum_j \hbar\omega_j \sigma_j^+ \sigma_j^- + \sum_{\mathbf{k}} \hbar\omega_{\mathbf{k}} a_{\mathbf{k}}^\dagger a_{\mathbf{k}} \\
\mathcal{H}_I &= \sum_{j,k} \hbar \left[g_{\mathbf{k}}(\mathbf{r}_j) \sigma_j^+ a_{\mathbf{k}} + g_{\mathbf{k}}^*(\mathbf{r}_j) \sigma_j^- a_{\mathbf{k}}^\dagger \right],
\end{aligned} \tag{4.15}$$

where j is the label of the dot, which can be either 1 or 2 and σ_j^\pm are the excitonic creation and annihilation operators. The index \mathbf{k} denotes the different modes of the EM field with frequency $\omega_{\mathbf{k}}$, creation and annihilation operators $a_{\mathbf{k}}^\dagger$, $a_{\mathbf{k}}$ and coupling constant $g_{\mathbf{k}}(\mathbf{r}_j)$. Here $g_{\mathbf{k}}(\mathbf{r}_j)$ contains a phase which is related to the position of the two dots.

Let us introduce the states

$$\begin{aligned}
|\psi_0\rangle &= |0\rangle_s \otimes |0\rangle_{\mathbf{k}}, & |\psi_1\rangle &= |1\rangle_s \otimes |0\rangle_{\mathbf{k}}, \\
|\psi_2\rangle &= |2\rangle_s \otimes |0\rangle_{\mathbf{k}}, & |\psi_{\mathbf{k}}\rangle &= |0\rangle_s \otimes |\mathbf{k}\rangle_{\mathbf{k}},
\end{aligned} \tag{4.16}$$

where $|0\rangle_s = \sigma_1^- |1\rangle_s$ and $|1\rangle_s = \sigma_1^+ |0\rangle_s$ indicate the ground and excited state of the quantum dot in our system. The subscript s indicates system of interest. The state $|0\rangle_{\mathbf{k}}$ denotes the vacuum state of the EM field and $|\mathbf{k}\rangle_{\mathbf{k}}$ denotes the state with one photon in mode \mathbf{k} .

A general state of our system can be expressed as:

$$|\phi(t)\rangle = C_0(t)|\psi_0\rangle + C_1(t)|\psi_1\rangle + C_2(t)|\psi_2\rangle + \sum_{\mathbf{k}} C_{\mathbf{k}}(t)|\psi_{\mathbf{k}}\rangle. \tag{4.17}$$

Since our Hamiltonian conserves the number of excitations, we will restrict the discussion to a single excitation in our system. If we only allow for a single excitation, the coefficient

$C_0(t)$ is a constant which equals 0. In this thesis, we keep this $C_0(t)$ term, so that our derivation can be applied to more general systems in which the total number of excitations is not conserved.

Our interest is the exciton dynamics in the quantum dots. We can trace out the photon degrees of freedom from the total density matrix. The reduced density matrix for the excitons in the quantum dots reads as

$$\begin{aligned}
\rho_s(t) &= \text{tr}_{\mathbf{k}} |\phi(t)\rangle\langle\phi(t)| = \sum_{\mathbf{k}'} \langle\mathbf{k}'|\phi(t)\rangle\langle\phi(t)|\mathbf{k}'\rangle \\
&= |C_0(t)|^2 |0\rangle_s \langle 0| + |C_1(t)|^2 |1\rangle_s \langle 1| + |C_2(t)|^2 |2\rangle_s \langle 2| + \sum_{\mathbf{k}} |C_{\mathbf{k}}(t)|^2 |0\rangle_s \langle 0| \\
&\quad + C_0(t)C_1(t)^* |0\rangle_s \langle 1| + C_0(t)C_2(t)^* |0\rangle_s \langle 2| + C_1(t)C_0(t)^* |1\rangle_s \langle 0| \\
&\quad + C_2(t)C_0(t)^* |2\rangle_s \langle 0| + C_1(t)C_2(t)^* |1\rangle_s \langle 2| + C_2(t)C_1(t)^* |2\rangle_s \langle 1|. \tag{4.18}
\end{aligned}$$

This can be represented in matrix form as:

$$\rho_s(t) = \begin{pmatrix} |C_2(t)|^2 & C_2(t)C_1(t)^* & C_2(t)C_0(t)^* \\ C_2^*(t)C_1(t) & |C_1(t)|^2 & C_1(t)C_0(t)^* \\ C_2^*(t)C_0(t) & C_1^*(t)C_0(t) & 1 - |C_1(t)|^2 - |C_2(t)|^2 \end{pmatrix}. \tag{4.19}$$

Therefore, the time derivative of the density matrix can be written explicitly as

$$\frac{d}{dt}\rho_s(t) = \begin{pmatrix} \frac{d}{dt}|C_2(t)|^2 & \dot{C}_2(t)C_1(t)^* + C_2(t)\dot{C}_1(t)^* & \dot{C}_2(t)C_0(t)^* \\ \dot{C}_2^*(t)C_1(t) + C_2^*(t)\dot{C}_1(t) & \frac{d}{dt}|C_1(t)|^2 & \dot{C}_1(t)C_0(t)^* \\ \dot{C}_2^*(t)C_0(t) & \dot{C}_1^*(t)C_0(t) & -\frac{d}{dt}|C_1(t)|^2 - \frac{d}{dt}|C_2(t)|^2 \end{pmatrix} \tag{4.20}$$

According to \mathcal{H}_I , $|\psi_0\rangle$ is totally decoupled with the other states $|\psi_1\rangle$ and $|\psi_2\rangle$, so $C_0(t)$ is

a constant, $\dot{C}_0(t)$.

The excitonic creation and annihilation operators can also be expressed in matrix form using the same basis of the density matrix:

$$\begin{aligned}\sigma_2^+ &= \begin{pmatrix} 0 & 0 & 1 \\ 0 & 0 & 0 \\ 0 & 0 & 0 \end{pmatrix}, \quad \sigma_2^- = \begin{pmatrix} 0 & 0 & 0 \\ 0 & 0 & 0 \\ 1 & 0 & 0 \end{pmatrix}, \quad \sigma_2^+ \sigma_2^- = \begin{pmatrix} 1 & 0 & 0 \\ 0 & 0 & 0 \\ 0 & 0 & 0 \end{pmatrix}, \\ \sigma_1^+ &= \begin{pmatrix} 0 & 0 & 0 \\ 0 & 0 & 1 \\ 0 & 0 & 0 \end{pmatrix}, \quad \sigma_1^- = \begin{pmatrix} 0 & 0 & 0 \\ 0 & 0 & 0 \\ 0 & 1 & 0 \end{pmatrix}, \quad \sigma_1^+ \sigma_1^- = \begin{pmatrix} 0 & 0 & 0 \\ 0 & 1 & 0 \\ 0 & 0 & 0 \end{pmatrix}.\end{aligned}\quad (4.21)$$

Therefore, we have the following relations between these operators and the density matrix:

$$\begin{aligned}\sigma_2^+ \sigma_2^- \rho_s(t) &= \begin{pmatrix} |C_2(t)|^2 & C_2(t)C_1(t)^* & C_2(t)C_0(t)^* \\ 0 & 0 & 0 \\ 0 & 0 & 0 \end{pmatrix}, \quad \rho_s(t) \sigma_2^+ \sigma_2^- = \begin{pmatrix} |C_2(t)|^2 & 0 & 0 \\ C_2^*(t)C_1(t) & 0 & 0 \\ C_2^*(t)C_0(t) & 0 & 0 \end{pmatrix} \\ \sigma_1^+ \sigma_1^- \rho_s(t) &= \begin{pmatrix} 0 & 0 & 0 \\ C_2^*(t)C_1(t) & |C_1(t)|^2 & C_1(t)C_0(t)^* \\ 0 & 0 & 0 \end{pmatrix}, \quad \rho_s(t) \sigma_1^+ \sigma_1^- = \begin{pmatrix} 0 & C_2(t)C_1(t)^* & 0 \\ 0 & |C_1(t)|^2 & 0 \\ 0 & C_1^*(t)C_0(t) & 0 \end{pmatrix} \\ \sigma_2^- \rho_s(t) \sigma_2^+ &= \begin{pmatrix} 0 & 0 & 0 \\ 0 & 0 & 0 \\ 0 & 0 & |C_2(t)|^2 \end{pmatrix}, \quad \sigma_1^- \rho_s(t) \sigma_1^+ = \begin{pmatrix} 0 & 0 & 0 \\ 0 & 0 & 0 \\ 0 & 0 & |C_1(t)|^2 \end{pmatrix}.\end{aligned}\quad (4.22)$$

We can use these relations to rewrite the equation of motion Eq.(4.20) by defining the quantities $S_2(t) = -2\Im\{\frac{\dot{C}_2(t)}{C_2(t)}\}$, $\gamma_2(t) = -2\Re\{\frac{\dot{C}_2(t)}{C_2(t)}\}$, $S_1(t) = -2\Im\{\frac{\dot{C}_1(t)}{C_1(t)}\}$, $\gamma_1(t) =$

$-2\Re\{\frac{\dot{C}_1(t)}{C_1(t)}\}$, after some algebraic simplification, the equation of motion can be written as

$$\begin{aligned}\frac{d}{dt}\rho_S(t) &= \sum_{j=1,2} -\frac{i}{2}S_j(t)[\sigma_j^+\sigma_j^-, \rho_S(t)] + \gamma_j(t)\{\sigma_j^-\rho_S(t)\sigma_j^+ - \frac{1}{2}\sigma_j^+\sigma_j^-\rho_S(t) - \frac{1}{2}\rho_S(t)\sigma_j^+\sigma_j^-\} \\ &= K_S(t)\rho_S(t),\end{aligned}\tag{4.23}$$

where $K_S(t)$ is a super-operator defined by the above equation which has the same form of a TCL equation (discussed in the Appendix A.3). $K_S(t)$ is called the TCL generator. At this point, we have not done any approximation, Eq.(4.23) is an exact equation. Our goal is to obtain a separate equation for $K_S(t)$, which is derived from the system Hamiltonian that can be integrated in parallel with Eq.(4.23). To reach this goal, we first note that the products between the excitonic operators are given by

$$\sigma_1^+\sigma_2^- = \begin{pmatrix} 0 & 0 & 0 \\ 1 & 0 & 0 \\ 0 & 0 & 0 \end{pmatrix}, \sigma_2^+\sigma_1^- = \begin{pmatrix} 0 & 1 & 0 \\ 0 & 0 & 0 \\ 0 & 0 & 0 \end{pmatrix}.\tag{4.24}$$

Other products combining σ_1 and σ_2 are zero. Using these relations, we can find a relation for the super-operator $K_S(t)$ by applying $K_S(t)$ to $(\sigma_1^+ + \sigma_2^+)$,

$$K_S(t)(\sigma_1^+ + \sigma_2^+) = -\frac{1}{2}[\gamma_1(t) + iS_1(t)]\sigma_1^+ - \frac{1}{2}[\gamma_2(t) + iS_2(t)]\sigma_2^+.\tag{4.25}$$

The remaining step is to link the quantities γ_i and S_i with the interaction between the exciton in the quantum dots and the electromagnetic field. Let's start with the Schrödinger

equation in the interaction picture:

$$\frac{d}{dt}|\phi(t)\rangle = -i\tilde{\mathcal{H}}_I(t)|\phi(t)\rangle, \quad (4.26)$$

where $\tilde{\mathcal{H}}_I(t)$ is defined as

$$\begin{aligned} \tilde{\mathcal{H}}_I(t) &= \sum_{j,\mathbf{k}} \hbar \left[g_{\mathbf{k}}(\mathbf{r}_j) \sigma_j^+(t) a_{\mathbf{k}}(t) + g_{\mathbf{k}}^*(\mathbf{r}_j) \sigma_j^-(t) a_{\mathbf{k}}^\dagger(t) \right] \\ &= \sum_j \sigma_j^+(t) B_j(t) + \sigma_j^-(t) B_j^\dagger(t). \end{aligned} \quad (4.27)$$

Here, $\sigma_j^\pm(t) = \sigma_j^\pm \exp(\pm i\omega_j t)$. We have also defined a new operator $B_j(t)$ combining photons in all field modes and their coupling to quantum dots, which are defined as $B_j(t) = \sum_{\mathbf{k}} \hbar g_{\mathbf{k}}(\mathbf{r}_j) a_{\mathbf{k}}(t)$ with

$$a_{\mathbf{k}}^\dagger(t) = a_{\mathbf{k}}^\dagger \exp(i\omega_{\mathbf{k}} t), \quad (4.28)$$

$$a_{\mathbf{k}}(t) = a_{\mathbf{k}} \exp(-i\omega_{\mathbf{k}} t). \quad (4.29)$$

The Liouville equation for the coupled double QD system is described by

$$\frac{d\rho(t)}{dt} = \mathcal{L}(t)\rho(t) = -i[\tilde{\mathcal{H}}_I(t), \rho(t)], \quad (4.30)$$

where $\tilde{\mathcal{H}}_I(t)$ is the interaction Hamiltonian for double QD system.

With the TCL operator method [38], as shown in Appendix A.3, Eq.(4.25) can be rewritten as

$$K_S(t)(\sigma_1^+ + \sigma_2^+) = \int_0^t dt' \text{tr}_{\mathbf{k}} \{ \mathcal{L}(t) \mathcal{L}(t') (\sigma_1^+ + \sigma_2^+) \otimes \rho_{\mathbf{k}} \}, \quad (4.31)$$

where we define the vacuum state of the reservoir of photons as $\rho_{\mathbf{k}} = |0\rangle_{\mathbf{k}}\langle 0|$. Using Eq.(4.30), we obtain:

$$\begin{aligned} [\tilde{\mathcal{H}}_I(t'), \sigma_1^+ \otimes \rho_{\mathbf{k}}] &= \sigma_1^- \sigma_1^+ B_1^\dagger(t') \rho_{\mathbf{k}} \exp(-i\omega_1 t') - \sigma_1^+ \sigma_1^- \rho_{\mathbf{k}} B_1^\dagger(t') \exp(-i\omega_1 t') \\ &\quad - \sigma_1^+ \sigma_2^- \rho_{\mathbf{k}} B_2^\dagger(t') \exp(-i\omega_2 t') \\ &= \sigma_1^- \sigma_1^+ B_1^\dagger(t') \rho_{\mathbf{k}} \exp(-i\omega_1 t'), \end{aligned} \quad (4.32)$$

since $\rho_{\mathbf{k}} B_j^\dagger = 0$.

In addition, going to the second order, we have,

$$\begin{aligned} [\tilde{\mathcal{H}}_I(t), [\tilde{\mathcal{H}}_I(t'), \sigma_1^+ \otimes \rho_{\mathbf{k}}]] &= [\sigma_1^+(t) B_1(t) + \sigma_2^+(t) B_2(t), [\tilde{\mathcal{H}}_I(t'), \sigma_1^+ \otimes \rho_{\mathbf{k}}]] \\ &= \sigma_1^+ \sigma_1^- \sigma_1^+ B_1(t) B_1^\dagger(t') \rho_{\mathbf{k}} \exp(-i\omega_1(t-t')) \\ &\quad + \sigma_2^+ \sigma_1^- \sigma_1^+ B_2(t) B_1^\dagger(t') \rho_{\mathbf{k}} \exp(-i\omega_2 t - i\omega_1 t') \\ &= \sigma_1^+ B_1(t) B_1^\dagger(t') \rho_{\mathbf{k}} \exp(-i\omega_1(t-t')) \\ &\quad + \sigma_2^+ B_2(t) B_1^\dagger(t') \rho_{\mathbf{k}} \exp(-i\omega_1(t-t')) \exp(-i(\omega_2 - \omega_1)t), \end{aligned} \quad (4.33)$$

and, in the same way,

$$\begin{aligned} [\tilde{\mathcal{H}}_I(t), [\tilde{\mathcal{H}}_I(t'), \sigma_2^+ \otimes \rho_{\mathbf{k}}]] &= \sigma_2^+ B_2(t) B_2^\dagger(t') \rho_{\mathbf{k}} \exp(-i\omega_2(t-t')) \\ &\quad + \sigma_1^+ B_1(t) B_2^\dagger(t') \rho_{\mathbf{k}} \exp(-i\omega_2(t-t')) \exp(-i(\omega_1 - \omega_2)t). \end{aligned} \quad (4.34)$$

With the results of Eqs.(4.32, 4.34, 4.35) and Eq.(4.25), we get,

$$\begin{aligned}
K_s(t)(\sigma_1^+ + \sigma_2^+) &= \int_0^t dt' \text{tr}_{\mathbf{k}} \{ \mathcal{L}(t) \mathcal{L}(t') (\sigma_1^+ + \sigma_2^+) \otimes \rho_{\mathbf{k}} \} \\
&= -\frac{1}{2} [\gamma_1(t) + iS_1(t)] \sigma_1^+ - \frac{1}{2} [\gamma_2(t) + iS_2(t)] \sigma_2^+. \quad (4.35)
\end{aligned}$$

By comparing the corresponding terms, we finally find the relation between γ_i , S_i and the exciton-photon interaction constant $g_{\mathbf{k}}$,

$$\begin{aligned}
-\frac{1}{2} [\gamma_1(t) + iS_1(t)] &= \int_0^t dt' \text{tr}_{\mathbf{k}} [B_1(t) B_1^\dagger(t') \rho_{\mathbf{k}} \exp(-i\omega_1(t-t')) \\
&\quad + B_1(t) B_2^\dagger(t') \rho_{\mathbf{k}} \exp(-i\omega_2(t-t')) \exp(-i(\omega_1 - \omega_2)t)] \\
&= \int_0^t dt' F(t-t', \omega_1, 0) + F(t-t', \omega_2, \mathbf{R}) \exp(-i(\omega_1 - \omega_2)t) \\
-\frac{1}{2} [\gamma_2(t) + iS_2(t)] &= \int_0^t dt' \text{tr}_{\mathbf{k}} [B_2(t) B_2^\dagger(t') \rho_{\mathbf{k}} \exp(-i\omega_2(t-t')) \\
&\quad + B_2(t) B_1^\dagger(t') \rho_{\mathbf{k}} \exp(-i\omega_1(t-t')) \exp(-i(\omega_2 - \omega_1)t)] \\
&= \int_0^t dt' F(t-t', \omega_2, 0) + F(t-t', \omega_1, -\mathbf{R}) \exp(-i(\omega_2 - \omega_1)t).
\end{aligned}$$

The function $F(\tau, \omega, \mathbf{r})$ is defined as in the previous chapter,

$$F(\tau, \omega, \mathbf{r}) = \sum_{\mathbf{k}} |g_{\mathbf{k}}|^2 \exp(-i\omega_{\mathbf{k}}\tau) \exp(i\omega\tau) \exp(i\mathbf{k}\mathbf{r}). \quad (4.36)$$

As a result,

$$\begin{aligned}
\gamma_1(t) &= 2 \int_0^t dt' \Re[F(t-t', \omega_1, 0)] + \Re[F(t-t', \omega_2, \mathbf{R}) \exp(-i(\omega_1 - \omega_2)t)] \\
S_1(t) &= 2 \int_0^t dt' \Im[F(t-t', \omega_1, 0)] + \Im[F(t-t', \omega_2, \mathbf{R}) \exp(-i(\omega_1 - \omega_2)t)] \quad (4.37) \\
\gamma_2(t) &= 2 \int_0^t dt' \Re[F(t-t', \omega_2, 0)] + \Re[F(t-t', \omega_1, -\mathbf{R}) \exp(-i(\omega_2 - \omega_1)t)] \\
S_2(t) &= 2 \int_0^t dt' \Im[F(t-t', \omega_2, 0)] + \Im[F(t-t', \omega_1, -\mathbf{R}) \exp(-i(\omega_2 - \omega_1)t)].
\end{aligned}$$

As shown above, the TCL projection operator technique has several advantages applied to our dot system. These quantities γ_i and S_i can be calculated before looking at the evolution of the quantum dot system and they keep the system history. Therefore, without Markovian approximation, we equivalently divide the whole integro-differential equations (3.12, 3.13) into integrals (4.37) and a PDE (4.23) for the density matrix. In addition, we can expand our two-dot approach to describe a situation with many dots (such as a quantum dot array) without going through the whole derivation of the equation of motion. We may calculate the γ_i and S_i coefficient for the new configuration, and solve the PDE with an expanded density matrix to simulate the dynamics of the quantum dot array.

4.2.2 Multi-dot array

As discussed in previous section, we could expand our dot system to multi dots system with the help of TCL method. In this section, we go through the derivation of the equation of motion for dot array with the same method. We first start from the system Hamiltonian,

$$\begin{aligned}
\mathcal{H} &= \mathcal{H}_0 + \mathcal{H}_I \\
\mathcal{H}_0 &= \sum_j \hbar\omega_j \sigma_j^+ \sigma_j^- + \sum_{\mathbf{k}} \hbar\omega_{\mathbf{k}} a_{\mathbf{k}}^\dagger a_{\mathbf{k}} \\
\mathcal{H}_I &= \sum_{j,k} \hbar \left[g_{\mathbf{k}}(\mathbf{r}_j) \sigma_j^+ a_{\mathbf{k}} + g_{\mathbf{k}}^*(\mathbf{r}_j) \sigma_j^- a_{\mathbf{k}}^\dagger \right],
\end{aligned} \tag{4.38}$$

where j is the label of the dot, which can be from 1 to N (the total number of dots). σ_j^\pm are the excitonic creation and annihilation operators. The index k denotes the different modes of the EM field with frequency $\omega_{\mathbf{k}}$, creation and annihilation operators $a_{\mathbf{k}}^\dagger$, $a_{\mathbf{k}}$ and coupling constant $g_{\mathbf{k}}(\mathbf{r}_j)$. Here $g_{\mathbf{k}}(\mathbf{r}_j)$ contains a phase which is related to the position of the dots.

With the same notation, a general state of our system can be expressed as:

$$|\phi(t)\rangle = C_0(t)|\psi_0\rangle + \sum_{j=1}^N C_j(t)|\psi_j\rangle + \sum_{\mathbf{k}} C_{\mathbf{k}}(t)|\psi_{\mathbf{k}}\rangle. \tag{4.39}$$

where $|0\rangle_s = \sigma_j^- |j\rangle_s$ and $|j\rangle_s = \sigma_j^+ |0\rangle_s$ indicate the ground and excited state of the quantum dot in our system.

The reduced density matrix for the excitons in the quantum dots is now expanded into a $N + 1$ by $N + 1$ matrix,

$$\rho_S(t) = \text{tr}_{\mathbf{K}} |\phi(t)\rangle\langle\phi(t)| \quad (4.40)$$

$$= \begin{pmatrix} |C_N(t)|^2 & \cdots & C_N(t)C_1(t)^* & C_N(t)C_0(t)^* \\ \vdots & \ddots & & \\ C_N(t)^*C_1(t) & & |C_1(t)|^2 & C_1(t)C_0(t)^* \\ C_N(t)^*C_0(t) & & C_1(t)^*C_0(t) & 1 - \sum_{j=1}^N |C_j(t)|^2 \end{pmatrix}. \quad (4.41)$$

Therefore, the time derivative of the density matrix can be written explicitly as

$$\frac{d}{dt}\rho_S(t) = \begin{pmatrix} \frac{d}{dt}|C_N(t)|^2 & \cdots & \dot{C}_N(t)C_1(t)^* + C_N(t)\dot{C}_1(t)^* & \dot{C}_N(t)C_0(t)^* \\ \vdots & \ddots & & \\ \dot{C}_N(t)^*C_1(t) + C_N(t)^*\dot{C}_1(t) & & \frac{d}{dt}|C_1(t)|^2 & \dot{C}_1(t)C_0(t)^* \\ \dot{C}_N(t)^*C_0(t) & & \dot{C}_1(t)^*C_0(t) & -\sum_{j=1}^N \frac{d}{dt}|C_j(t)|^2 \end{pmatrix}.$$

According to \mathcal{H}_I , $|\psi_0\rangle$ is totally decoupled with the other states $|\psi_j\rangle$, so $C_0(t)$ is a constant, $\dot{C}_0(t) = 0$.

The excitonic creation and annihilation operators can also be expressed in matrix form using the same basis of the density matrix. The elements in the density matrix can be expressed as,

$$[\sigma_j^+]_{i,k} = \begin{cases} 1 & \text{For } i = N - j \text{ and } k = N + 1 \\ 0 & \text{Otherwise} \end{cases}$$

$$[\sigma_j^-]_{i,k} = \begin{cases} 1 & \text{For } i = N + 1 \text{ and } k = N - j \\ 0 & \text{Otherwise} \end{cases}$$

$$[\sigma_j^+ \sigma_j^-]_{i,k} = \begin{cases} 1 & \text{For } i = N - j \text{ and } k = N - j \\ 0 & \text{Otherwise} \end{cases}. \quad (4.42)$$

Explicitly in matrix form,

$$\sigma_j^+ = \begin{pmatrix} 0 & \cdots & 0 \\ \vdots & \cdots & \vdots & N - j - 1 \\ 0 & \cdots & 1 \\ \vdots & \cdots & \vdots & j - 1 \\ 0 & \cdots & 0 \\ N - 1 \end{pmatrix}, \quad \sigma_j^- = \begin{pmatrix} 0 & \cdots & 0 & \cdots & 0 \\ \vdots & \vdots & \vdots & \vdots & \vdots & N - 1 \\ 0 & \cdots & 1 & \cdots & 0 \\ N - j - 1 & & j - 1 \end{pmatrix},$$

$$\sigma_j^+ \sigma_j^- = \begin{pmatrix} 0 & \cdots & 0 & \cdots & 0 \\ \vdots & \ddots & \vdots & \vdots & \vdots & N - j - 1 \\ 0 & \cdots & 1 & \cdots & 0 \\ \vdots & \cdots & \vdots & \ddots & \vdots & j - 1 \\ 0 & \cdots & 0 & \cdots & 0 \\ N - j - 1 & & j - 1 \end{pmatrix}. \quad (4.43)$$

With these definitions of creation and annihilation operators, we can simply represent $\sigma_j^+ \sigma_j^- \rho_S(t)$, $\rho_S(t) \sigma_j^+ \sigma_j^-$ and $\sigma_j^- \rho_S(t) \sigma_j^+$ in matrix form, so that we are able to rewrite the equation of motion by defining the quantities $S_j(t) = -2\Im\{\frac{\dot{C}_j(t)}{C_j(t)}\}$, $\gamma_j(t) = -2\Re\{\frac{\dot{C}_j(t)}{C_j(t)}\}$, the equation of motion can be expressed in a compact form,

$$\begin{aligned} \frac{d}{dt} \rho_S(t) &= \sum_{j=1}^N -\frac{i}{2} S_j(t) [\sigma_j^+ \sigma_j^-, \rho_S(t)] + \gamma_j(t) \{ \sigma_j^- \rho_S(t) \sigma_j^+ - \frac{1}{2} \sigma_j^+ \sigma_j^- \rho_S(t) - \frac{1}{2} \rho_S(t) \sigma_j^+ \sigma_j^- \} \\ &= K_S^N(t) \rho_S(t), \end{aligned} \quad (4.44)$$

where $K_s^N(t)$ is a super-operator for a N dot array defined by the above equation.

Using the same approach we used in deriving Eq.(4.25), we obtain a equation for the new defined super-operator $K_s^N(t)$.

First, we need to check the products between the excitonic operators.

$$[\sigma_j^+ \sigma_{j'}^-]_{i,k} = \begin{cases} 1 & \text{For } i = N - j \text{ and } k = N - j' \\ 0 & \text{Otherwise} \end{cases}. \quad (4.45)$$

In matrix form, it reads,

$$\sigma_j^+ \sigma_{j'}^- = \begin{pmatrix} 0 & \dots & 0 & \dots & 0 \\ \vdots & \ddots & \vdots & \vdots & \vdots & N - j - 1 \\ 0 & \dots & 1 & \dots & 0 \\ \vdots & \dots & \vdots & \ddots & \vdots & j - 1 \\ 0 & \dots & 0 & \dots & 0 \\ N - j' - 1 & & j' - 1 & & \end{pmatrix}. \quad (4.46)$$

Other products combining σ_j and $\sigma_{j'}$ are all zero. Using these relations, we find a relation for the super-operator $K_s^N(t)$.

$$K_s^N(t) \sum_{j=1}^N \sigma_j^+ = -\frac{1}{2} \sum_{j=1}^N [\gamma_j(t) + iS_j(t)] \sigma_j^+ \quad (4.47)$$

The remaining question is to link the quantities γ_i and S_i with the interaction between the exciton in the quantum dots and the electromagnetic field. Let's start with the Schrödinger

equation in the interaction picture:

$$\frac{d}{dt}|\phi(t)\rangle = -i\tilde{\mathcal{H}}_I(t)|\phi(t)\rangle, \quad (4.48)$$

where $\tilde{\mathcal{H}}_I(t)$ is defined as

$$\begin{aligned} \tilde{\mathcal{H}}_I(t) &= \sum_{j,k} \hbar \left[g_{\mathbf{k}}(\mathbf{r}_j) \sigma_j^+(t) a_{\mathbf{k}}(t) + g_{\mathbf{k}}^*(\mathbf{r}_j) \sigma_j^-(t) a_{\mathbf{k}}^\dagger(t) \right] \\ &= \sum_j \sigma_j^+(t) B_j(t) + \sigma_j^-(t) B_j^\dagger(t). \end{aligned} \quad (4.49)$$

Here, $\sigma_j^\pm(t) = \sigma_j^\pm \exp(\pm i\omega_j t)$. We have also defined a new operator $B_j(t)$ combining photons in all field modes and their coupling to quantum dots, which are defined as $B_j(t) = \sum_{\mathbf{k}} \hbar g_{\mathbf{k}}(\mathbf{r}_j) a_{\mathbf{k}}(t)$ with

$$a_{\mathbf{k}}^\dagger(t) = a_{\mathbf{k}}^\dagger \exp(i\omega_{\mathbf{k}} t), \quad (4.50)$$

$$a_{\mathbf{k}}(t) = a_{\mathbf{k}} \exp(-i\omega_{\mathbf{k}} t). \quad (4.51)$$

The Liouville equation for the coupled double QD system is described by

$$\frac{d\rho_S}{dt} = \mathcal{L}(t)\rho = -i[\tilde{\mathcal{H}}_I(t), \rho], \quad (4.52)$$

where $\tilde{\mathcal{H}}_I(t)$ is the interaction Hamiltonian for double QD system.

With the time convolutionless operator method,

$$K_s^N(t)(\sum_j \sigma_j^+) = \int_0^t dt' \text{tr}_{\mathbf{k}}\{\mathcal{L}(t)\mathcal{L}(t')(\sum_j \sigma_j^+) \otimes \rho_{\mathbf{k}}\}, \quad (4.53)$$

Using Eq.(4.52), we obtain:

$$\begin{aligned} [\tilde{\mathcal{H}}_I(t'), \sigma_j^+ \otimes \rho_{\mathbf{k}}] &= \sigma_j^- \sigma_j^+ B_j^\dagger(t') \rho_{\mathbf{k}} \exp(-i\omega_j t') - \sigma_j^+ \sigma_j^- \rho_{\mathbf{k}} B_j^\dagger(t') \exp(-i\omega_j t') \\ &\quad - \sigma_j^+ \sigma_l^- \rho_{\mathbf{k}} B_l^\dagger(t') \exp(-i\omega_l t') \\ &= \sigma_j^- \sigma_j^+ B_j^\dagger(t') \rho_{\mathbf{k}} \exp(-i\omega_j t'), \end{aligned} \quad (4.54)$$

since $\rho_{\mathbf{k}} B_l^\dagger = 0$.

In addition, going to the next order, we have,

$$\begin{aligned} [\tilde{\mathcal{H}}_I(t), [\tilde{\mathcal{H}}_I(t'), \sigma_j^+ \otimes \rho_{\mathbf{k}}]] &= \left[\sum_l \sigma_l^+(t) B_l(t), [\tilde{\mathcal{H}}_I(t'), \sigma_j^+ \otimes \rho_{\mathbf{k}}] \right] \\ &= \sum_l \sigma_l^+ \sigma_j^- \sigma_j^+ B_l(t) B_j^\dagger(t') \rho_{\mathbf{k}} \exp(-i\omega_l t - i\omega_j t') \\ &= \sigma_j^+ B_j(t) B_j^\dagger(t') \rho_{\mathbf{k}} \exp(-i\omega_j(t - t')) \\ &\quad + \sum_{l \neq j} \sigma_l^+ B_l(t) B_j^\dagger(t') \rho_{\mathbf{k}} \exp(-i\omega_j(t - t')) \exp(-i(\omega_l - \omega_j)t), \end{aligned} \quad (4.55)$$

With the results of Eqs.(4.54, 4.56) and Eq.(4.53),

$$\begin{aligned} K_s^N(t)(\sum_j \sigma_j^+) &= \int_0^t dt' \text{tr}_{\mathbf{k}}\{\mathcal{L}(t)\mathcal{L}(t')(\sum_j \sigma_j^+) \otimes \rho_{\mathbf{k}}\} \\ &= \sum_j -\frac{1}{2}[\gamma_j(t) + iS_j(t)]\sigma_j^+, \end{aligned} \quad (4.56)$$

By comparing the corresponding terms, we finally find the relation between γ_i , S_i and the

exciton-photon interaction constant $g_{\mathbf{k}}$,

$$\begin{aligned}
-\frac{1}{2}[\gamma_j(t) + iS_j(t)] &= \int_0^t dt' \text{tr}_{\mathbf{k}}[B_j(t)B_j^\dagger(t')\rho_{\mathbf{k}} \exp(-i\omega_j(t-t')) \\
&+ \sum_{l \neq j} B_j(t)B_l^\dagger(t')\rho_{\mathbf{k}} \exp(-i\omega_l(t-t')) \exp(-i(\omega_j - \omega_l)t)] \\
&= \int_0^t dt' F(t-t', \omega_j, 0) + \sum_{l \neq j} F(t-t', \omega_l, (l-j)\mathbf{R}) \exp(-i(\omega_j - \omega_l)t)
\end{aligned} \tag{4.57}$$

The function $F(\tau, \omega, \mathbf{r})$ is defined as in the previous chapter,

$$F(\tau, \omega, \mathbf{r}) = \sum_{\mathbf{k}} |g_{\mathbf{k}}|^2 \exp(-i\omega_{\mathbf{k}}\tau) \exp(i\omega\tau) \exp(i\mathbf{k}\mathbf{r}). \tag{4.58}$$

As a result,

$$\begin{aligned}
\gamma_j(t) &= 2 \int_0^t dt' \Re[F(t-t', \omega_j, 0)] + \Re[\sum_{l \neq j} F(t-t', \omega_l, (l-j)\mathbf{R}) \exp(-i(\omega_j - \omega_l)t)] \\
S_j(t) &= 2 \int_0^t dt' \Im[F(t-t', \omega_j, 0)] + \Im[\sum_{l \neq j} F(t-t', \omega_l, (l-j)\mathbf{R}) \exp(-i(\omega_j - \omega_l)t)].
\end{aligned} \tag{4.59}$$

It is shown in the above equation, the first term in $\gamma_j(t)$ and $S_j(t)$ indicates the on-site interaction. The second term with the summation over all dots l different from dot j shows the interaction between different dots which effectively causes the energy transfer. With the

set of $\gamma_j(t)$ and $S_j(t)$, we can finally obtain the equation of motion for N dots,

$$\frac{d}{dt}\rho_S(t) = \sum_{j=1}^N -\frac{i}{2}S_j(t)[\sigma_j^+\sigma_j^-, \rho_S(t)] + \gamma_j(t)\{\sigma_j^-\rho_S(t)\sigma_j^+ - \frac{1}{2}\sigma_j^+\sigma_j^-\rho_S(t) - \frac{1}{2}\rho_S(t)\sigma_j^+\sigma_j^-\}. \quad (4.60)$$

For different systems, the form of Eq.(4.60) remains the same. Eq.(4.60) can be treated as a general starting point of the simulation for different multi dot systems.

Compared with master equation in the Lindblad form which has time independent coupling terms, Eq.(4.60) has time dependent terms $S_j(t)$ and $\gamma_j(t)$, which contain the history of the system. In addition, the details of the system such as the configuration of the dots and the coupling between the dots is only specified in $S_j(t)$ and $\gamma_j(t)$. This method we adopted is a general method which could apply to different multi-dot systems. Thus, finding $S_j(t)$ and $\gamma_j(t)$ for a certain system setup is the key to simulate the exciton dynamics in that particular system. This theory is ready to applied to specific devices which has not been done in this thesis.

Chapter 5

Conclusion and outlook

We have presented in Chapter 2 a theoretical review of concepts important to the physics of energy transfer in semiconductor nanostructures. In particular a full quantum mechanical treatment of the Wannier-Mott exciton was provided. We have obtained the energy of the exciton by exploiting the well-known solution to the Schrödinger equation for the hydrogen atom. Furthermore, we have extended the discussion from excitons in bulk materials to excitons in quantum dots. In disk-like quantum dots which are the main focus of this thesis, we obtained a 2D hydrogen-like problem, due to the strong confinement in the growth direction of the sample (z -direction). The modification to the exciton energy due to the confinement has two different contributions. The first is the quantization energy of electrons and holes in the z -direction. The second is the difference between the hydrogenic eigenenergies for a 3D and 2D Coulomb problems.

In the description of exciton energy transfer in photon-confined system, two novel approaches have been used. First of all, instead of treating the exciton-photon interaction semiclassically [18, 19, 20, 21], we started from the quantized EM field operator to calculate

the coupling constant of the exciton-photon interaction. The advantage of the approach is that this method can be used to calculate the exciton-photon interaction in planar microcavity by replacing the free space EM field operator by the EM field operator of the microcavity. Generally speaking, this approach can be applied to any photon confined system as long as the EM field operator for that system is given. With the Hamiltonian given, in Chapter 3, we were able to do the numerical simulation of the dynamics of the exciton transfer in a cavity by solving the Schrödinger equation for the coupled system of excitons and photons. For the single dot simulation, the spontaneous exciton recombination was obtained without including a phenomenological damping term in the equations. This is a nice feature of the full quantum mechanical treatment. In the same simulation, the Purcell effect is recovered from the result that the spontaneous emission rate is highly suppressed when the microcavity is off-resonance (when the exciton energy in the quantum dot is lower than the energy of the lowest allowed cavity mode). Although these results were obtained in a single dot simulation, they proved the validity of our treatment to describe the exciton-photon interaction and cavity effects. For two-dot simulation, we have found that the exciton energy transfer only occurs when the two dots have the same exciton energy, which corresponds to the resonant condition or the elastic transfer. We have also found that the inter-dot separation dependence of the effective transfer rate is R^{-1} in the planar cavity, compared with the energy transfer rate in the free space which is either R^{-6} for Förster transfer or R^{-2} for radiative transfer. This difference originates from the different photon density of state and indicates the possibility of ultra-long range energy transfer in a 2D system [14].

The second novel approach introduced in this thesis was to include phonon effect in our simulation. Although exciton energy transfer phenomenon between quantum dots have

been widely studied [13, 14, 15, 16, 17, 18, 19, 20, 21], the mechanism of phonon assisted inelastic energy transfer had not been explored before this thesis. In order to investigate the inelastic energy transfer, we added to the Hamiltonian the exciton-phonon interaction by the deformation potential of the material [36, 49]. Using the independent boson model [49], we have derived an effective exciton-photon-phonon interaction from the combined effect of exciton-photon interaction and exciton-phonon interaction. In the inelastic energy transfer, the phonon can bring in or take away the extra energy to compensate the energy detuning between the two dots, and enables the inelastic energy transfer process between the two dots in the presence of detuning. As shown in the simulation, although the transition rate for inelastic transfer is lower than the transition rate for the elastic transfer, a relatively efficient energy transfer is still observed compared to the spontaneous exciton recombination. This result suggests a possible mechanism of the exciton energy transfer between self-assembled quantum dots of different size.

One direct application of the phonon-assisted energy transfer model is in the field of quantum computing. A semiconductor based Quantum Zeno gate has been proposed in this thesis based on Dr. Y.P. Huang and Prof. M. Moore's idea [37]. In the gate operation, the phonon-assisted energy transfer, acting as fast dissipation channels, is regarded as a continuous measurement that enables the Quantum Zeno effect [7]. Three lateral dots are proposed in system configuration to realize a two qubit conditional phase gate. In the gate design, only the ancillary dot is operated by the laser. The two target dots in which the electron spins represent the qubits interact with the ancillary dot through the Quantum Zeno effect. There are three main physical quantities that control the whole gate operation. Ω is the Rabi strength of the driving laser. γ is the spontaneous photon-emission rate of

the ancillary dot. Γ the dissipation rate from the ancillary dot to the target dots. The criterion for a successful gate operation is that $\gamma \ll \Omega \ll \Gamma$. After the discussion of the possibility of the Quantum Zeno gate, the fidelity of the gate was optimized theoretically. The optimized fidelity can be expressed as $\mathcal{F}_{\text{opt}} \geq \mathcal{F}(\Omega_{\text{opt}}) = \exp\left[-\frac{10}{3}\sqrt{\frac{\gamma}{\Gamma}}\right]$ for the optimized $\Omega_{\text{opt}} = \sqrt{\gamma\Gamma/8}$. With given physical parameters, the gate was also calculated numerically. The gate fidelity reached up to 0.85, when we choose a set of realistic parameters in GaAs quantum dots ($\Gamma = 20 \text{ ns}^{-1}$, $\gamma = 0.08 \text{ ns}^{-1}$, $\Omega = 0.45 \text{ ns}^{-1}$).

Finally, we extended our exciton energy transfer model to describe innovative light harvesting systems. The subject of the study changed from excitons in two dots to exciton in multiple dots. This required the formulation of a theory with good scalability. The non-Markovian time-convolutionless technique (TCL), which was used to describe the spontaneous emission in a two level system in Breuer and Petruccione's book [38] provided a good starting point. First of all, this approach keeps the system memory in the dynamics, i.e. including non-Markovian effects. Secondly, as derived in Chapter 4, it is straight forward to expand this method to a N dot system and the complexity of the problem grows only quadratically with the number of the dots. This TCL model is a general theory that can be applied to any physical system characterized by exciton-photon interaction and exciton and photon confinement. So far, the theory we have developed for multi-dot systems has not yet been applied to a specific device. It could be applied to light harvesting devices and quantum computing implementations where interactions between photons and quantum dots play a critical role. One possible application to quantum computation could be the simulation of the so-called quantum cellular automation. As proposed in Seth Lloyd's paper [90], arrays of weakly coupled quantum dots interacting with a sequence of laser pulse of well-defined

frequency and length can be regarded as a quantum-mechanical micromanipulator. It is capable of both creating any desired quantum state(qubit) of the array and transforming that state(qubit configuration) in the array in any desired way. This micromanipulator is believed to be a realizable quantum computer.

For future study, we have several ideas to explore. We could simulate the energy transfer in more complex geometries (any arbitrary cavity shape), which could be helpful in real device design. As an application of the multi-dot TCL model, it would be interesting to explore the open question about enhancing the energy transfer by optimizing the configuration of the quantum dots. In this problem, there are many controllable parameters, such as the size of the dots, the distance between the dots, the material of the dots and the type of photon confinement that can be adjusted. Finally, a challenging but interesting task would be to include the phonon effect into our multi-dot model. This could be very important in describing dissipative process in systems with many dots.

APPENDICES

Appendix A

Projection operator techniques

A.1 Projection operators

Projection operator techniques provide a general framework to derive exact equations of motion of an open quantum system. The basic idea is to define the operation of tracing over the environment as a formal projection $\rho \rightarrow \mathcal{P}\rho$ in the state space of the total system. The super-operator \mathcal{P} has the property of a projection operator, and the density matrix $\mathcal{P}\rho$ is said to be the relevant part of the density matrix ρ of the total system which contains the complete information required to reconstruct the reduced density matrix ρ_S of the open system. Explicitly, ρ_S is the reduced density matrix that indicates the system of interest; ρ_B the reduced density matrix that indicates the bath. We have then

$$\rho \rightarrow \mathcal{P}\rho = tr_B\{\rho\} \otimes \rho_B \equiv \rho_S \otimes \rho_B, \quad (\text{A.1})$$

where ρ_B is some fixed state of the environment bath. tr_B is the partial trace over the bath. Correspondingly, a complementary super-operator \mathcal{Q} which represents a projection $\rho \rightarrow \mathcal{Q}\rho$

onto the irrelevant part can be defined as,

$$\rho \rightarrow \mathcal{Q}\rho = \rho - \mathcal{P}\rho \quad (\text{A.2})$$

The aim for this approach is to derive a closed equation of motion for the relevant part $\mathcal{P}\rho$.

These super-operators have the obvious properties

$$\mathcal{P} + \mathcal{Q} = I, \quad (\text{A.3})$$

$$\mathcal{P}^2 = \mathcal{P}, \quad (\text{A.4})$$

$$\mathcal{Q}^2 = \mathcal{Q}, \quad (\text{A.5})$$

$$\mathcal{P}\mathcal{Q} = \mathcal{Q}\mathcal{P} = 0, \quad (\text{A.6})$$

which can be easily checked using the definitions Eq.(A.1) and (A.2) and assuming ρ_B to be normalized.

A.2 The Nakajima-Zwanzig equation

We consider the time evolution of an open system S coupled to an environment B. The dynamics of the density matrix $\rho(t)$ of the combined system is specified by Hamiltonian of the form,

$$H = H_0 + \alpha H_I, \quad (\text{A.7})$$

where H_0 generates the uncoupled time evolution of the system and environment. H_I indicates the interaction between the system and environment. In interaction picture, the

equation of motion for the density matrix reads,

$$\frac{\partial}{\partial t}\rho(t) = -i\alpha[H_I(t), \rho(t)] \equiv \alpha\mathcal{L}(t)\rho(t). \quad (\text{A.8})$$

The Liouville super-operator is denoted by $\mathcal{L}(t)$. This equation is known as the Liouville-von Neumann equation.

By applying the projection operators \mathcal{P} and \mathcal{Q} to the Liouville-von Neumann equation and assuming the environment state ρ_B to be time independent, the relevant and the irrelevant part of the density matrix $\mathcal{P}\rho(t)$ and $\mathcal{Q}\rho(t)$ satisfy the equations,

$$\frac{\partial}{\partial t}\mathcal{P}\rho(t) = \mathcal{P}\frac{\partial}{\partial t}\rho(t) = \alpha\mathcal{P}\mathcal{L}(t)\rho(t), \quad (\text{A.9})$$

$$\frac{\partial}{\partial t}\mathcal{Q}\rho(t) = \mathcal{Q}\frac{\partial}{\partial t}\rho(t) = \alpha\mathcal{Q}\mathcal{L}(t)\rho(t). \quad (\text{A.10})$$

These two equations can be rewritten by inserting the identity $\mathcal{I} = \mathcal{P} + \mathcal{Q}$ between $\mathcal{L}(t)$ and $\rho(t)$,

$$\frac{\partial}{\partial t}\mathcal{P}\rho(t) = \alpha\mathcal{P}\mathcal{L}(t)\mathcal{P}\rho(t) + \alpha\mathcal{P}\mathcal{L}(t)\mathcal{Q}\rho(t), \quad (\text{A.11})$$

$$\frac{\partial}{\partial t}\mathcal{Q}\rho(t) = \alpha\mathcal{Q}\mathcal{L}(t)\mathcal{P}\rho(t) + \alpha\mathcal{Q}\mathcal{L}(t)\mathcal{Q}\rho(t). \quad (\text{A.12})$$

In order to get a closed equation for the relevant part of the density matrix $\mathcal{P}\rho$, we solve Eq.(A.12) and insert the solution into Eq.(A.11). The formal solution of Eq.(A.12) corresponding to a given $\rho(t_0)$ at some initial time t_0 may be expressed as

$$\mathcal{Q}\rho(t) = \mathcal{G}(t, t_0)\mathcal{Q}\rho(t_0) + \alpha \int_{t_0}^t ds \mathcal{G}(t, s) \mathcal{Q}\mathcal{L}(s) \mathcal{P}\rho(s), \quad (\text{A.13})$$

where the propagator $\mathcal{G}(t, s)$ is defined as

$$\mathcal{G}(t, s) \equiv T_{\leftarrow} \exp \left[\alpha \int_s^t ds' \mathcal{Q}\mathcal{L}(s') \right]. \quad (\text{A.14})$$

The time ordering operator T_{\leftarrow} orders any product of super-operators such that the time arguments increase from right to left. The propagator $\mathcal{G}(t, s)$ satisfies the differential equation

$$\frac{\partial}{\partial t} \mathcal{G}(t, s) = \alpha \mathcal{Q}\mathcal{L}(t) \mathcal{G}(t, s) \quad (\text{A.15})$$

with the initial condition $\mathcal{G}(s, s) = I$.

In order to check the validity of the solution to Eq.(A.12), we take a partial time derivative on both sides of Eq. (A.13), and we obtain,

$$\begin{aligned} \frac{\partial}{\partial t} \mathcal{Q}\rho(t) &= \frac{\partial}{\partial t} \mathcal{G}(t, t_0) \mathcal{Q}\rho(t_0) + \alpha \frac{\partial}{\partial t} \int_{t_0}^t ds \mathcal{G}(t, s) \mathcal{Q}\mathcal{L}(s) \mathcal{P}\rho(s), \\ &= \alpha \mathcal{Q}\mathcal{L}(t) \mathcal{G}(t, t_0) \mathcal{Q}\rho(t_0) + \alpha \mathcal{G}(t, t) \mathcal{Q}\mathcal{L}(t) \mathcal{P}\rho(t), \\ &= \alpha \mathcal{Q}\mathcal{L}(t) \mathcal{Q}\rho(t) + \alpha \mathcal{Q}\mathcal{L}(t) \mathcal{P}\rho(t), \end{aligned} \quad (\text{A.16})$$

which is exactly Eq.(A.12).

Inserting the expression Eq.(A.13) for $\mathcal{Q}\rho(t)$ into the equation of motion Eq.(A.11), we

obtain the the desired closed equation for the relevant part of the density matrix $\mathcal{P}\rho(t)$,

$$\begin{aligned}
\frac{\partial}{\partial t}\mathcal{P}\rho(t) &= \alpha\mathcal{P}\mathcal{L}(t)\mathcal{G}(t, t_0)\mathcal{Q}\rho(t_0) + \alpha\mathcal{P}\mathcal{L}(t)\mathcal{P}\rho(t) \\
&\quad + \alpha^2 \int_{t_0}^t ds \mathcal{P}\mathcal{L}(t)\mathcal{G}(t, s)\mathcal{Q}\mathcal{L}(s)\mathcal{P}\rho(s), \\
&= \alpha\mathcal{P}\mathcal{L}(t)\mathcal{G}(t, t_0)\mathcal{Q}\rho(t_0) + \alpha\mathcal{P}\mathcal{L}(t)\mathcal{P}\rho(t) \\
&\quad + \int_{t_0}^t ds \mathcal{P}\mathcal{K}(t, s)\mathcal{P}\rho(s). \tag{A.17}
\end{aligned}$$

This equation is known as the Nakajima-Zwanzig equation. It is an exact equation for the relevant degrees of freedom of the reduced system. It describes non-Markovian memory effects in the dynamics with an integral over the past history of the system. The memory kernel $\mathcal{K}(t, s) = \alpha^2\mathcal{P}\mathcal{L}(t)\mathcal{G}(t, s)\mathcal{Q}\mathcal{L}(s)\mathcal{P}$ represents a super-operator in the relevant subspace.

A.3 Time-convolutionless projection operator method

The Nakajima-Zwanzig equation with time convolution in the memory kernel is usually as difficult to solve as the Liouville equation describing the dynamics of the total system. In this section we show how to remove the time convolution through a method which is known as the time convolutionless projection operator method. In order to achieve this objective, we first replace the density matrix $\rho(s)$ on the right-hand side of Eq.(A.13) by

$$\rho(s) = G(t, s)\rho(t) = G(t, s)(\mathcal{P} + \mathcal{Q})\rho(t), \tag{A.18}$$

where $G(t, s)$ is the backward propagator of the system defined as

$$G(t, s) \equiv T_{\rightarrow} \exp \left[-\alpha \int_s^t ds' \mathcal{L}(s') \right]. \quad (\text{A.19})$$

The equation for the irrelevant part of the density matrix Eq.(A.13) can be rewritten as

$$\mathcal{Q}\rho(t) = \mathcal{G}(t, t_0)\mathcal{Q}\rho(t_0) + \alpha \int_{t_0}^t ds \mathcal{G}(t, s)\mathcal{Q}\mathcal{L}(s)\mathcal{P}G(t, s)(\mathcal{P} + \mathcal{Q})\rho(t). \quad (\text{A.20})$$

Introducing another new super-operator

$$\Sigma(t) = \alpha \int_{t_0}^t ds \mathcal{G}(t, s)\mathcal{Q}\mathcal{L}(s)\mathcal{P}G(t, s), \quad (\text{A.21})$$

and rearranging the equation above, we can express the irrelevant part of the density matrix as

$$[1 - \Sigma(t)]\mathcal{Q}\rho(t) = \mathcal{G}(t, t_0)\mathcal{Q}\rho(t_0) + \Sigma(t)\mathcal{P}\rho(t). \quad (\text{A.22})$$

Note that the super-operator $\Sigma(t)$ contains both propagators \mathcal{G} and G , so that it does not specify a well-defined chronological order. By its definition, $\Sigma(t)$ has the properties, $\Sigma(t_0) = 0$ and $\Sigma(t)|_{\alpha=0} = 0$. Hence, $1 - \Sigma(t)$ can be inverted in case for small $t - t_0$ or small coupling α . We get

$$\mathcal{Q}\rho(t) = [1 - \Sigma(t)]^{-1}\mathcal{G}(t, t_0)\mathcal{Q}\rho(t_0) + [1 - \Sigma(t)]^{-1}\Sigma(t)\mathcal{P}\rho(t). \quad (\text{A.23})$$

This equation shows that the irrelevant part $\mathcal{Q}\rho(t)$ of the density matrix can be determined from the relevant part $\mathcal{P}\rho(t)$ at time t and from the initial condition $\mathcal{Q}\rho(t_0)$. The explicit dependence on the history of the relevant part which occurs in the Nakajima-Zwanzig equa-

tion (A.17) has thus been removed by introducing history dependent super-operator $\Sigma(t)$ which contains the propagator $\mathcal{G}(t, s)$ and the backward propagator $G(t, s)$.

By inserting this equation for the irrelevant part into the right hand side of Eq.(A.11), we get

$$\frac{\partial}{\partial t} \mathcal{P}\rho(t) = \mathcal{K}(t)\mathcal{P}\rho(t) + \mathcal{I}(t)\mathcal{Q}\rho(t_0), \quad (\text{A.24})$$

with the Time Convolutionless(TCL) generator,

$$\mathcal{K}(t) = \alpha\mathcal{P}\mathcal{L}(t) [1 - \Sigma(t)]^{-1} \mathcal{P}, \quad (\text{A.25})$$

and the inhomogeneity operator defined as

$$\mathcal{I}(t) = \alpha\mathcal{P}\mathcal{L}(t) [1 - \Sigma(t)]^{-1} \mathcal{G}(t, t_0) \mathcal{Q}. \quad (\text{A.26})$$

For a factorized initial condition $\rho(t_0) = \rho_S(t_0) \otimes \rho_B$, we have $\mathcal{P}\rho(t_0) = \rho(t_0)$ and $\mathcal{Q}\rho(t_0) = 0$. Hence the inhomogeneous term vanishes and the TCL equation reduces to

$$\frac{\partial}{\partial t} \mathcal{P}\rho(t) = \mathcal{K}(t)\mathcal{P}\rho(t). \quad (\text{A.27})$$

The super-operator $\mathcal{K}(t)$ only exists when it is possible to invert the operator $[1 - \Sigma(t)]$. Let's assume that $[1 - \Sigma(t)]^{-1}$ may be expanded into a geometric series,

$$[1 - \Sigma(t)]^{-1} = \sum_{n=0}^{\infty} [\Sigma(t)]^n \quad (\text{A.28})$$

Inserting this expansion into the definition of super-operator $\mathcal{K}(t)$, we get

$$\mathcal{K}(t) = \alpha \sum_{n=0}^{\infty} \mathcal{P}\mathcal{L}(t) [\Sigma(t)]^n \mathcal{P} = \sum_{n=0}^{\infty} \alpha^n \mathcal{K}_n(t). \quad (\text{A.29})$$

Here, we expand the super-operator $\mathcal{K}(t)$ in power series of the coupling α , $\mathcal{K}_n(t)$ is the n -th order contribution.

We can find the explicit expression for $\mathcal{K}_n(t)$ according to the definition of the super-operator $\Sigma(t)$ in Eq.(A.36). It is convenient if we also expand $\Sigma(t)$ in powers of α ,

$$\Sigma(t) = \sum_{n=1}^{\infty} \alpha^n \Sigma_n(t). \quad (\text{A.30})$$

By inserting this into Eq.(A.29), we get

$$\alpha \sum_{n=0}^{\infty} \mathcal{P}\mathcal{L}(t) \left[\sum_{n'=1}^{\infty} \alpha^{n'} \Sigma_{n'}(t) \right]^n \mathcal{P} = \sum_{n=0}^{\infty} \alpha^n \mathcal{K}_n(t). \quad (\text{A.31})$$

By sorting equal powers of α , up to fourth order in α , we obtain,

$$\mathcal{K}_1(t) = \mathcal{P}\mathcal{L}(t)\mathcal{P}, \quad (\text{A.32})$$

$$\mathcal{K}_2(t) = \mathcal{P}\mathcal{L}(t)\Sigma_1(t)\mathcal{P}, \quad (\text{A.33})$$

$$\mathcal{K}_3(t) = \mathcal{P}\mathcal{L}(t) \left\{ [\Sigma_1(t)]^2 + \Sigma_2(t) \right\} \mathcal{P}, \quad (\text{A.34})$$

$$\mathcal{K}_4(t) = \mathcal{P}\mathcal{L}(t) \left\{ [\Sigma_1(t)]^3 + \Sigma_1(t)\Sigma_2(t) + \Sigma_2(t)\Sigma_1(t) + \Sigma_3(t) \right\} \mathcal{P}. \quad (\text{A.35})$$

In order to have a better understanding of the expansion of $\Sigma(t)$, we list the definition of $\Sigma(t)$ which is already shown in previous section.

$$\Sigma(t) = \alpha \int_{t_0}^t ds \mathcal{G}(t, s) \mathcal{Q} \mathcal{L}(s) \mathcal{P} G(t, s), \quad (\text{A.36})$$

with the propagator $\mathcal{G}(t, s)$ defined as

$$\mathcal{G}(t, s) \equiv T_{\leftarrow} \exp \left[\alpha \int_s^t ds' \mathcal{Q} \mathcal{L}(s') \right], \quad (\text{A.37})$$

and also with the backward propagator $G(t, s)$ defined as

$$G(t, s) \equiv T_{\rightarrow} \exp \left[-\alpha \int_s^t ds' \mathcal{L}(s') \right]. \quad (\text{A.38})$$

The first order contribution $\Sigma_1(t)$ can be obtained by taking the zeroth order term in both expansions of $\mathcal{G}(t, s)$ and $G(t, s)$.

$$\Sigma_1(t) = \int_{t_0}^t ds \mathcal{Q} \mathcal{L}(s) \mathcal{P}, \quad (\text{A.39})$$

which yields

$$\mathcal{K}_2(t) = \int_{t_0}^t ds \mathcal{P} \mathcal{L}(t) \mathcal{Q} \mathcal{L}(s) \mathcal{P}, \quad (\text{A.40})$$

To simplify the expression, we take $t_0 = 0$. In many cases it may also be assumed that the odd moments of the interaction Hamiltonian with respect to the reference state vanish, which leads to the relation

$$\mathcal{P} \mathcal{L}(t_1) \mathcal{L}(t_2) \dots \mathcal{L}(t_{2n+1}) \mathcal{P} = 0. \quad (\text{A.41})$$

Then we have the contribution \mathcal{K}_n up to second order,

$$\mathcal{K}_1(t) = \mathcal{P}\mathcal{L}(t)\mathcal{P} = 0, \quad (\text{A.42})$$

$$\begin{aligned} \mathcal{K}_2(t) &= \int_0^t ds \mathcal{P}\mathcal{L}(t)\mathcal{Q}\mathcal{L}(s)\mathcal{P} \\ &= \int_0^t ds \mathcal{P}\mathcal{L}(t)\mathcal{L}(s)\mathcal{P} - \int_0^t ds \mathcal{P}\mathcal{L}(t)\mathcal{P}\mathcal{L}(s)\mathcal{P} \\ &= \int_0^t ds \mathcal{P}\mathcal{L}(t)\mathcal{L}(s)\mathcal{P}. \end{aligned} \quad (\text{A.43})$$

Using the same notation in Chapter 4, up to second order expansion, the general TCL method leads to the relation

$$K_S(t)\sigma_j^\dagger = \int_0^t dt' \text{tr}_{\mathbf{k}}\{\mathcal{L}(t)\mathcal{L}(t')\sigma_j^\dagger \otimes \rho_{\mathbf{k}}\} \quad (\text{A.44})$$

where $\rho_{\mathbf{k}} = |0\rangle_{\mathbf{k}}\langle 0|$ is the vacuum state of the reservoir.

Here we only study the second order expansion in TCL equation since in our simulation, higher order contributions are not considered. A more general derivation is available in the book *'The Theory of Open Quantum System'* [38].

Appendix B

Perturbation theory check

In this appendix, we provide an alternative approach to investigate the microscopic properties of phonon assisted energy transfer qualitatively. We establish a link between the effective exciton-photon-phonon interaction and the combined effect of exciton-photon interaction and exciton-phonon interaction, which could be considered as a validation of the results of our numerical simulation in Chapter 3. This approach is based on the perturbation theory. Let us start from the Schrödinger equation assuming $\hbar = 1$.

$$\mathcal{H}|\psi(t)\rangle = i\frac{\partial}{\partial t}|\psi(t)\rangle. \quad (\text{B.1})$$

Given the state $|\psi(t_0)\rangle$ at some initial time t_0 , we can solve the Schrödinger equation to obtain the state at any subsequent time t . In particular, if \mathcal{H} is time independent, then

$$|\psi(t)\rangle = e^{-i\mathcal{H}t}|\psi(t_0)\rangle. \quad (\text{B.2})$$

The time evolution operator of a system with Hamiltonian \mathcal{H} can be expressed as an integral

$$e^{-i\mathcal{H}t} = \int_{-\infty}^{\infty} \frac{d\omega}{-2\pi i} \frac{e^{-i(\omega+i\epsilon)t}}{\omega+i\epsilon-\mathcal{H}}, \quad (\text{B.3})$$

where $\mathcal{H} = \mathcal{H}_0 + \mathcal{H}_I$. We can expand the denominator $\frac{1}{\omega+i\epsilon-\mathcal{H}}$ when \mathcal{H}_I is a small perturbation compared to the unperturbed hamiltonian \mathcal{H}_0 .

$$\begin{aligned} \frac{1}{\omega+i\epsilon-\mathcal{H}} &= (\omega+i\epsilon-\mathcal{H})^{-1} \\ &= (\omega+i\epsilon-\mathcal{H}_0-\mathcal{H}_I)^{-1} \\ &= (\omega+i\epsilon-\mathcal{H}_0 - (\omega+i\epsilon-\mathcal{H}_0)(\omega+i\epsilon-\mathcal{H}_0)^{-1}\mathcal{H}_I)^{-1} \\ &= \left\{ (\omega+i\epsilon-\mathcal{H}_0) [1 - (\omega+i\epsilon-\mathcal{H}_0)^{-1}\mathcal{H}_I] \right\}^{-1} \\ &= [1 - (\omega+i\epsilon-\mathcal{H}_0)^{-1}\mathcal{H}_I]^{-1} (\omega+i\epsilon-\mathcal{H}_0)^{-1} \\ &= \sum_{n=0}^{\infty} [(\omega+i\epsilon-\mathcal{H}_0)^{-1}\mathcal{H}_I]^n (\omega+i\epsilon-\mathcal{H}_0)^{-1}. \end{aligned} \quad (\text{B.4})$$

In the last line of the above equation, $[1 - (\omega+i\epsilon-\mathcal{H}_0)^{-1}\mathcal{H}_I]^{-1}$ is expanded into a geometric series. The matrix element of the transition from initial state $|i\rangle$ to the final state $|f\rangle$ is given by,

$$\langle f | e^{-i\mathcal{H}t} | i \rangle = \int_{-\infty}^{\infty} \frac{d\omega}{-2\pi i} e^{-i(\omega+i\epsilon)t} \langle f | \sum_{n=0}^{\infty} [(\omega+i\epsilon-\mathcal{H}_0)^{-1}\mathcal{H}_I]^n (\omega+i\epsilon-\mathcal{H}_0)^{-1} | i \rangle. \quad (\text{B.5})$$

According to Fermi's Golden rule, the transition probability is proportional to $|\langle f | e^{-i\mathcal{H}t} | i \rangle|^2$.

This is a general relation which could be applied to any perturbative system to study the transition rate from initial state $|i\rangle$ to final state $|f\rangle$.

B.1 Exciton energy transfer between two dots

In this section, we try to study the exciton energy transfer between two quantum dots denoted as dot A and dot B. A general theory is derived to understand the physical nature of the energy transfer which is a supplementary to the numerical simulation in Chapter 3. Quantitative work is not needed to be presented in this section. Hence, the physical quantities and the coupling constant in the Hamiltonian are not specified.

The Hamiltonian for a two dot system with the presence of photon bath reads as,

$$\begin{aligned}
 \mathcal{H}_0 &= \sum_{\alpha} E_{\alpha} a_{\alpha}^{\dagger} a_{\alpha} + \sum_{\beta} E_{\beta} a_{\beta}^{\dagger} a_{\beta} + \sum_{k\gamma} \hbar\omega_{k\gamma} c_{k\gamma}^{\dagger} c_{k\gamma} \\
 \mathcal{H}_{ex-pht} &= \sum_{k\gamma,\alpha} \hbar \left(g_{k\gamma,\alpha}^{*} c_{k\gamma} a_{\alpha}^{\dagger} + g_{k\gamma,\alpha} c_{k\gamma}^{\dagger} a_{\alpha} \right) + \sum_{k\gamma,\beta} \hbar \left(g_{k\gamma,\beta}^{*} c_{k\gamma} a_{\beta}^{\dagger} + g_{k\gamma,\beta} c_{k\gamma}^{\dagger} a_{\beta} \right) \\
 &= \sum_{k\gamma,\alpha} V_{k\gamma,\alpha} + \sum_{k\gamma,\beta} V_{k\gamma,\beta}. \tag{B.6}
 \end{aligned}$$

Here \mathcal{H}_0 is the unperturbed Hamiltonian. E_{α} and E_{β} are the exciton energy in quantum dot A and quantum dot B respectively. $a_{\alpha}^{\dagger}(a_{\beta}^{\dagger})$ and $a_{\alpha}(a_{\beta})$ are the exciton creation and annihilation operators with exciton energy $E_{\alpha}(E_{\beta})$. The summation over α indicates that all excited states of exciton in quantum dot A are considered. $\hbar\omega_{k\gamma}$ is the photon energy with wavevector $k\gamma$. $c_{k\gamma}^{\dagger}$ and $c_{k\gamma}$ are the photon creation and annihilation operators. All photon modes are considered in the summation over $k\gamma$.

Perturbative term \mathcal{H}_{ex-pht} represents exciton-photon interaction. The first(second) term indicates the interaction between exciton with energy $E_{\alpha}(E_{\beta})$ in quantum dot A(B) and the photon with wavevector $k\gamma$. An exciton is created or destroyed when a photon is absorbed or emitted. $g_{k\gamma,\alpha}$ and $g_{k\gamma,\beta}$ are the coupling constants. To shorten the derivation, these

interaction terms are denoted as $V_{k\gamma,\alpha}$ and $V_{k\gamma,\beta}$ without losing any physical meanings.

With this interaction term, and according to Eq.(B.5), the first order perturbation gives zero, so we go to second order:

$$\begin{aligned} \langle f|e^{-i\mathcal{H}t}|i\rangle &= \int_{-\infty}^{\infty} \frac{d\omega}{-2\pi i} e^{-i(\omega+i\epsilon)t} \langle f| \frac{1}{\omega+i\epsilon-\mathcal{H}_0} V_{k\gamma,\beta_0} \frac{1}{\omega+i\epsilon-\mathcal{H}_0} V_{k\gamma,\alpha_0} \frac{1}{\omega+i\epsilon-\mathcal{H}_0} |i\rangle \\ &= \int_{-\infty}^{\infty} \frac{d\omega}{-2\pi i} e^{-i(\omega+i\epsilon)t} \frac{1}{\omega+i\epsilon-E_{\beta_0}} \frac{1}{\omega+i\epsilon-E_{\alpha_0}} \sum_{k\gamma} g_{k\gamma,\beta_0}^* g_{k\gamma,\alpha_0} \hbar^2 \frac{1}{\omega+i\epsilon-\omega_{k\gamma}}. \end{aligned} \quad (\text{B.7})$$

The initial state $|i\rangle$ is chosen as one exciton in quantum dot A with exciton energy E_{α_0} . The final state $|f\rangle$ is one exciton in quantum dot B with exciton energy E_{β_0} . The transition from $|i\rangle$ to $|f\rangle$ represents the exciton energy transfer from quantum dot A to quantum dot B. Both E_{α_0} and E_{β_0} are the lowest energy for exciton in quantum dot A and quantum dot B. The excited exciton states do not appear in either initial state or final state, but they play a important role in the process when phonons are taken into consideration. In principle, we can omit all the higher exciton levels when only photon bath is included, but in order to keep the consistency, we still include these excited exciton levels in the Hamiltonian.

To calculate the integral Eq.(B.7), we have two different cases. First, the initial state and final state have different energy, which is the off-resonance case. Second, the initial state and final state have same energy, which is the resonance case.

When $E_{\alpha_0} \neq E_{\beta_0}$, we have a second order pole,

$$\begin{aligned}
\langle f|e^{-i\mathcal{H}t}|i\rangle &= e^{-iE_{\beta_0}t} \frac{1}{E_{\beta_0} - E_{\alpha_0}} \sum_{k_\gamma}^{\omega_{k_\gamma} \neq E_{\alpha_0} \neq E_{\beta_0}} g_{k_\gamma, \beta_0}^* g_{k_\gamma, \alpha_0} \hbar^2 \frac{1}{E_{\beta_0} - \omega_{k_\gamma}} \\
&+ e^{-iE_{\alpha_0}t} \frac{1}{E_{\alpha_0} - E_{\beta_0}} \sum_{k_\gamma}^{\omega_{k_\gamma} \neq E_{\alpha_0} \neq E_{\beta_0}} g_{k_\gamma, \beta_0}^* g_{k_\gamma, \alpha_0} \hbar^2 \frac{1}{E_{\alpha_0} - \omega_{k_\gamma}} \\
&+ e^{-iE_{\beta_0}t} g_{k_\gamma, \beta_0}^* g_{k_\gamma, \alpha_0} \hbar^2 \left[\frac{-it}{E_{\beta_0} - E_{\alpha_0}} + \frac{-1}{(E_{\beta_0} - E_{\alpha_0})^2} \right] \\
&+ e^{-iE_{\alpha_0}t} g_{k_\gamma, \beta_0}^* g_{k_\gamma, \alpha_0} \hbar^2 \left[\frac{-it}{E_{\alpha_0} - E_{\beta_0}} + \frac{-1}{(E_{\alpha_0} - E_{\beta_0})^2} \right].
\end{aligned}$$

When $E_{\alpha_0} = E_{\beta_0} = E_0$, we have a third order pole,

$$\begin{aligned}
\langle f|e^{-i\mathcal{H}t}|i\rangle &= e_{k_\gamma}^{-iE_0\omega_{k_\gamma} \neq E_0} g_{k_\gamma, \beta_0}^* g_{k_\gamma, \alpha_0} \hbar^2 \left[\frac{-it}{E_0 - \omega_{k_\gamma}} + \frac{-1}{(E_0 - \omega_{k_\gamma})^2} \right] \\
&+ e^{-iE_0t} g_{k_\gamma, \beta_0}^* g_{k_\gamma, \alpha_0} \hbar^2 (-t^2).
\end{aligned}$$

Let's compare these two results. For the off-resonance case, $\langle f|e^{-i\mathcal{H}t}|i\rangle$ only has terms proportional to t . Meanwhile, for the resonance case, $\langle f|e^{-i\mathcal{H}t}|i\rangle$ has terms with t^2 . In addition, for the off-resonance case, when the detuning between E_{α_0} and E_{β_0} is decreasing, the transition rate keeps increasing. For the limiting case, $|E_{\alpha_0} - E_{\beta_0}| \rightarrow 0$, the transition rate for off-resonance case should approach the limit of the resonance case. Hence, it can be concluded that the transition rate for the resonance case is significantly larger. As shown in Chapter 3, when two dots are off-resonant, the energy transfer is highly suppressed. We have a good agreement with this perturbation theory and the numerical simulation.

B.2 Phonon assisted exciton energy transfer

It is commonly known that phonon is a source of dissipation and decoherence in the excitonic dynamics in semiconductor. However, phonon plays a different role in exciton energy transfer when two dots are off-resonant. We call this process 'phonon assisted exciton energy transfer'.

In order to include phonon effect, the Hamiltonian is modified as,

$$\begin{aligned}
\mathcal{H}_0 &= \sum_{\alpha} E_{\alpha} A_{\alpha}^{\dagger} A_{\alpha} + \sum_{\beta} E_{\beta} A_{\beta}^{\dagger} A_{\beta} + \sum_{k\gamma} \hbar\omega_{k\gamma} a_{k\gamma}^{\dagger} a_{k\gamma} + \sum_q \hbar c|q| b_q^{\dagger} b_q \\
\mathcal{H}_{ex-phn} &= \sum_{k\gamma,\alpha} \hbar \left(g_{k\gamma,\alpha}^* a_{k\gamma} A_{\alpha}^{\dagger} + g_{k\gamma,\alpha} a_{k\gamma}^{\dagger} A_{\alpha} \right) + \sum_{k\gamma,\beta} \hbar \left(g_{k\gamma,\beta}^* a_{k\gamma} B_{\beta}^{\dagger} + g_{k\gamma,\beta} a_{k\gamma}^{\dagger} B_{\beta} \right) \\
&= \sum_{k\gamma,\alpha} V_{k\gamma,\alpha} + \sum_{k\gamma,\beta} V_{k\gamma,\beta} \\
\mathcal{H}_{ex-phn} &= \sum_q \sum_{\alpha,\alpha'} \hbar g_{q,\alpha,\alpha'} A_{\alpha'}^{\dagger} A_{\alpha} (b_q^{\dagger} + b_{-q}) + \sum_q \sum_{\beta,\beta'} \hbar g_{q,\beta,\beta'} B_{\beta'}^{\dagger} B_{\beta} (b_q^{\dagger} + b_{-q}) \\
&= \sum_q \sum_{\alpha,\alpha'} V_{q,\alpha,\alpha'} + \sum_q \sum_{\beta,\beta'} V_{q,\beta,\beta'}. \tag{B.8}
\end{aligned}$$

We have one additional term $\sum_q \hbar c|q| b_q^{\dagger} b_q$ in \mathcal{H}_0 which indicates the energy of acoustic phonon. b_q^{\dagger} (b_q) is the creation (annihilation) operator of phonon with wavevector q . \mathcal{H}_{ex-phn} represents the exciton-phonon interaction. In this interaction term, we include the scattering process between exciton and phonon. Explicitly, a phonon is created or destroyed when the exciton is jumping between different energy levels. Optical phonon is not considered in the Hamiltonian since its energy is not comparable to the scattering process. With this Hamiltonian, we have two kinds of interactions, one is the exciton-photon interaction, that could create or destroy an exciton in the quantum dot. The other one is the

exciton-phonon scattering process which can only shift the energy of the exciton with the presence of phonon bath. It is very interesting to see total effect of these two interactions.

Similarly, we use Eq.(B.5) to study to phonon assisted process. we try to investigate the terms with both exciton-photon interaction and exciton-phonon interaction. The lowest order non zero contribution in this perturbation expansion reads,

$$\begin{aligned}
\langle f|e^{-i\mathcal{H}t}|i\rangle &= \int_{-\infty}^{\infty} \frac{d\omega}{-2\pi i} e^{-i(\omega+i\epsilon)t} \langle f| \frac{1}{\omega+i\epsilon-\mathcal{H}_0} V_{q,\beta x,\beta_0} \frac{1}{\omega+i\epsilon-\mathcal{H}_0} \\
&\quad V_{k\gamma,\beta x} \frac{1}{\omega+i\epsilon-\mathcal{H}_0} V_{k\gamma,\alpha_0} \frac{1}{\omega+i\epsilon-\mathcal{H}_0} |i\rangle \\
&+ \int_{-\infty}^{\infty} \frac{d\omega}{-2\pi i} e^{-i(\omega+i\epsilon)t} \langle f| \frac{1}{\omega+i\epsilon-\mathcal{H}_0} V_{k\gamma,\beta_0} \frac{1}{\omega+i\epsilon-\mathcal{H}_0} \\
&\quad V_{k\gamma,\alpha x} \frac{1}{\omega+i\epsilon-\mathcal{H}_0} V_{q,\alpha_0,\alpha x} \frac{1}{\omega+i\epsilon-\mathcal{H}_0} |i\rangle \\
&= \int_{-\infty}^{\infty} \frac{d\omega}{-2\pi i} e^{-i(\omega+i\epsilon)t} \sum_q \frac{1}{\omega+i\epsilon-E_{\beta_0}-E_q} \frac{1}{\omega+i\epsilon-E_{\alpha_0}} \cdot \\
&\quad \sum_{\beta x} g_{q,\beta x,\beta_0} \hbar \frac{1}{\omega+i\epsilon-E_{\beta x}} \sum_{k\gamma} g_{k\gamma,\beta x}^* g_{k\gamma,\alpha_0} \hbar^2 \frac{1}{\omega+i\epsilon-\omega_{k\gamma}} \\
&+ \int_{-\infty}^{\infty} \frac{d\omega}{-2\pi i} e^{-i(\omega+i\epsilon)t} \sum_q \frac{1}{\omega+i\epsilon-E_{\beta_0}-E_q} \frac{1}{\omega+i\epsilon-E_{\alpha_0}} \cdot \\
&\quad \sum_{\alpha x} g_{q,\alpha_0,\alpha x} \hbar \frac{1}{\omega+i\epsilon-E_{\alpha x}-E_q} \sum_{k\gamma} g_{k\gamma,\beta_0}^* g_{k\gamma,\alpha x} \hbar^2 \frac{1}{\omega+i\epsilon-\omega_{k\gamma}-E_q}. \tag{B.9}
\end{aligned}$$

Compared with Eq.(B.7) which is a two step process including exciton-photon interacting only, Eq.(B.9) consists three steps. One additional step is the exciton-phonon scattering process, which change the energy of the exciton by emitting or absorbing a phonon. This additional step plays an important role when the initial state and the final state are detuned.

Eq.(B.9) is quite complicated to integrate, since we have multiple summations in the expression. In order to better demonstrate the physics in phonon assisted process, we simplify the integral by picking one phonon mode whose energy gives $E_{\alpha_0} = E_{\beta_0} + E_q$. This is the

case when the phonon energy compensates the detuning between the two quantum dots.

As discussed above, the integral is calculated under the condition when $E_{\alpha_0} = E_{\beta_0} + E_q = E_0 \neq E_{\beta_x} \neq E_{\alpha_x}$. It is a messy integral, but it is helpful to understand the physical meaning of the phonon assisted process. We list the complete result here,

$$\begin{aligned}
& \langle f | e^{-i\mathcal{H}t} | i \rangle \\
= & e^{-iE_0 t} \sum_{\beta_x} g_{q,\beta_x,\beta_0} \hbar \sum_{k_\gamma}^{\omega_{k_\gamma} \neq E_0} g_{k_\gamma,\beta_x}^* g_{k_\gamma,\alpha_0} \hbar^2 \\
& \left[\frac{-it}{(E_0 - E_{\beta_x})(E_0 - \omega_{k_\gamma})} - \frac{1}{(E_0 - E_{\beta_x})^2(E_0 - \omega_{k_\gamma})} - \frac{1}{(E_0 - E_{\beta_x})(E_0 - \omega_{k_\gamma})^2} \right] \\
+ & \sum_{\beta_x} e^{-iE_{\beta_x} t} g_{q,\beta_x,\beta_0} \sum_{k_\gamma}^{\omega_{k_\gamma} \neq E_{\beta_x}} g_{k_\gamma,\beta_x}^* g_{k_\gamma,\alpha_0} \hbar^2 \frac{1}{(E_{\beta_x} - E_0)^2(E_{\beta_x} - \omega_{k_\gamma})} \\
+ & \sum_{\beta_x} g_{q,\beta_x,\beta_0} \sum_{k_\gamma}^{\omega_{k_\gamma} \neq E_0 \neq E_{\beta_x}} e^{-i\omega_{k_\gamma} t} g_{k_\gamma,\beta_x}^* g_{k_\gamma,\alpha_0} \hbar^2 \frac{1}{(\omega_{k_\gamma} - E_0)^2(\omega_{k_\gamma} - E_{\beta_x})} \\
+ & e^{-iE_0 t} \sum_{\beta_x} g_{q,\beta_x,\beta_0} \hbar g_{k_\gamma,\beta_x}^* g_{k_\gamma,\alpha_0} \hbar^2 \left[\frac{-t^2}{E_0 - E_{\beta_x}} + \frac{-2it}{(E_0 - E_{\beta_x})^2} + \frac{2}{(E_0 - E_{\beta_x})^3} \right] \\
+ & \sum_{\beta_x} e^{-iE_{\beta_x} t} g_{q,\beta_x,\beta_0} \hbar g_{k_\gamma,\beta_x}^* g_{k_\gamma,\alpha_0} \hbar^2 \left[\frac{-it}{(E_{\beta_x} - E_0)^2} + \frac{-2}{(E_{\beta_x} - E_0)^3} \right] \\
+ & e^{-iE_0 t} \sum_{\alpha_x} g_{q,\alpha_0,\alpha_x} \hbar \sum_{k_\gamma}^{\omega_{k_\gamma} \neq E_0 - E_q} g_{k_\gamma,\beta_0}^* g_{k_\gamma,\alpha_x} \hbar^2 \\
& \left[\frac{-it}{(E_0 - E_{\alpha_x} - E_q)(E_0 - \omega_{k_\gamma} - E_q)} - \frac{(E_0 - E_{\alpha_x} - E_q) + (E_0 - \omega_{k_\gamma} - E_q)}{(E_0 - E_{\alpha_x} - E_q)^2(E_0 - \omega_{k_\gamma} - E_q)^2} \right] \\
+ & \sum_{\alpha_x} e^{-i(E_{\alpha_x} + E_q)t} g_{q,\alpha_0,\alpha_x} \sum_{k_\gamma}^{\omega_{k_\gamma} \neq E_{\alpha_x}} g_{k_\gamma,\beta_0}^* g_{k_\gamma,\alpha_x} \hbar^2 \frac{1}{(E_{\alpha_x} + E_q - E_0)^2(E_{\alpha_x} - \omega_{k_\gamma})}
\end{aligned}$$

$$\begin{aligned}
& + \sum_{\alpha_x} g_{q,\alpha_0,\alpha_x} \sum_{k_\gamma}^{\omega_{k_\gamma} \omega_{k_\gamma} \neq E_{\alpha_x} \neq E_0 - E_q} e^{-i(\hbar\omega_{k_\gamma} + E_q)t} g_{k_\gamma,\beta_0}^* g_{k_\gamma,\alpha_x} \hbar^2 \\
& \frac{1}{(\omega_{k_\gamma} + E_q - E_0)^2 (\omega_{k_\gamma} - E_{\alpha_x})} \\
& + e^{-iE_0 t} \sum_{\alpha_x} g_{q,\alpha_0,\alpha_x} \hbar g_{k_\gamma,\beta_0}^* g_{k_\gamma,\alpha_x} \hbar^2 \\
& \left[\frac{-t^2}{E_0 - E_{\alpha_x} - E_q} + \frac{-2it}{(E_0 - E_{\alpha_x} - E_q)^2} + \frac{2}{(E_0 - E_{\alpha_x} - E_q)^3} \right] \tag{B.10} \\
& + \sum_{\alpha_x} e^{-i(E_{\alpha_x} + E_q)t} g_{q,\alpha_0,\alpha_x} \hbar g_{k_\gamma,\beta_0}^* g_{k_\gamma,\alpha_x} \hbar^2 \left[\frac{-it}{(E_{\alpha_x} + E_q - E_0)^2} + \frac{-2}{(E_{\alpha_x} + E_q - E_0)^3} \right].
\end{aligned}$$

In this result, there are many terms because we have to consider all possible poles in different conditions related to the variables ω_{k_γ} , E_0 , E_{α_x} and E_{β_x} . All the terms have the product of three coupling constants g because we are describing a three step process. In the expression, we can find terms proportional to t^2 , which indicate that a phonon assisted process might be more efficient than off-resonant energy transfer without phonon. Compared with the resonant two step case, which also has terms with t^2 in this phonon assisted process, we have a product of three coupling constants multiplied by terms like $1/(E_0 - E_{\beta_x})$. In the weak coupling regime, $\hbar g$, which has the dimension of energy, is usually much smaller compared to the energy scale. Hence, this three step process is less effective than the resonant two step process, as seen in the simulations presented in Chapter 3. We can conclude that exciton energy transfer between quantum dots with detuned exciton energy level can be enhanced by the presence of the phonon bath. Phonons in this process provide a compensation to the energy detuning by turning a two step off-resonant process into a more effective three step resonant process.

B.3 Exciton-photon-phonon interaction

In the previous section, we have introduced the exciton-phonon interaction in the Hamiltonian as a source of the scattering between exciton and phonon. In the calculation, we have included all possible combinations between the three interactions (two exciton photon interactions and one exciton-phonon interaction). The result turns out to be complicated with many lower order contributions. In this section, we develop a two step process model, in which we combine one exciton-photon interaction and one exciton-phonon interaction into an exciton-photon-phonon interaction. By doing so, we simplify the integrals a lot without losing the leading terms. \mathcal{H}_{ex-phn} represents a process in which exciton phonon scattering is combined with the creation (annihilation) of the exciton. The new Hamiltonian needs as follows: $\mathcal{H}_0 + \mathcal{H}_{ex-phn} + \mathcal{H}_{ex-phn-phn}$ where

$$\begin{aligned}
\mathcal{H}_0 &= \sum_{\alpha} E_{\alpha} A_{\alpha}^{\dagger} A_{\alpha} + \sum_{\beta} E_{\beta} A_{\beta}^{\dagger} A_{\beta} + \sum_{k\gamma} \hbar\omega_{k\gamma} a_{k\gamma}^{\dagger} a_{k\gamma} + \sum_q \hbar c|q| b_q^{\dagger} b_q \\
\mathcal{H}_{ex-phn} &= \sum_{k\gamma,\alpha} V_{k\gamma,\alpha} + \sum_{k\gamma,\beta} V_{k\gamma,\beta} \\
&= \sum_{k\gamma,\alpha} \hbar \left(g_{k\gamma,\alpha}^* a_{k\gamma} A_{\alpha}^{\dagger} + g_{k\gamma,\alpha} a_{k\gamma}^{\dagger} A_{\alpha} \right) + \sum_{k\gamma,\beta} \hbar \left(g_{k\gamma,\beta}^* a_{k\gamma} A_{\beta}^{\dagger} + g_{k\gamma,\beta} a_{k\gamma}^{\dagger} A_{\beta} \right) \\
\mathcal{H}_{ex-phn-phn} &= \sum_{q,k\gamma,\alpha} V_{q,k\gamma,\alpha} + \sum_{q,k\gamma,\beta} V_{q,k\gamma,\beta} \\
&= \sum_{q,k\gamma,\alpha} \hbar \left(g_{q,k\gamma,\alpha}^* a_{k\gamma} A_{\alpha}^{\dagger} + g_{q,k\gamma,\alpha} a_{k\gamma}^{\dagger} A_{\alpha} \right) (b_q^{\dagger} + b_{-q}) \\
&+ \sum_{q,k\gamma,\beta} \hbar \left(g_{q,k\gamma,\beta}^* a_{k\gamma} A_{\beta}^{\dagger} + g_{q,k\gamma,\beta} a_{k\gamma}^{\dagger} A_{\beta} \right) (b_q^{\dagger} + b_{-q}).
\end{aligned} \tag{B.11}$$

As we discussed above, for the off-resonant case when $E_{\alpha_0} \neq E_{\beta_0}$, the first non zero

term in the perturbation expansion contains one exciton-photon interaction and one exciton photon phonon interaction.

$$\begin{aligned}
\langle f|e^{-i\mathcal{H}t}|i\rangle &= \int_{-\infty}^{\infty} \frac{d\omega}{-2\pi i} e^{-i(\omega+i\epsilon)t} \langle f| \frac{1}{\omega+i\epsilon-\mathcal{H}_0} V_{q,k\gamma,\beta_0} \frac{1}{\omega+i\epsilon-\mathcal{H}_0} V_{k\gamma,\alpha_0} \frac{1}{\omega+i\epsilon-\mathcal{H}_0} |i\rangle \\
&+ \int_{-\infty}^{\infty} \frac{d\omega}{-2\pi i} e^{-i(\omega+i\epsilon)t} \langle f| \frac{1}{\omega+i\epsilon-\mathcal{H}_0} V_{k\gamma,\beta_0} \frac{1}{\omega+i\epsilon-\mathcal{H}_0} V_{q,k\gamma,\alpha_0} \frac{1}{\omega+i\epsilon-\mathcal{H}_0} |i\rangle \\
&= \int_{-\infty}^{\infty} \frac{d\omega}{-2\pi i} e^{-i(\omega+i\epsilon)t} \sum_q \frac{1}{\omega+i\epsilon-E_{\beta_0}-E_q} \frac{1}{\omega+i\epsilon-E_{\alpha_0}} \\
&\quad \sum_{k\gamma} g_{q,k\gamma,\beta_0}^* g_{k\gamma,\alpha_0} \hbar^2 \frac{1}{\omega+i\epsilon-\omega_{k\gamma}} \\
&+ \int_{-\infty}^{\infty} \frac{d\omega}{-2\pi i} e^{-i(\omega+i\epsilon)t} \sum_q \frac{1}{\omega+i\epsilon-E_{\beta_0}-E_q} \frac{1}{\omega+i\epsilon-E_{\alpha_0}} \\
&\quad \sum_{k\gamma} g_{k\gamma,\beta_0}^* g_{q,k\gamma,\alpha_0} \hbar^2 \frac{1}{\omega+i\epsilon-\omega_{k\gamma}-E_q}.
\end{aligned} \tag{B.12}$$

In the expression of $\langle f|e^{-i\mathcal{H}t}|i\rangle$ we do not have the excited energy levels E_{α_x} and E_{β_x} explicitly. All the information about the excited levels are not thrown away but included in the exciton-photon-phonon coupling constant $g_{q,k\gamma,\alpha_0}$ and $g_{q,k\gamma,\beta_0}$. The remaining problem is to figure out the properties of the coupling constant $g_{q,k\gamma,\alpha_0}$ and $g_{q,k\gamma,\beta_0}$. With the exciton-photon-phonon interaction, we simplifies the expression a lot without losing any physics. This is the advantage of introducing the exciton-photon-phonon interaction. Compare Eq.(B.12) with Eq.(B.5), Eq.(B.12) is very similar to the resonant energy transfer between the two dots without phonon, although the two dots in this case are detuned.

The physical meaning of the Hamiltonian with exciton-phonon interaction and the Hamiltonian with exciton-photon-phonon interaction need to be clarified here. In our model, the exciton photon phonon interaction is treated as the combined effect of one exciton-photon interaction and one exciton-phonon interaction. In the following discussion, the relation

between these two Hamiltonians will be shown.

When $E_{\alpha_0} = E_{\beta_0} + E_q = E_0$, Eq.(B.12) leads to,

$$\begin{aligned}
\langle f | e^{-i\mathcal{H}t} | i \rangle &= e^{-iE_0 t} \sum_{k_\gamma}^{\omega_{k_\gamma} \neq E_0} g_{q,k_\gamma,\beta_0}^* g_{k_\gamma,\alpha_0} \hbar^2 \left[\frac{-it}{E_0 - \omega_\gamma} - \frac{1}{(E_0 - \omega_\gamma)^2} \right] \\
&+ \sum_{k_\gamma}^{\omega_{k_\gamma} \neq E_0} e^{-i\omega_{k_\gamma} t} g_{q,k_\gamma,\beta_0}^* g_{k_\gamma,\alpha_0} \hbar^2 \frac{1}{(\omega_{k_\gamma} - E_0)^2} \\
&+ e^{-iE_0 t} g_{q,k_\gamma,\beta_0}^* g_{k_\gamma,\alpha_0} \hbar^2 (-t^2) \\
&+ e^{-iE_0 t} \sum_{k_\gamma}^{\omega_{k_\gamma} \neq E_0 - E_q} g_{k_\gamma,\beta_0}^* g_{q,k_\gamma,\alpha_0} \hbar^2 \left[\frac{-it}{E_0 - \omega_\gamma - E_q} - \frac{1}{(E_0 - \omega_\gamma - E_q)^2} \right] \\
&+ \sum_{k_\gamma}^{\hbar\omega_{k_\gamma} \neq E_0 - E_q} e^{-i\hbar\omega_{k_\gamma} t} g_{k_\gamma,\beta_0}^* g_{q,k_\gamma,\alpha_0} \hbar^2 \frac{1}{(\omega_{k_\gamma} + E_q - E_0)^2} \\
&+ e^{-iE_0 t} g_{k_\gamma,\beta_0}^* g_{q,k_\gamma,\alpha_0} \hbar^2 (-t^2).
\end{aligned}$$

From this expression we can see that the energy transfer for the case $E_{\alpha_0} = E_{\beta_0} + E_q$ originates from two different processes. One contains the factor $g_{q,k_\gamma,\beta_0}^* g_{k_\gamma,\alpha_0}$ which indicates the exciton-photon interaction in dot A and the exciton-photon-phonon interaction in dot B. The other one contains the factor $g_{k_\gamma,\beta_0}^* g_{q,k_\gamma,\alpha_0}$ which indicates the exciton-photon-phonon interaction in dot A and the exciton photon interaction in dot B. The leading terms in the expression which is proportional to t^2 occur when the photon energy $\omega_{k_\gamma} = E_{\alpha_0}$ or $\omega_{k_\gamma} = E_{\beta_0}$. In these two cases, the phonon energy $E_q = E_{\alpha_0} - E_{\beta_0}$ compensates the detuning between the two dots and highly enhances the exciton energy transfer.

In the following, we establish the link between the two Hamiltonians. Neglecting the terms related to excited energy levels α_x , and keeping the leading terms related to β_x , we

have

$$\begin{aligned}
& \langle f | e^{-i\mathcal{H}t} | i \rangle \\
&= e^{-iE_0t} \sum_{\beta_x} g_{q,\beta_x,\beta_0} \hbar \sum_{k_\gamma}^{\omega_{k_\gamma} \neq E_0} g_{k_\gamma,\beta_x}^* g_{k_\gamma,\alpha_0} \hbar^2 \frac{-it}{(E_0 - E_{\beta_x})(E_0 - \omega_{k_\gamma})} \\
&+ e^{-iE_0t} \sum_{\beta_x} g_{q,\beta_x,\beta_0} \hbar g_{k_\gamma,\beta_x}^* g_{k_\gamma,\alpha_0} \hbar^2 \frac{-t^2}{E_0 - E_{\beta_x}}. \tag{B.13}
\end{aligned}$$

On the other hand for the Hamiltonian with exciton-photon-phonon interaction, we have

$$\begin{aligned}
\langle f | e^{-i\mathcal{H}t} | i \rangle &= e^{-iE_0t} \sum_{k_\gamma}^{\omega_{k_\gamma} \neq E_0} g_{q,k_\gamma,\beta_0}^* g_{k_\gamma,\alpha_0} \hbar^2 \frac{-it}{E_0 - \omega_\gamma} \\
&+ e^{-iE_0t} g_{q,k_\gamma,\beta_0}^* g_{k_\gamma,\alpha_0} \hbar^2 (-t^2). \tag{B.14}
\end{aligned}$$

By comparing these two expressions, we get

$$g_{q,k_\gamma,\beta_0}^* = \sum_{\beta_x} g_{q,\beta_x,\beta_0} g_{k_\gamma,\beta_x}^* \frac{1}{E_0 - E_{\beta_x}}. \tag{B.15}$$

Other terms in the expression for $\langle f | e^{-i\mathcal{H}t} | i \rangle$ give the same relation between g_{q,k_γ,β_0}^* and $g_{q,\beta_x,\beta_0} g_{k_\gamma,\beta_x}^*$ which means this relation is originated from the same physics.

In this appendix, we have applied a perturbation theory to check the validity of introducing a exciton-photon-phonon interaction into the Hamiltonian in order to describe the phonon assisted exciton energy transfer. It is proved analytically that one exciton-photon interaction together with one exciton-phonon interaction can be treated as a single exciton-

photon-phonon interaction with a properly estimated coupling constant. And the relation between the coupling constants are given in Eq.(B.15). This analytical work could serve as a reference to the numerical simulation in Chapter 3.

BIBLIOGRAPHY

BIBLIOGRAPHY

- [1] M. A. Reed, J. N. Randall, R. J. Aggarwal, R. J. Matyi, T. M. Moore, and A. E. Wetsel. Observation of discrete electronic states in a zero-dimensional semiconductor nanostructure. *Phys. Rev. Lett.*, 60:535–537, Feb 1988.
- [2] G. Ramon, U. Mizrahi, N. Akopian, S. Braitbart, D. Gershoni, T. L. Reinecke, B. D. Gerardot, and P. M. Petroff. Emission characteristics of quantum dots in planar microcavities. *Phys. Rev. B*, 73:205330, May 2006.
- [3] L P. Kouwenhoven, D G. Austing, and S Tarucha. Few-electron quantum dots. *Rep. Prog. Phys*, 64:701–736, 2001.
- [4] P. Peumans, A. Yakimov, and S. R. Forrest. Small molecular weight organic thin-film photodetectors and solar cells. *J. Appl. Phys.*, 93(7):3693, April 2003.
- [5] Y. Cao, I. D. Parker, G. Yu, C. Zhang, and A. J. Heeger. Improved quantum efficiency for electroluminescence in semiconducting polymers. *Nature*, 397(6718):414, February 1999.
- [6] V. G. Kozlov, V. Bulovic, P. E. Burrows, M. Baldo, V. B. Khalfin, G Parthasarathy, S. R. Forrest, Y. You, and M. E. Thompson. Study of lasing action based on frster energy transfer in optically pumped organic semiconductor thin films. *J. Appl. Phys.*, 94(8):4096, October 1998.
- [7] K. J. Xu, Y. P. Huang, M. G. Moore, and C. Piermarocchi. Two-qubit conditional phase gate in laser-excited semiconductor quantum dots using the quantum zeno effect. *Phys. Rev. Lett.*, 103(3):037401, Jul 2009.
- [8] A.S. Davydov and A.A. Serikov. Energy transfer between impurity molecules of a crystal in the presence of relaxation. *Phys. Stat. Sol. B*, 51:57, 1972.

- [9] Ho Trung Dung, Ludwig Knöll, and Dirk Gunnar Welsch. Resonant dipole-dipole interaction in the presence of dispersing and absorbing surroundings. *Phys. Rev. A*, 66(6):063810, Dec 2002.
- [10] Dae Gwi Kim, Shinya Okahara, Masaaki Nakayama, and Yong Gu Shim. Experimental verification of Förster energy transfer between semiconductor quantum dots. *Phys. Rev. B*, 78(15):153301, Oct 2008.
- [11] K. Nishibayashi, T. Kawazoe, M. Ohtsu, K. Akahane, and N. Yamamoto. Observation of interdot energy transfer between inas quantum dots. *Appl. Phys. Lett.*, 93(15):153301, Jul 2008.
- [12] T. Kazimierczuk, J. Suffczyński, A. Golnik, J. A. Gaj, P. Kossacki, and P. Wojnar. Optically induced energy and spin transfer in nonresonantly coupled pairs of self-assembled cdte/znte quantum dots. *Phys. Rev. B*, 79(15):153301, Apr 2009.
- [13] A. O. Govorov. Spin and energy transfer in nanocrystals without tunneling. *Phys. Rev. B*, 68:075315, 2003.
- [14] G. Parascandolo and V. Savona. Long-range radiative interaction between semiconductor quantum dots. *Phys. Rev. B*, 71:045335, January 2005.
- [15] Gregory D. Scholes and David L. Andrews. Resonance energy transfer and quantum dots. *Phys. Rev. B*, 72(12):125331, Sep 2005.
- [16] Alexander O. Govorov. Spin-Förster transfer in optically excited quantum dots. *Phys. Rev. B*, 71(15):155323, Apr 2005.
- [17] S. Yu. Kruchinin, A. V. Fedorov, A. V. Baranov, T. S. Perova, and K. Berwick. Resonant energy transfer in quantum dots: Frequency-domain luminescent spectroscopy. *Phys. Rev. B*, 78(12):125311, Sep 2008.
- [18] Anna Sitek and Pawel Machnikowski. Collective fluorescence and decoherence of a few nearly identical quantum dots. *Phys. Rev. B*, 75(3):035328, Jan 2007.
- [19] Pawel Machnikowski, K. Roszak, and Anna Sitek. Collective luminescence and phonon-induced processes in double quantum dots. *Acta Phys. Pol.*, 116:818, 2009.
- [20] J. Danckwerts, K. J. Ahn, J. Förstner, and A. Knorr. Theory of ultrafast nonlinear optics of coulomb-coupled semiconductor quantum dots: Rabi oscillations and pump-probe spectra. *Phys. Rev. B*, 73(16):165318, Apr 2006.

- [21] M. Richter, K. J. Ahn, A. Knorr, A. Schliwa, D. Bimberg, M. E.-A. Madjet, and T. Renger. Theory of excitation transfer in coupled nanostructures c from quantum dots to light harvesting complexes. *Phys. Stat Sol. (b)*, 243(10):2302, 2006.
- [22] M. Sugawara. Theory of exciton spontaneous emission in semiconductor mesoscopic quantum disk embedded in a planar microcavity. *Jpn. J. Appl. Phys.*, 36:2151–2162, April 1997.
- [23] Girish S. Agarwal and S. Dutta Gupta. Microcavity-induced modification of the dipole-dipole interaction. *Phys. Rev. A*, 57(1):667–670, Jan 1998.
- [24] D. M. Basko, F. Bassani, G. C. La Rocca, and V. M. Agranovich. Electronic energy transfer in a microcavity. *Phys. Rev. B*, 62(23):15962–15977, Dec 2000.
- [25] G. Tarel, G Parascandolo, and V. Savona. Ultralong-range radiative excitation transfer between quantum dots in a planar microcavity. *Phys. Stat. Sol.(b)*, 245(6):1085, 2008.
- [26] B. Krummheuer, V. M. Axt, and T. Kuhn. Theory of pure dephasing and the resulting absorption line shape in semiconductor quantum dots. *Phys. Rev. B*, 65(19):195313, May 2002.
- [27] J. Förstner, C. Weber, J. Danckwerts, and A. Knorr. Phonon-assisted damping of rabi oscillations in semiconductor quantum dots. *Phys. Rev. Lett.*, 91(12):127401, Sep 2003.
- [28] T. Stauber and R. Zimmermann. Optical absorption in quantum dots: Coupling to longitudinal optical phonons treated exactly. *Phys. Rev. B*, 73(11):115303, Mar 2006.
- [29] U. Hohenester, G. Pfanner, and M. Seliger. Phonon-assisted decoherence in the production of polarization-entangled photons in a single semiconductor quantum dot. *Phys. Rev. Lett.*, 99:047402, 2007.
- [30] Emil Rozbicki and Pawel Machnikowski. Quantum kinetic theory of phonon-assisted excitation transfer in quantum dot molecules. *Phys. Rev. Lett.*, 100(2):027401, Jan 2008.
- [31] P. Machnikowski. Radiative and phonon-induced dephasing in double quantum dots. *J. Phys.: Conf. Ser.*, 193:012136, 2009.
- [32] G. Tarel and V. Savona. Linear spectrum of a quantum dot coupled to a nanocavity. *Phys. Rev. B*, 81(7):075305, Feb 2010.

- [33] S. Hughes, P. Yao, F. Milde, A. Knorr, D. Dalacu, K. Mnaymneh, V. Sazonova, P. J. Poole, G. C. Aers, J. Lapointe, R. Cheriton, and R. L. Williams. Influence of electron-acoustic phonon scattering on off-resonant cavity feeding within a strongly coupled quantum-dot cavity system. *Phys. Rev. B*, 83(16):165313, Apr 2011.
- [34] K. J. Xu and C. Piermarocchi. Dynamics of elastic and inelastic energy transfer between quantum dots in a microcavity. *Phys. Rev. B*, 84:115316, Sep 2011.
- [35] G. Barton. Quantum electrodynamics of spinless particles between conducting plates. *Proc. Roy. Soc. Lond. A.*, 320(1541):251–275, December 1970.
- [36] T. Takagahara. Localization and energy transfer of quasi-two-dimensional excitons in gaas-alas quantum-well heterostructures. *Phys. Rev. B*, 31(10):6552–6573, May 1985.
- [37] Y. P. Huang and M. G. Moore. Interaction- and measurement-free quantum zeno gates for universal computation with single-atom and single-photon qubits. *Phys. Rev. A*, 77(062332), 2008.
- [38] Heinz-Peter Breuer and Francesco Petruccione. *The Theory of Open Quantum System*. Oxford University Press, 2002.
- [39] J Frenkel. On the transformation of light into heat in solids. i. *Physical Review*, 37:17, 1931.
- [40] Gregory H Wannier. The structure of electronic excitation levels in insulating crystals. *Physical Review*, 52:191, 1937.
- [41] L. J. Sham and T. M. Rice. Many-particle derivation of the effective-mass equation for the wannier exciton. *Phys. Rev.*, 144:708–714, Apr 1966.
- [42] Victor I. Klimov. Nanocrystal quantum dots. *Los Alamos Science*, 28:214, 2003.
- [43] Weiming Que. Excitons in quantum dots with parabolic confinement. *Phys. Rev. B*, 45:11036–11041, May 1992.
- [44] Garnett W. Bryant. Excitons in quantum boxes: Correlation effects and quantum confinement. *Phys. Rev. B*, 37:8763–8772, May 1988.
- [45] Edward Mills Purcell. Spontaneous emission probabilities at radio frequencies. *Physical Review*, 69:681, 1946.

- [46] Claude Cohen-Tannoudji, Jacques Dupont-Roc, and Gilbert Grynberg. *Photons and Atoms: Introduction to Quantum Electrodynamics*. Wiley & Sons, 1989.
- [47] E. M. Kessler, M. Grochol, and C. Piermarocchi. Light-mass bragg cavity polaritons in planar quantum dot lattices. *Phys. Rev. B*, 77(8):085306, Feb 2008.
- [48] Neil W Ashcroft and N David Mermin. *Solid State Physics*. 1976.
- [49] G.D. Mahan. *Many-particle Physics*. Plenum Press, New York, 1981.
- [50] M. I. Vasilevskiy, E. V. Anda, and S. S. Makler. Electron-phonon interaction effects in semiconductor quantum dots:a nonperturbative approach. *Phys. Rev. B*, 70(3):035318, Jul 2004.
- [51] T. Takagahara. Theory of exciton dephasing in semiconductor quantum dots. *Phys. Rev. B*, 60(4):2638–2652, Jul 1999.
- [52] L. Besombes, K. Kheng, L. Marsal, and H. Mariette. Acoustic phonon broadening mechanism in single quantum dot emission. *Phys. Rev. B*, 63(15):155307, Mar 2001.
- [53] A. Grodecka and P. Machnikowski. Partly noiseless encoding of quantum information in quantum dot arrays against phonon-induced pure dephasing. *Phys. Rev. B*, 73(12):125306, Mar 2006.
- [54] D. Gammon, E. S. Snow, B. V. Shanabrook, D. S. Katzer, and D. Park. Fine structure splitting in the optical spectra of single gaas quantum dots. *Phys. Rev. Lett.*, 76(16):3005–3008, Apr 1996.
- [55] M. Grochol, F. Grosse, and R. Zimmermann. Exciton wave function properties probed by diamagnetic shift in disordered quantum wells. *Phys. Rev. B*, 71(12):125339, Mar 2005.
- [56] G. Bastard. *Wave Mechanics Applied to Semiconductor Hetrostructures*. Les éditions de physique, Paris, 1992.
- [57] E. Rosencher and B. Vinter. *Optoelectronics*. Cambridge University Press, Cambridge, 2002.
- [58] Dirk Englund, David Fattal, Edo Waks, Glenn Solomon, Bingyang Zhang, Toshihiro Nakaoka, Yasuhiko Arakawa, Yoshihisa Yamamoto, and Jelena Vuckovic. Controlling

- the spontaneous emission rate of single quantum dots in a two-dimensional photonic crystal. *Phys. Rev. Lett.*, 95(1):013904, Jul 2005.
- [59] K. Hennessy, A. Badolato, M. Winger, D. Gerace, M. Atatüre, S. Gulde, S. Fält, E. L. Hu, and A. Imamoglu. Quantum nature of a strongly coupled single quantum dot-cavity system. *Nature*, 445:896, 2007.
- [60] R. H. Dicke. Coherence in spontaneous radiation processes. *Phys. Rev.*, 93:99–110, Jan 1954.
- [61] Mitchel Weissbluth. *Photon-Atom Interactions*. Academic Press Inc.(London) LTD, 1989.
- [62] David E. Pritchard. Cooling neutral atoms in a magnetic trap for precision spectroscopy. *Phys. Rev. Lett.*, 51:1336–1339, Oct 1983.
- [63] C. Piermarocchi, Pochung Chen, Y. S. Dale, and L. J. Sham. Theory of fast quantum control of exciton dynamics in semiconductor quantum dots. *Phys. Rev. B*, 65(7):075307, Jan 2002.
- [64] Daniel Loss and David P. DiVincenzo. Quantum computation with quantum dots. *Phys. Rev. A*, 57:120–126, Jan 1998.
- [65] B. Misra and E.C.G. Sudarshan. The zeno’s paradox in quantum theory. *Journal of Mathematical Physics*, 18:756, 1977.
- [66] C. B. Chiu, E. C. G. Sudarshan, and B. Misra. Time evolution of unstable quantum states and a resolution of zeno’s paradox. *Phys. Rev. D*, 16(2):520–529, Jul 1977.
- [67] Asher Peres. Zeno paradox in quantum-theory. *American Journal of Physics*, 48:931, 1980.
- [68] W. M. Itano, D. J. Heinzen, J. J. Bollinger, and Wineland D. J. Quantum zeno effect. *Phys. Rev. Lett.*, 41:2295, 1990.
- [69] Paul Kwiat, Harald Weinfurter, Thomas Herzog, Anton Zeilinger, and Mark A. Kasevich. Interaction-free measurement. *Phys. Rev. Lett.*, 74(24):4763–4766, Jun 1995.
- [70] P. Horodecki. ”interaction-free” interaction: Entangling evolution coming from the possibility of detection. *Phys. Rev. A*, 63:022108, 2001.

- [71] P. Zanardi M. Rasetti. A possible strategy to defeat decoherence in quantum computation: The role of symmetries, dynamical algebras, and all that. *Fortschritte Der Physik-Progress of Physics*, 48:559, 2000.
- [72] P. Facchi and S Pascazio. Quantum zeno subspaces. *Phys. Rev. A*, 89:080401, 2002.
- [73] J. D. Franson, B. C. Jacobs, and T. B. Pittman. Quantum computing using single photons and the zeno effect. *Phys. Rev. A*, 70:062302, 2004.
- [74] P. M Leung and T. C Ralph. Improving the fidelity of optical zeno gates via distillation. *Phys. Rev. A*, 74:062325, 2006.
- [75] C. R. Myers and A. Gilchrist. Photon-loss-tolerant zeno controlled-sign gate. *Phys. Rev. A*, 75:052339, 2007.
- [76] Almut Beige, Daniel Braun, Ben Tregenna, and Peter L. Knight. Quantum computing using dissipation to remain in a decoherence-free subspace. *Phys. Rev. Lett.*, 85(8):1762–1765, Aug 2000.
- [77] X. B. Wang, J. Q. You, and F. Nori. Quantum entanglement via two-qubit quantum zeno dynamics. *Phys. Rev. A*, 77:062339, 2008.
- [78] L. Robledo, J. Elzerman, G. Jundt, M Atatüre, A Högele, S. Fält, and A. Imamoglu. Conditional dynamics of interacting quantum dots. *Science*, 320:772, 2008.
- [79] T. H. Stievater, X. Li, D. G. Steel, D. Gammon, D. S. Katzer, D. Park, C. Piermarocchi, and L. J. Sham. Rabi oscillations of excitons in single quantum dots. *Phys. Rev. Lett.*, 87:133603, 2001.
- [80] Q. Q. Wang, A. Muller, P. Bianucci, E. Rossi, Q. K. Xue, T. Takagahara, C. Piermarocchi, A. H. MacDonald, and C. K. Shih. Decoherence processes during optical manipulation of excitonic qubits in semiconductor quantum dots. *Phys. Rev. B*, 72:035306, 2005.
- [81] Pierre Meystre. *Atom Optics*. Springer-Verlag, New York, 2001.
- [82] Gustavo A. Narvaez, Gabriel Bester, Alberto Franceschetti, and Alex Zunger. Excitonic exchange effects on the radiative decay time of monoexcitons and biexcitons in quantum dots. *Physical Review B (Condensed Matter and Materials Physics)*, 74(20):205422, 2006.

- [83] J. F. Poyatos, J. I. Cirac, and P. Zoller. Complete characterization of a quantum process: The two-bit quantum gate. *Phys. Rev. Lett.*, 78(2):390–393, Jan 1997.
- [84] R. D. Schaller and V. I. Klimov. High efficiency carrier multiplication in pbse nanocrystals: Implications for solar energy conversion. *Phys. Rev. Lett.*, 92:186601, May 2004.
- [85] R. J. Ellingson, M. C. Beard, J. C. Johnson, P. Yu, O. I. Micic, A. J. Nozik, A. Shabaev, and A. L. Efros. Highly efficient multiple exciton generation in colloidal pbse and pbs quantum dots. *Nano Letters*, 5:865–871, May 2005.
- [86] Octavi E. Semonin, Joseph M. Luther, Sukgeun Choi, Hsiang-Yu Chen, Jianbo Gao, Arthur J. Nozik, and Matthew C. Beard. Peak external photocurrent quantum efficiency exceeding 100% via meq in a quantum dot solar cell. *Science*, 334:1530–1533, Dec 2011.
- [87] Heinz-Peter Breuer, Bernd Kappler, and Francesco Petruccione. The time-convolutionless projection operator technique in the quantum theory of dissipation and decoherence. *Ann. Phys.*, 291:1633–1643, 2001.
- [88] Sadao Nakajima. On quantum theory of transport phenomena. *Prog. Theor. Phys.*, 20:948–959, 1958.
- [89] Robert Zwanzig. Ensemble method in the theory of irreversibility. *J. Chem. Phys.*, 33:1338–1341, 1960.
- [90] Seth Lloyd. A potentially realizable quantum computer. *Science*, 261:1569, Sep 1993.